DOCTOR OF PHILOSOPHY

Adaptive Optical OFDM for Local and Access Networks

Giacoumidis, Elias

Award date:
2011

Awarding institution:
Bangor University

Adaptive Optical OFDM for Local and Access Networks

Elias Giacoumidis

PRIFYSGOL
BANGOR
UNIVERSITY

A Thesis submitted for the degree of

Doctor of Philosophy

School of Electronic Engineering

Bangor University

July 2011

Abstract

To satisfy the continuously increasing bandwidth requirements from individual and business end-users, Optical Orthogonal Frequency Division Multiplexing (OOFDM) has been widely considered as one of the strongest contenders for high-speed Local Area Networks (LANs) and Next Generation (NG)-Passive Optical Networks (PONs). The aim of the PhD dissertation research is to extensively explore the feasibility of implementing the OOFDM technique in the aforementioned application scenarios. Special attention is given to investigating the transmission performance of Adaptively Modulated Optical OFDM (AMOOFDM) in cost-sensitive Directly-Modulated DFB Lasers (DML)-based, Intensity-Modulation and Direct-Detection (IM/DD) systems utilising Multi-Mode Fibres (MMFs) or Single-Mode Fibres (SMFs). The impacts of a wide range of different parameters of various components involved in the AMOOFDM modems on the transmission performance of the un-amplified IM/DD AMOOFDM signals are thoroughly explored, in single-channel MMF/SMF systems, and Dense Wavelength Division Multiplexing (DWDM) PON systems. The validity of numerical simulations presented in the thesis is also rigorously verified by comparing with real-time experimental measurements conducted in Bangor University.

Following an extensive review of OOFDM operating principles as well as challenges and opportunities of existing transmission techniques associated with LANs and NG-PONs, detailed investigations are first undertaken of the impact of Adaptive Cyclic Prefix (ACP) on the transmission performance of AMOOFDM over DML-based, IM/DD systems using both MMFs and SMFs. Three ACP mechanisms are identified, each of which can, depending upon the system properties, affect significantly the

AMOOFDM transmission performance. In comparison with AMOOFDM having a fixed cyclic prefix duration of 25%, AMOOFDM with ACP can not only improve the transmission capacity by a factor of >2 (>1.3) for >1000m MMFs (<80km SMFs) with 1dB link loss margin enhancement, but also relax considerably the requirement on the DFB modulation bandwidth.

Further investigations of the AMOOFDM technique in multi-channel NG-PON systems are also undertaken. It is shown that AMOOFDM not only significantly reduces the nonlinear WDM impairments induced by the effects of cross-phase modulation and four-wave mixing but also effectively compensates for the DML-induced frequency chirp effect. In comparison with conventional OOFDM using an identical signal modulation format across all the subcarriers, AMOOFDM improves the maximum achievable signal transmission capacity of a central WDM channel by a factor of 1.3 and 3.6 for 40- and 80-km standard SMFs, respectively, with the corresponding dynamic input optical power ranges being extended by approximately 5dB. In addition, AMOOFDM also causes the occurrence of cross-channel complementary modulation format mapping among various WDM channels, leading to considerably improved transmission capacities for all individual WDM channels.

To further maximize the OOFDM transmission performance and simultaneously improve the system flexibility and performance robustness, the widely adopted adaptive loading algorithms including Bit Loading (BL), Power Loading (PL), and Bit-and-Power Loading (BPL) are compared in terms of transmission performance for different transceiver parameters in both SMF and MMF systems. As different MMF links reveal large variations in both the 3dB bandwidths and the system frequency responses, any explorations of the topic of interest over a specific MMF link are not

adequate. Hence, statistical investigations of the performance of these three algorithms are undertaken over 1000 statistically constructed worst-case MMF links. The thesis tenders for the first time complete evaluations of adaptive loading algorithms over MMF and SMF-based systems. It is shown that the BPL (PL) algorithm always offers the best (worst) transmission performance. The absolute transmission capacity differences between these algorithms are independent of signal bit rate and increase with both transmission distance and digital-to-analog converter/analog-to-digital converter (DAC/ADC) sampling rate. More importantly, numerical results also indicate that, for PON systems and worst-case MMF links of less than 300 m, in comparison with the most sophisticated BPL algorithm, the simplest PL algorithm is sufficiently effective in escalating the OOFDM system performance to its maximum potential. The effectiveness of the PL algorithm can be further improved when a large number of subcarriers are utilized. On the other hand, for relatively transmission systems with their 3-dB bandwidths being much less than the transmitted OOFDM signal spectrum, the BPL algorithm has to be adopted. The aforementioned results have great potential for practical cost-effective OOFDM transceiver architecture design.

Having explored OOFDM in cost-sensitive LANs and PONs, further investigations of the OOFDM technique are conducted in transparent optical Metro/Regional Reconfigurable Optical Add/Drop Multiplexer (ROADM)-based networks without employing optoelectronic regeneration. In Metro/Regional networks using ROADMs, one significant source of penalty is signal degradation due to transmission through cascaded ROADMs, referred to as the filter concatenation effect. The use of AMOOFDM to improve the network tolerance to the filter concatenation effect is

theoretically investigated. It is shown that, compared to the conventional identical modulation OOFDM, adaptive modulation can not only improve the maximum achievable transmission capacity by up to 60%, but also enhances the network tolerance to the filter impairments. More importantly, it is shown that the utilization of adaptive modulation is essential due to its vital tolerance to the filter misalignment penalty.

Acknowledgements

Above all, I would like to express my deep and sincere gratitude to my supervisor, Prof. Jianming Tang from Bangor University, for his guidance, advice, patience and support during my research. His wide knowledge, attention to detail, and logic way of thinking have been of great values for the completion of the current PhD Thesis. He was always accessible and willing to help all of his students with their research. As a result, research life in Bangor University became smooth and rewarding for me.

I am also deeply grateful to Prof. I. Tomkos, who hired me as a Senior Research Scientist in Athens Information Technology (AIT) centre, during writing my PhD Thesis, and helped me considerably with his constructive comments and important support throughout this work.

Special thanks go to the colleagues in Bangor University, Dr. Jinlong Wei, Dr. Xing Zheng, Dr. Xianqing Jin, Dr. Roger Giddings, Dr. Emilio-Hugues Salas, and also to Dr. Athanasios Kavatzikidis, Dr. Kostis Kanonakis, Mrs. Marianna Angelou, Dr. Christoforos Kachris, Dr. Dimitrios Klonidis, Mr. Ioannis Nellas, Dr. Christos Tsekrekos, Dr. Siamak Adomolsky, and Dr. Arvind Mishra from AIT centre for their constructive suggestions, discussions and encouragement. Many thanks also to Dr. Xuelin Yang, Dr. Anoop Menachery and Prof. S. P. Spencer.

I wish to thank my family for supporting me all these years. Special thanks to my sister Amalia Giacoumidou and my brother Marios Giacoumidis.

Lastly, and most importantly, I wish to thank my mother, Eleni Triviza-Giacoumidou. To her I dedicate this Thesis.

ABBREVIATIONS

3D	3Dimensional
ACP	Adaptive Cyclic Prefix
ADC	Analogue-to-Digital Converter
ADM	Add/Drop Multiplexers
ADSL	Asymmetric Digital Subscriber Line
AIT	Athens Information Technology
AM	Amplitude Modulation
AMOOFDM	Adaptively Modulated Optical Orthogonal Frequency Division Multiplexing
ANSI	American National Standards Institute
APD	Avalanche Photo-Diode
ASE	Amplified Spontaneous Emission
ATM	Asynchronous Transfer Mode
AT&T	American Telephone and Telegraph Company
AWG	Arrayed Wavelength Grating
BER	Bit-Error-Rate
BL	Bit Loading
BLS	Broadband Light Source
BPL	Bit-and-Power Loading
BPON	Broadband Passive Optical Network
BPSK	Binary Phase Shift Keying
BS	Band Splitter

CAPEX	Cost Capital Expenditures
CATV	Cable Television
CD	Chromatic Dispersion
CDF	Cumulative Density Function
CDM	Code Division Multiplexing
CFO	Carrier Frequency Offset
CO	Centre Office
COFDM	Coded OFDM
CO-OOFDM	Coherent Optical Orthogonal Frequency Division Multiplexing
CP	Cyclic Prefix
CPE	Customer Premises Equipment
CPEr	Carrier Phase Error
CSI	Channel State Information
CMTS	Connection Mode Transport Service
DAC	Digital-to-Analogue Converter
DBPSK	Differential Binary Phase Shift Keying
DC	Direct Current
DCF	Dispersion Compensation Fibre
DEMUX	De- multiplexer
DD	Direct-Detection
DFE	Decision Feedback Equalizers
DFB	Distributed Feedback Laser
DFT	Discrete Fourier Transform
DMD	Differential Mode Delay
DML	Directly Modulated Laser

DMT	Discrete Multi-Tone modulation
DOCSIS	Data Over Cable Service Interface Specification
DQPSK	Differential Quaternary Phase Shift Keying
DSB	Double-Side Band
DSL	Digital Subscriber Line
DSLAM	Digital Subscriber Line Access Multiplexer
DSP	Digital Signal Processing
DWDM	Dense Wavelength Division Multiplexing
DXC	Digital Cross Connects
EAM	Electro-Absorption Modulator
EDFA	Erbium Doped Fibre Amplifier
ETRI	Electronics and Telecommunications Research Institute, Korea
E/O	Electrical/Optical
ER	Extensive Reach
EPON	Ethernet Passive Optical Network
EVC	Ethernet Virtual Connection
FBG	Fibre-Bragg Grating
FDD-LTE	Frequency Division Duplex-Long Term Evolution
FDM	Frequency Division Multiplexing
FFE	Feed-Forward Equalizers
FFT	Fast Fourier Transform
FOFDM	Fast Orthogonal Frequency Division Multiplexing
FOMA	Freedom of Multimedia Access
FPGA	Field-Programmable Gate Array

FSAN	Full Service Access Network
FTTH	Fibre-to-the-Home
FTTx	Fibre to the x
FWA	Fixed Wireless Access
FWM	Four-Wave Mixing
GDR	Group Delay Ripple
GSM	Global System for Mobile communications
GPON	Gigabit Passive Optical Network
GEM	GPON Encapsulation Method
HDSL	High-bit-rate Digital Subscriber Line
HFC	Hybrid Fibre Coaxial
HGW	Home Gate Way
HSPA	High Speed Packet Access
ICI	Inter-Carrier Interference
IEEE	Institute of Electrical and Electronic Engineers
IFFT	Inverse Fast Fourier Transform
I	In-phase
IF	Intermediate Frequency
IMD	Inter-Modulation
IM/DD	Intensity-Modulation and Direct-Detection
IMT	International Mobile Telecommunication
IP	Internet Protocol
IPTV	Internet Protocol Television
ISDN	Integrated Services Digital Network

ISI	Inter-Symbol Interference
ITU	International Telecommunications Union
L2	Layer 2
LAN	Local Area Network
LD	Laser Diode
LED	Light-Emitting Diode
LO	Local Oscillator
LP	Loss Ripple
LPF	Low-Pass Filter
LTE	Line Terminating Equipment
MAC	Media Access Control
MAN	Metropolitan Area Network
MBWA	Mobile Broadband Wireless Access
MCM	Multi-Carrier Modulation
MFL	Multi-Frequency Laser
MMF	Multi-Mode Fibre
MPEG	Moving Picture Expert Group
MSL	Mode Selective Loss
MUX	Multiplexer
MWA	Maintenance Work Area
MZM	Mach-Zehnder Modulator
N-CDMA	Narrowband - Code Division Multiple Access
NDSF	Non-Dispersion Shifted Fibre
NGA	Next-Generation Access

NG-PON	Next Generation-Passive Optical Network
NRZ	Non-Return to Zero
NTI	National Tyndall Institute
NWA	Native Web Applications
ODN	Optical Distribution Network
OE	Optical-to-Electrical
OEO	Optical-Electronic-Optical
OFDM	Orthogonal Frequency Division Multiplexing
OOFDM	Optical Orthogonal Frequency Division Multiplexing
OLT	Optical Line Terminal
ONT	Optical Network Termination
ONU	Optical Network Unit
OPEX	Operating Expenditure
OSI	Open System Interconnect
OSNR	Optical Signal-to-Noise Ratio
P2P	Point-to-Point
PAL	Phase Alternation Line
PAN	Personal Area Network
PAPR	Peak-to-Average Power Ratio
PC	Personal Computer
PCM	Pulse Code Modulation
PDC	Personal Digital Cellular
PDH	Plesiochronous Digital Hierarchy
PFS	Platform Service
PHY	Physical

PIN	P-type Intrinsic N-type material
PL	Power Loading
PMD	Polarization-Mode Dispersion
PON	Passive Optical Networks
PoP	Point-of-Presence
POTS	Plain Old Telephony Service
PS	Power Splitter
PSD	Power Spectral Density
Q	Quadrature
QAM	Quadrature Amplitude Modulation
QPSK	Quaternary Phase Shift Keying
QoS	Quality-of-Signal
R&D	Research & Development
RB	Rayleigh Backscattering
RBOC	Regional Bell Operating Company
RF	Radio Frequency
ROADM	Reconfigurable Optical Add/Drop Multiplexer
RSOA	Reflective Semiconductor Optical Amplifier
SCM	Sub-Carrier Modulation
SCO	Sampling Clock Offset
SDH	Synchronous Digital Hierarchy
SEC	Service Equipment Custer
SMF	Single-Mode Fibre

SNR	Signal-to-Noise Ratio
SONET	Synchronous Optical Network
SPM	Self-Phase Modulation
SSB	Single-Side Band
SSMF	Standard Single-Mode Fibre
STM	Synchronous Transfer Mode
STO	Symbol Timing Offset
T1	Digital transmission line T-carrier 1
TC	Transmission Convergence
TD-CDMA	Time Division - CDMA
TDD-LTE	Time Division Duplex - Long Term Evolution
TDM	Time Division Multiplexing
TDMA	Time Division Multiplexing Access
TEI	Technological Educational Institute
UCC	University College Cork
UHDTV	Ultra High Definition Television
UWB	Ultra Wide Band
VOA	Variable Optical Attenuator
VoD	Video-on-Demand
VoIP	Voice over Internet Protocol
VPN	Virtual Private Network
WAN	Wide Area Network
WB/WSS	Wavelength Blocker/Wavelength Selective Switch

W-CDMA	Wideband - CDMA
WDM	Wavelength Division Multiplexing
WE-PON	WDM Ethernet PON
Wi-Fi	Wireless - Fidelity
WiMAX	Worldwide Interoperability for Microwave Access
WIPAS	Wireless Internet Protocol Access System
WLAN	Wireless Local Area Network
WPAN	Wireless Personal Area Network
WWAN	Wireless Wide Area Networks
WXC	Wavelength Cross Connect
XG-PON	10 Gigabit Passive Optical Network
XPM	Cross-Phase Modulation

Contents

Abstract.....I

Acknowledgements.....V

Abbreviations.....VI

Chapter 1: Introduction

1.1 Evolution of Optical Communication.....1

1.2 Next-Generation PONs.....5

1.3 Optical OFDM.....11

1.4 Challenges in MMF/SMF-based OOFDM systems.....12

1.5 Major Achievements of the Dissertation Research.....16

1.6 Thesis Structure.....20

References.....23

Chapter 2: Reviews of High-Speed Optical Networks and OOFDM

2.1 Introduction.....32

2.2 General Network Concepts.....33

2.3 Access Network Technology Evaluations.....36

2.3.1 Digital Subscriber Line (DSL).....37

2.3.2 Hybrid Fibre Coaxial (HFC).....39

2.4 Passive Optical Networks (PONs).....41

2.5 PON Evolution.....45

2.6 NG-PON Evolution.....47

2.6.1 NG-PON General Requirements.....50

2.6.2 Service Requirements.....51

2.6.3 General Requirements on Architecture/Infrastructure.....52

2.7 Promising Technologies for NG-PONs.....53

2.7.1 WDM-PON.....53

2.7.2 Hybrid WDM/TDM-PON.....56

2.8 Optical OFDM technology for Next Generation Optical Networks

2.8.1 OFDM concept and description.....57

2.8.1.1 Bit Encoding....59
2.8.1.2 IFFT/FFT....60
2.8.1.3 Cyclic Prefix....64
2.8.1.4 Serialization....65
2.8.1.5 DAC/ADC....66
2.8.1.6 Pilot-Assisted Channel Estimation and Equalization....68
2.8.1.7 Synchronization....69
2.8.2 Optical OFDM....71
2.8.2.1 Coherent OOFDM (CO-OFDM) Transceivers....71
2.8.2.2 IM/DD OOFDM Transceivers....73
2.8.2.3 Comparison between CO-OFDM and IM/DD OOFDM....75
2.8.2.4 AMOOFDM....77
2.9 OOFDM PON....80
2.10 Conclusion....81
References....83

Chapter 3: Transmission Performance Improvement of AMOOFDM Signals using Adaptive Cyclic Prefix

3.1 Introduction
3.1.1 Background....91
3.1.2 Scope....94
3.2 Transmission Link Model, Signal Characteristics and Simulation Parameters....95
3.2.1 Transmission Link Model....96
3.2.2 Signal Characteristics....100
3.2.3 Simulation Parameters....102
3.3 Performance of AMOOFDM-ACP Signals over MMFs
3.3.1 Capacity versus Reach Transmission Performance....107
3.3.2 Link Loss Margin....110
3.4 Performance of AMOOFDM-ACP Signals over SMFs
3.4.1 Capacity versus Reach Transmission Performance....113
3.4.2 Link Loss Margin....116
3.5 ACP-Enabled DFB Bandwidth Relaxation....117

3.6 Conclusions.....120
References.....121

Chapter 4: Adaptive Loading Algorithms
4.1 Introduction.....126
4.2 Theoretical OOFDM SMF/MMF-Based Model, Statistical Construction of Worst-Case MMF links, and Simulation Parameters.....129
4.2.1 Statistical Construction of Worst-Case MMF links.....130
4.2.2 Simulation Parameters for SMF/MMF-based links.....132
4.3 Implementation of Adaptive Loading Algorithms.....133
4.4 Statistical Performance of Adaptive Loading Algorithms over MMF links.....138
4.4.1 Impact of Transmission Distance on Adaptive Loading Algorithms.....138
4.4.2 Impact of Subcarrier Number and Sampling Speeds 141
4.5 Adaptive Loading Algorithm Performance over SMF links.....144
4.5.1 Impact of Transmission Distance and Launched Optical Power.....144
4.5.2 Impact of Subcarrier Number and Sampling Speeds.....149
4.6 Conclusions.....152
References.....154

Chapter 5: WDM Impairment Reduction using Adaptive Modulation in Multi-channel OOFDM Transmission Systems for NG-PONs
5.1 Introduction.....158
5.2 WDM AMOOFDM Transmission System
5.2.1 WDM AMOOFDM Transmission System Models.....161
5.2.2 WDM Channel-Bit-Loading Algorithm.....163
5.2.3 Simulation Parameters.....167
5.3 Cross-Channel Complementary Modulation Format Mapping.....168
5.4 Adaptive-Modulation-Induced Reduction in WDM Impairments.....171
5.5 DML Frequency Chirp Compensation.....175
5.6 Conclusion.....177
References.....178

Chapter 6: Filter Concatenation Impairments Reduction using AMOOFDM

6.1 Introduction.....183

6.2 Transmission System Model.....184

6.3 Conventional OOFDM using Identical Modulation.....188

6.4 OOFDM with Adaptive Modulation 192

6.5 Conclusions.....199

References.....200

Chapter 7: Conclusions and Future Work

7.1 Conclusions.....203

7.2 Future Work.....207

References.....209

Appendix

A.1 Journals Publications.....211

A.2 Conference Publications.....212

CHAPTER 1

Introduction

1.1 Evolution of Optical Communications

Optical communications has evolved out of the necessity for a transmission medium with increased bandwidth capacity. The evolution of fibre optic data communications has stemmed from the telecommunications industry's need to multiplex voice channels for interconnecting call distribution centres. In the 1930s communications engineers became aware that the current infrastructure deployment strategy would not support the service demand of future telephone usage. At that time, each concurrent connection required an allocated physical connection [1]. Massive physical networks were implemented and could not possibly have supported future expansions. The infrastructure problem was not strictly a United States issue. Europeans were also dealing with demand-based expansion problems. Early multiplexing techniques included Frequency Division Multiplexing (FDM), which attained little success due to cost issues. In the late 1960s, researches into a digitization technique called "Pulse Code Modulation" (PCM) were performed. PCM utilizes 8000 8-bit samples per second, creating a 64 kb/s digital channel for carrying voice. Digitizing the audio channel made multiplexing easier. Early multiplexing techniques involved simple bit interleaving which proved ineffective for dense multiplexing operations [1]. At this

time the European and United States telecommunications industries diverged. The United States systems multiplexed 24×64 kb/s channels, and added some control overhead, to yield a 1.544 Mb/s channel, referred to as a "T1". Europe, on the other hand, multiplexed 30×64 kbps channels and 2 control channels to yield a 2.048 Mb/s channel, referred to as an "E1".

Interoperability between the two networks became expensive and complicated. As further multiplexing was performed on the trunk lines, distance and vendor differences led to extensive transmission problems. Clock signal skew and distance-related delays caused signal timings to be compromised. To resolve these problems, the Plesiochronous Digital Hierarchy (PDH) standard was adopted by the International Telecommunications Union (ITU) in the 1970s. PDH allowed successful interoperability of these communications networks, but problems with network scalability and the introduction of additional value-added services for fibre optic media made PDH obsolete. To add or remove a data channel at a point along the network, extensive network infrastructure was needed to provide for de-multiplexing, channel addition or removal, and re-multiplexing of the channel [1]. PDH does not provide for channel addition without de-multiplexing down to the channel hierarchy level of the channel to be added [1]. The court-ordered breakup of the American Telephone and Telegraph Company (AT&T) at the end of 1983 created the need for a new American National Standards Institute (ANSI) standard for the interoperability of the Regional Bell Operating Companies (RBOCs). Synchronous Optical Network (SONET), which allows for the addition or modification of a channel without extensive de-multiplexing, became the United States standard. SONET was designed to be compatible with the United States PDH systems. Having observed SONET's

integration benefits, the ITU adopted a Synchronous Digital Hierarchy (SDH) standard. SDH was designed to be interoperable with both the new U.S.-based SONET equipment and the large investment in European PDH equipment [1]. Both SONET and SDH operate by means of Synchronous Transfer Mode (STM) digital transmission. STM is a time division multiplexed technology with consistent framing every 125 microseconds [1].

The SONET standard supports synchronous framing for data and overhead octets. Several protocols can be run over SONET, such as Asynchronous Transfer Mode (ATM) or Internet Protocol (IP). When running over the optical transmission medium of single-mode fibre, SONET can be utilized as an interfacing protocol for long distance fibres. Typical SONET networks consist of Digital Cross Connects (DXC), Add/Drop Multiplexers (ADM), and Line Terminating Equipment (LTE). DXCs are the interconnecting structures of SONET network rings. These provide the Optical-Electronic-Optical (OEO) conversions, multiplexing and de-multiplexing functions, and programmable mapping for network interconnection and switching. The ADMs allow for the direct insertion and removal of individual services onto the same SONET connection [1]. This ability is an improvement over PDH which requires de-multiplexing down to the speed of the inserted channel. The Line Terminating Equipment allows users to interface with the SONET network. Such devices could be a telephone switch or network gateway. SONET also provides for network management and fault detection/traffic redirection. Cost effective ways of increasing optical network capacity could save corporations substantial capital.

Wavelength Division Multiplexing (WDM) entered into the picture and dramatically increased effective fibre optic bandwidth. WDM, and its Dense Wavelength Division

Multiplexing (DWDM) counterpart, operate under the premise of multiplexing different optical signals by wavelength on the same physical medium. This allows network engineers to increase network capacity without extensive and expensive infrastructure redesign. Similar in functionality to SONET's ADMs, but different in method, DWDM's Wavelength Cross Connects (WXCs) populate the DWDM ring topology. WXCs coexist with ADMs and can provide substantial benefit to the infrastructure when implemented together within the backbone. DWDMs provide wavelength conversion to allow for optical routing and cross-wavelength traffic redirection. SONET provides the network management and control protocol to ensure the integrity of the optical transmission. Thus, a hybrid of SONET and DWDM network infrastructures provides effective, efficient, and dependable backbone architecture. Missing from the DWDM/SONET hybrid is the concept of high-speed fully optical switching, also known as "photonic switching".

Currently, for network layer switching to occur, a conversion must be done from the optical domain to the electrical domain. The necessary routing and switching is performed electrically and the signal is converted back into the optical domain for transport. This process becomes increasingly difficult as the speed disparity of optical transport and electronic switch backplanes increases almost daily. As networks evolve towards all-optical networks, also known as "transparent networks", protocols must be developed to ensure manageability and controllability without inefficient OEO conversions [1].

1.2 Next-Generation PONs

The evolution of communications exhibits endless pursuit of larger bandwidths, longer distances and better quality of services. Nowadays, the high bandwidth demand arises from the rapid increase in IP traffic and newly emerging applications such as IP Television (IPTV), Video-on-Demand (VoD) and video surveillance. Such a continuous growth of bandwidth demand places great pressures on the network infrastructures at every scale, from core to metro, access networks and even in-building networks. Present core networks have an amazing transmission capacity of 100 Pbit/s-km, which is equivalent to 400 DVDs per second over 7000km transoceanic cable according to Alcatel-Lucent Bell Labs, Sep. 2009 [2]. For such application scenarios, sophisticated and expensive solutions are often employed to ensure the capacity, quality and resilience needed for the networks.

In access networks, however, the presence of legacy copper pairs/cables in the home forces operators to improve their capacities by using advanced techniques such as Digital Subscriber Line (DSL) and Hybrid Fibre Coaxial (HFC) [3]. The best achievable DSL performance is symmetric 100Mbit/s transmission over 300m copper cable by using the Very fast data rate DSL2 (VDSL2: G.933.2) technique. Nevertheless, the copper cable is approaching its fundamental physical limits. This imposes a bottleneck between the end user and core network, thus limits the end users' ability to make full use of the huge capacity available in the core networks. Not surprisingly, the penetration of optical fibre directly to the home, referred to as Fibre-to-the Home (FTTH) or more generally FTTx (x can be H for home, B for building, and C for curb), has undergone a rapid mass deployment to offer "future-proof" cost-

effective solutions for access networks. This is because optical fibre offers potentially high and upgradable bandwidth.

Several different types of bandwidth-hungry applications and services, including multimedia-oriented applications such as High-Definition Tele-Vision (HDTV), are rapidly being deployed in the access network. Hence, telecommunication operators are driven to upgrade their access networks to provide broader bandwidth for their subscribers.

The Full Service Access Network (FSAN) [4], an affiliation of network operators and telecom vendors, has completed its mission on the Giga-bit-capable Passive Optical Network (GPON). The International Telecommunication Union — Telecommunication Standardization Sector (ITU-T) G.984 series specifies various aspects of GPON, including the general architecture, the physical layer, the Transmission Convergence (TC) layer, and the GPON management and control [5], [6]. A typical GPON system provides 2.488 Gb/s of downstream bandwidth and 1.244 Gb/s of upstream bandwidth. GPON possesses the following characteristics [7]:

- GPON directly reflects the requirements of network operators because the GPON standardization is driven by operators through FSAN.
- As with ITU-T G.983 broadband PON (BPON), GPON provides high product inter-operability by standardizing a management interface, referred to as the Optical-network-unit Management and Control Interface (OMCI), between Optical Line Terminals (OLTs) and Optical Network Units/Terminals (ONUs/ONTs). We use ONUs and ONTs interchangeably in this article.

- GPON accommodates three layer-2 networks: Asynchronous Transport Mode (ATM) for voice, Ethernet for data, and proprietary encapsulation for video, thus enabling GPON with full-service support capability, including voice, Time Division Multiplexing (TDM), Ethernet, ATM, leased lines, and wireless extension.

- GPON defines the GPON Encapsulation Method (GEM) to achieve efficient packaging of user traffic, with frame segmentation to better provide Quality of Service (QoS) for delay-sensitive traffic such as voice and video applications.

- GPON supports Radio Frequency (RF) video transmission in the waveband from 1550 nm to 1560 nm.

Having turned over the work of GPON standard maintenance to ITU, FSAN is now studying the Next-Generation Access (NGA). The objective of NGA is to facilitate high bandwidth provision, large split ratio, and extended network reach. FSAN has planned two stages of NGA evolution: NGA1 and NGA2 [4]. NGA1 focuses on PON technologies that are compatible with GPON standards (ITU-T G.984 series) and compatible with the current Optical Distribution Network (ODN) as well. In contrast, NGA2 is a long-term solution with an entirely new optical network type. The objective of NGA2 is to provision an independent PON scheme, without access-network traffic.

To practically realize cost-effective and flexible NG-PONs, a large number of techniques have been investigated, among which Optical OFDM (OOFDM) has attracted great R&D interest and is considered as one of the most competitive "future-

proof" techniques for implementation in cost-sensitive PON application scenarios since OOFDM offers superior physical layer transmission performance, linear dispersion tolerance, spectral efficiency, efficient channel estimation/equalization [6]. In addition, the use of Directly Modulated Distributed Feedback (DFB) Lasers (DMLs) is also preferable due to their advantages including, for example, low cost, compactness, low power consumption, relatively small driving voltage and high optical output power [3], [8], [9].

1.3 Optical OFDM

For satisfying the rapidly increasing end-users' data traffic, the concept of OOFDM was first proposed in 2005 [7]. Soon afterwards, opportunities for employing OOFDM signals converted by DFB Lasers (DMLs) were theoretically explored over Multi-Mode Fibre (MMF)-based Local Area Networks (LANs) [8] and Single-Mode Fibre (SMF)-based optical access networks [9]. Since then, world-wide extensive investigations of the transmission performance of the OOFDM technique have been reported for application scenarios: long-haul core networks [10], [11], [12], LANs [13], [14] Metropolitan Area Networks (MANs), access networks [15], [16], and PONs [6], [13].

The reason for the popularity of the OOFDM technique in optical communications is that OOFDM has unique and inherent advantages including potential for providing a cost-effective technical solution by fully exploiting the rapid advances in modern Digital Signal Processing (DSP) technologies and considerable reduction in optical network complexity owing to its great resistance to dispersion impairments and efficient utilization of channel spectral characteristics. Apart from the above-

mentioned features, OOFDM is also capable of offering, in both the frequency and time domains, hybrid dynamic allocation of broad bandwidth among various end-users [17]. Such ability significantly enhances not only the flexibility of optical networks but also their compatibility with existing optical networks, allowing transparent support for legacy services. Another advantage of OOFDM is that the Power Spectral Density (PSD) can be chosen according to the subcarrier Signal-to-Noise Ratio (SNR) in order to obtain optimal performance (e.g., maximum data rate or minimum power consumption).

OOFDM can be enhanced in terms of transmission performance, flexibility and robustness by the so-called adaptive loading algorithms which include Power Loading (PL) [18], Bit Loading (BL) [19], or Bit-and-Power Loading (BPL) [14]. For a given transmission system, the optimum choice of the loading algorithm is a critical issue in the design of OOFDM systems. The BL when applied for OOFDM also called, for simplicity, Adaptively Modulated OOFDM (AMOOFDM) [8], [9], offers the functionality of adaptive data rate to adapt the channel conditions via adjusting the signal modulation format taken on each individual subcarrier. In the PL, a fixed signal modulation format is taken on all the subcarriers and the individual subcarrier powers are optimised according to the system frequency response. The BPL combines variable power and bit loading, where both the signal modulation format and power are adjustable for all subcarriers. The employment of adaptive loading algorithms significantly enhances not only the networks' flexibility but also their compatibility with existing PONs, allowing transparent support for legacy services.

Generally speaking, there are two variants of the OOFDM technique: Coherent OFDM (CO-OFDM) [8], [10], and Intensity-Modulation and Direct-Detection (IM/DD) OFDM [1], [7], [8], [9], [11]. In CO-OFDM systems, the detection of OOFDM signals is carried out using coherent mixing between the incoming signals and a Local Oscillator (LO), in conjunction with sophisticated post-detection DSPs. Such detection can achieve, in theory, unlimited dispersion tolerance at high spectral efficiency, thus giving rise to a large bit rate-distance product [20]. For achieving a specific transmission performance, CO-OFDM also requires an Optical SNR (OSNR) as low as 19dB for Quaternary Phase Shift Keying (QPSK)-encoded OOFDM signals [10]. CO-OFDM also has great susceptibility to the Polarization-Mode Dispersion (PMD) effect. Very recently, 448-Gb/s CO-OFDM signals with reduced guard interval using 16-QAM of subcarrier modulation through orthogonal band multiplexing was demonstrated [21].

However, CO-OFDM requires a low linewidth laser (<100 kHz [12]) due to local optical carrier at the receiver. In addition, CO-OFDM signals are sensitive to the phase noise and frequency offset effects. The requirements on narrow linewidth LOs, optical phase locked loops and polarization controllers considerably complicate CO-OFDM transceiver design. From the above analysis, it is clear that the expensive and bulky CO-OFDM transceivers restrict the use of the CO-OFDM technique in cost-sensitive networks: LANs, MANs/access networks and PONs.

In IM/DD OOFDM systems, OOFDM signals are usually transmitted with intensity-modulation and afterward received with square-law detection. Due to direct-detection, unwanted subcarrier Inter-Modulation (IMD) products occur close to the Direct-Current (DC) component upon photo-detection [22]. The OOFDM signal spectrum

can be allocated away from the unwanted IMD products by inserting a spectral guard band between the optical carrier and the OOFDM signal band. However, this reduces the spectral efficiency and significantly complicates the transceiver design. Compared to CO-OFDM, simple direct-detection significantly reduces the system complexity with its tolerance to fibre dispersion still being maintained to some extent. IM/DD OOFDM has been considered as one of the promising candidates for cost-sensitive access and metro applications [23].

Recently, using low-cost, off-the-shelf optoelectronic components, the world-first real-time end-to-end OOFDM transceivers over IM/DD MMF systems had been successfully demonstrated [24], and the highest ever 11.25 Gb/s over 25km SMF real-time end-to-end transmission performance had also been achieved [25], [26], indicating great potential of OOFDM for practical applications in PONs. As the commercially deployed FTTx networks are overwhelmingly based on IM/DD SMF links, IM/DD OOFDM is therefore a preferred choice for NG-PONs.

1.4 Challenges in MMF/SMF-based OOFDM systems

Generally speaking, OOFDM SMF-based MAN/access networks and MMF-based LANs have been identified as considerably cost-sensitive, under the increasing pressure to meet the surge in demand for offering cost-effective >10 Gb/s over 100km SMF and 300m MMF transmission, respectively. On the other hand, there is an increasing demand to reduce the cost in PONs and deliver heterogeneous services for multiple customers. OOFDM provides cost-effective technical solutions by fully exploiting the rapid advances in modern DSP technology, and considerable reduction

in optical network complexity owing to its great resistance to dispersion impairments and efficient utilization of channel spectral characteristics [8], [9]. OOFDM is also capable of offering, in both the frequency and time domains, hybrid dynamic allocation of broad bandwidth among various end-users [8], [9]. To further upgrade the present 1 Gb/s MMF and SMF links to 10 Gb/s and above, AMOOFDM has been proposed [8], [9].

With the increase of network data rate and transparency, the Reconfigurable Optical Add/Drop Multiplexer (ROADM) [27] filtering concatenation effect [28] has been considered to be one dominant drawback. The filter concatenation impairments degrade severely the maximum achievable transmission performance [28]. To address this problem, AMOOFDM can be introduced. It is expected that AMOOFDM can improve the tolerance to the filter concatenation impairments by using low signal modulation formats on subcarriers located on the filter side lobes experiencing degraded subcarrier SNRs. AMOOFDM can also enhance the transmission performance by combating a number of cascaded ROADM impairments including Loss Ripple (LR), Group Delay Ripple (GDR) and frequency dip.

Furthermore, while external modulation schemes, like Electro-Absorption Modulator (EAM) and Mach-Zehnder Modulator (MZM) are the dominant technologies, their usage is limited since they are expensive. This problem can be addressed by the utilization of DMLs because of their characteristics including potentially low cost, compact size, low power consumption and high optical output power when compared with other transmitter sources using the external modulation scheme [9]. As it is well known, however, DMLs are carrier density modulation via drive current, giving rise

to inherent and highly component-specific frequency chirp, i.e. a residual phase modulation accompanying the desired intensity-modulation. This results in broad spectrum that severely limits the maximum achievable transmission performance due to its interaction with fibre dispersion along the transmission. It is expected that the use of AMOOFDM enhances the tolerance to the DML frequency chirp effect by taking low-signal-modulation formats on the most distorted spectral regions caused by the frequency chirp and by reducing the signal Peak-to-Average Power Ratio (PAPR), which will result in a small electrical signal current variation and, thus, a low DML frequency chirp. It should be noted that one of the major problems associated with OOFDM is its large PAPR [29], [30]. The high PAPR of OOFDM makes the system performance sensitive to the nonlinearity of involved devices. Therefore, a reduced PAPR can significantly increase the maximum achievable transmission capacity compared to the conventional identical modulation OOFDM technique.

In all AMOOFDM works reported previously [8], [9], [15], [19], a Cyclic Prefix (CP) of a fixed time duration has been utilised to combat Differential Mode Delays (DMDs) occurring in MMFs and CDs associated with SMFs. A CP is essentially a copy of the last fraction of each time domain OFDM symbol and added to the front of the corresponding symbol in the transmitter. This treatment produces quasi-periodically extended time domain OFDM symbols, leading to the maintenance of the orthogonality between subcarriers within the symbol. If the CP length is larger than the expected maximum delay spread to be encountered, after transmitting through the channel, the dispersive effect is localized within the prefix region only. As the CP duration can be chosen by design, in principle, AMOOFDM can be made free from any arbitrary delay spread. From the above analysis, it is clear that, if a CP time

duration is smaller than the DMD (CD) associated with a MMF (SMF) link, the imperfectly compensated DMD (CD) effect limits considerably the maximum achievable transmission performance of the AMOOFDM signals [8], [9]. In addition, a small CP may also affect the subcarrier orthogonality, resulting in a significant increase in the minimum required SNR for a specific signal modulation format being taken on a subcarrier [31]. On the other hand, if the CP is longer than the DMD (CD) of a MMF (SMF) link, for a fixed signal sampling speed, the CP wastes a large percentage of the transmitted signal power, giving rise to a degraded effective signal SNR. Furthermore, an excessive length of CP also prevents us from making full use of the available link bandwidth. Therefore, it is greatly advantageous if the CP lengths can be made variable, according to the properties of different optical transmission links, to ensure that the selected CP lengths are just sufficiently long to compensate for DMDs (CDs) and other effects in MMF (SMF)-based links. For simplification, the adjustable CP length technique is referred to as Adaptive Cyclic Prefix (ACP) and the AMOOFDM modem using ACP as AMOOFDM-ACP.

As mentioned in section 1.3, to maximize the OOFDM performance and simultaneously improve the system flexibility and performance robustness, full use can be made of orthogonality among different subcarriers within an OOFDM symbol by applying the adaptive loading algorithms (BL, PL, and BPL) on each individual subcarrier, according to the SNR experienced by the subcarrier. Detailed explorations of the validity of the adaptive loading algorithms in arbitrary SMF/MMF-based transmission links are of great importance. As different MMF links reveal large variations in both the 3dB bandwidths and the system frequency responses, any explorations of the topic of interest over a specific MMF link are not adequate.

Consequently, statistical analysis of the performance of these three algorithms should be undertaken.

In NG-PONs using the WDM technique, where multiple signals at different wavelengths propagating in the fibre, three major nonlinear impairments are introduced: (i) Self-Phase Modulation (SPM), which refers to the self-induced phase shift experienced by an optical field during its propagation in optical fibres; (ii) Cross-Phase Modulation (XPM), which induces nonlinear phase shift to an optical field which is dependent not only on the intensity of that wave but also on the intensity of a co-propagating field at a different wavelength; and (iii) Four-Wave Mixing (FWM), where the intensity dependence of refractive index causes the signals to interfere and generate refractive index gratings, and, such gratings interact with the signals and produce new frequencies. The aforementioned nonlinear impairments severely limit the maximum achievable WDM transmission performance. To address this problem, the exploration of multichannel AMOOFDM transmission performance is essential. It is expected that multichannel AMOOFDM will enhance the system performance through reducing the aforementioned WDM nonlinear impairments.

1.5 Major Achievements of the Dissertation Research

To deal with the challenges outlined above, the dissertation research work has been carried out to investigate the transmission performance of OOFDM signals over IM/DD MMF and SMF systems using DMLs as intensity modulators.

The work in this thesis has resulted in the publication of 15 papers in world-leading professional journals (4 papers) and international/national conferences (11 papers) including major international conferences such as OFC.

These papers have been completed by the author of this thesis and form the major contents of this dissertation work. Apart from that, the author also authored/co-authored another 2 journals papers and 2 conference papers, which have been published by collaborating with other people in the same research group in Bangor University, and also with people from the AIT research centre (where the author has been working over the last 9 months as a Senior Research Scientist), as well as people from the Technological Educational Institute (TEI) of Lamia (see Appendix A1: List of Publications). Even these co-authored papers are related to this thesis [25], [26], [30]; they are, however, not discussed in detail here.

The major achievements of my research work are summarized as follows:

- ***Improved transmission performance of AMOOFDM signals over directly modulated DFB laser-based IM/DD links using ACP for LANs and PONs*** [32], [33], [34].

  The impact of ACP on the transmission performance of AMOOFDM is explored thoroughly in DML-based, IM/DD links using MMFs/SMFs for

LANs and PONs. Three ACP mechanisms are identified, each of which can, depending upon the link properties, affect significantly the AMOOFDM transmission performance. In comparison with AMOOFDM having a typical fixed CP duration of 25%, AMOOFDM with ACP can not only improve the transmission capacity by a factor of >2 (>1.3) for >1000m MMFs (<80km SMFs) but also relax considerably the requirement on the DFB bandwidths. This work is detailed in Chapter 3.

- ***Performance comparisons of OOFDM adaptive loading algorithms in statistically constructed worst-case MMF links and SMF-based transmission systems for LANs and PONs, respectively*** [35], [36], [37], [38], [39].

  Detailed investigations of the effectiveness of three widely adopted OOFDM adaptive loading algorithms, including PL, BL (similar to AMOOFDM), and BPL, are undertaken, over 1000 statistically constructed worst-case MMF links and over <100km SMF links for LANs and PONs, respectively, without incorporating inline optical amplification and CD compensation. It is shown that, firstly, for both worst-case and normal-case MMF links of <300m, in comparison with the most sophisticated BPL algorithm, the simplest PL algorithm is sufficiently effective in escalating the OOFDM MMF links performance to its maximum potential. The effectiveness of the PL algorithm can be further improved when a large number of OOFDM subcarriers are utilized. On the other hand, for relatively long MMF links with their 3dB bandwidths being much less than the transmitted OOFDM signal spectrum, the sophisticated BPL algorithm has to be adopted. Secondly, for the case when SMF links are employed, it is shown that over a range of transmission

distances and launched optical powers of practical interest for PONs; the simplest PL algorithm is effective in escalating the OOFDM SMF link performance to its maximum potential compared to the sophisticated BPL algorithm. This work is detailed in Chapter 4.

- ***Adaptive-modulation-enabled WDM impairment reduction in multi-channel OOFDM transmission systems for NG-PONs*** [40], [41].

  The transmission performance of multichannel AMOOFDM signals is investigated numerically, in optical-amplification-free and CD-compensation-free IM/DD systems directly incorporating DMLs. It is shown that AMOOFDM not only significantly reduces the nonlinear WDM impairments induced by the effects of XPM and FWM but also effectively compensates for the DML-induced frequency chirp effect. In comparison with conventional OOFDM, which uses an identical signal modulation format across all the subcarriers, AMOOFDM improves the maximum achievable signal transmission capacity of a central WDM channel by a factor of 1.3 and 3.6 for 40km and 80km Standard SMFs (SSMFs), respectively, with the corresponding dynamic input optical power ranges being extended by approximately 5dB. In addition, AMOOFDM also causes the occurrence of cross-channel complementary modulation format mapping among various WDM channels, leading to considerably improved transmission capacities for all individual WDM channels. This work is detailed in Chapter 5.

- ***Significant reduction in filter concatenation impairments by AMOOFDM signals for transparent Metro/Regional networks*** [42], [43], [44].

  The impact of AMOOFDM on the filter concatenation effect is investigated, in IM/DD transparent Metro/Regional network systems incorporating cascaded ROADMs. The considered ROADMs are based on different optical filters including Fibre-Bragg Grating (FBG), Chebyshev, thin film and a Wavelength-Blocker (WB)/Wavelength Selective Switch (WSS) devices. It is shown that, in comparison with conventional identical OOFDM modulation, AMOOFDM can improve the system performance by a factor of up to 60%. The utilization of AMOOFDM can also significantly enhance the network tolerance to filter LRs, GDRs, and frequency dips. This work is detailed in Chapter 6.

It should also be noted that the author of the thesis has also involved in Bangor University's experimental demonstration of end-to-end real-time OOFDM systems [25], [26], [37], in terms of the following aspects: a) the provision of an in-depth understanding of various physical mechanisms limiting the maximum achievable system performance. Such understanding is critical for system design and optimization; b) conducting some experimental research activities with researchers from Bangor University and National Tyndall Institute (NTI), University College Cork (UCC). It has been planned that after the PhD dissertation research, the author will be undertaking experimental research to verify the feasibility of using the novel techniques proposed in the thesis in practical systems through collaborations between Bangor University and AIT research centre.

1.6 Thesis Structure

The thesis comprises 7 chapters in total. Chapter 2 presents review of fundamental concepts and Chapters 3 to 7 detail research results. These Chapters are outlined as following:

Chapter 2: This Chapter presents fundamental principles and evolution of PONs. General concepts with emphasis in access network architectures are first overviewed. As promising access network technologies, IEEE EPON and ITU Broadband PON (BPON)/GPON together with the corresponding standards (802.3ah and G.983/G.984) are discussed, followed by the review of 10G-EPON standard 802.3av and the current status of ITU XG-PON and NG-PON2 standard draft G.987. Various promising architectures for NG-PON2 such as WDM-PONs and OOFDM PONs are discussed in terms of their principles as well as strengthens and limitations. To gain a better understanding of OOFDM PONs, Chapter 2 also deals with the fundamental principles of OFDM, OOFDM and AMOOFDM. Discussions are also made of two main variants of OOFDM including CO-OOFDM and IM/DD OOFDM, and their advantages and drawbacks are highlighted.

Chapter 3: Based on the AMOOFDM technique described in Chapter 1, to further increase the transmission performance of AMOOFDM, as well as its flexibility and robustness, a novel ACP-AMOOFDM modem is presented and explored thoroughly in Chapter 3 over optical-amplification-free and CD-compensation-free DML-based, IM/DD links using Double-Side Band (DSB) signals for both MMFs and SMFs. This Chapter identifies three ACP mechanisms, each of which can, depending upon the link properties, affect significantly the AMOOFDM transmission performance. The

Chapter shows how the ACP-AMOOFDM modem can effectively improve the tolerance to the imperfectly compensated DMD (CD) effect over MMFs (SMFs) and the imperfect subcarrier orthogonality, which limit considerably the maximum achievable transmission performance of the AMOOFDM signals, and also reveals why ACP-AMOOFDM can relax the requirement on the DFB bandwidth.

Chapter 4: State-of-the-art DSP solutions for further improving the OOFDM Bit-Error-Rate (BER) include the adoption of adaptive loading algorithms which constitute of BL (i.e. the aforementioned AMOOFDM on Chapters 2-3), PL and BPL. Based on the developed OOFDM DML-based IM/DD model of Chapter 3, the adaptive loading algorithms are investigated in this Chapter to maximize the OOFDM performance and simultaneously improve the system flexibility and performance robustness over 1000 statistically constructed worst-case MMF links and over <100km SMF links for LANs and PONs, respectively. This Chapter details the benefits and drawback associated on each adaptive loading algorithm, but more importantly addresses the optimum choice of an adaptive loading algorithm for a specific transmission link.

Chapter 5: Following the adaptive loading algorithms investigations of Chapter 5 for PONs, Chapter 5 takes a step further to explore the transmission performance of multichannel AMOOFDM (BL in OOFDM) signals, in optical-amplification-free and CD-compensation-free IM/DD NG-PONs incorporating DMLs. This Chapter is dedicated to address the impact of nonlinear WDM impairments such as XPM and FWM, and explore a simple and effective approach to reduce such impairments in

NG-PONs. This Chapter also reveals that AMOOFDM can be considered as a PAPR mitigation technique for NG-PONs.

Chapter 6: Having explored thoroughly in all previous Chapters the impact of AMOOFDM in LANs and access networks, in Chapter 6 the AMOOFDM is investigated over IM/DD transparent Metro/Regional network systems incorporating cascaded ROADMs to reduce the filter concatenation effect. The considered ROADMs are based on different optical filters including FBG, Chebyshev, thin film and WB/WSS devices. This Chapter represents the importance and effectiveness of using AMOOFDM in ROADM-based networks.

Finally, Chapter 7 summarizes the Thesis and suggests future research work.

References

[1] "Special Report: Next Generation Internet Applications", 2005 http://www.photuris.com/future-internet-applications-3.html

[2] Available at http://www.alcatel-lucent.com.

[3] J. L. Wei, "Intensity Modulation of Optical OFDM Signals Using Low-Cost Semiconductor Laser Devices for Next-Generation PONs", PhD Thesis Manuscript, Bangor University, 2010.

[4] IDATE Consulting & Research, "FTTx 2010," 2010. Available at www.idate.org

[5] D. Qian, J. Hu, J. Yu, and et al., "Experimental Demonstration of a Novel OFDM-A Based 10Gb/s PON Architecture", European Conference on Optical Communication, 2007, pp. 1–2.

[6] J. Zhang, N. Ansari, Y. Luo, F. Effenberger, and F. Ye, "Next-Generation PONs: A Performance Investigation of Candidate Architectures for Next-Generation Access Stage 1", IEEE Communications Magazine, Topics in Optical Communications, 2009.

[7] N. E. Jolley, H. Kee, R. Rickard, J. Tang, and K. Cordina, "Generation and propagation of a 1550 nm 10 Gb/s optical orthogonal frequency division multiplexed signal over 1000 m of multimode fibre using a directly modulated DFB", Proc. OFC/NFOEC, (OSA, 2005), Paper OFP3.

[8] J. M. Tang, P. M. Lane, and K. A. Shore, "High-speed transmission of adaptively modulated optical OFDM signals over multimode fibres using directly modulated DFBs", IEEE J. Lightwave. Technol., vol. 24, no. 1, pp. 429–441, Jan. 2006.

[9] J. M. Tang and K. A. Shore, "30 Gb/s signal transmission over 40-km directly modulated DFB-laser-based single-mode-fibre links without optical amplification and

dispersion compensation", IEEE J. Lightwave Technol., vol.24, no. 6, pp. 2318-2327, 2006.

[10] H. Masuda, E. Yamazaki, A. Sano, T. Yoshimatsu, T. Kobayashi, E. Yoshida, Y. Miyamoto, S. Matsuoka, Y. Takatori, M. Mizoguchi, K. Okada, K. Hagimoto, T. Yamada, and S. Kamei, "13.5-Tb/s (135×111-Gb/s/ch) no-guard-interval coherent OFDM transmission over 6248km using SNR maximized second-order DRA in the extended L-band", Optical Fiber Communication/National Fiber Optic Engineers Conference (OFC/NFOEC), (OSA, 2009), Paper PDPB5.

[11] B. J. C. Schmidt, Z. Zan, L. B. Du, and A. J. Lowery, "100 Gbit/s transmission using single-band direct-detection optical OFDM", Optical Fiber Communication/National Fiber Optic Engineers Conference (OFC/NFOEC), (OSA, 2009), Paper PDPC3.

[12] Y. Ma, Q. Yang, Y. Tang, S. Chen, and W. Shieh, "1-Tb/s single-channel coherent optical OFDM transmission over 600-km SSMF fibre with subwavelength bandwidth access", Opt. Express, vol. 17, no. 11, pp. 9421–9427, May 2009.

[13] D. Qian, N. Cvijetic, J. Hu, and T. Wang, "108 Gb/s OFDMA-PON with polarization multiplexing and direct-detection", Optical Fiber Communication/National Fiber Optic Engineers Conference (OFC/NFOEC), (OSA, 2009), Paper PDPD5.

[14] H. Yang, S. C. J. Lee, E. Tangdiongga, F. Breyer, S. Randel, and A. M. J. Koonen, "40-Gb/s transmission over 100m graded-index plastic optical fibre based on discrete multitone modulation", Optical Fiber Communication/National Fiber Optic Engineers Conference (OFC/NFOEC), (OSA, 2009), Paper PDPD8.

[15] T. Duong, N. Genay, P. Chanclou, B. Charbonnier, A. Pizzinat, and R. Brenot, "Experimental demonstration of 10 Gbit/s for upstream transmission by remote

modulation of 1 GHz RSOA using Adaptively Modulated Optical OFDM for WDM PON single fiber architecture", European Conference on Optical Communication (ECOC), (Brussels, Belgium, 2008), PD paper Th.3.F.1.

[16] C.-W. Chow, C.-H. Yeh, C.-H. Wang, F.-Y. Shih, C.-L. Pan and S. Chi, "WDM extended reach passive optical networks using OFDM-QAM", Opt. Express, vol. 16, no.16, pp. 12096–12101, Jul. 2008.

[17] D. Qian, J. Hu, P. N. Ji, and T. Wang, "10-Gb/s OFDMA-PON for delivery of heterogeneous services", Optical Fiber Communication/National Fiber Optic Engineers Conference (OFC/NFOEC), (OSA, 2008), Paper OWH4.

[18] C. S. Park and K. B. Lee, "Transmit power allocation for BER performance improvement in multicarrier systems", IEEE Trans. Commun., vol. 52, no. 10, pp. 1658–1663, Oct. 2004.

[19] Y. George and O. Amrani, "Bit loading algorithms for OFDM", in Proc. ISIT, Chicago, IL, 2004, p. 391.

[20] S. L. Jansen, A. A. Amin, H. Takahashi, I. Morita, and H. Tanaka, "132.2-Gb/s PDM-8QAM-OFDM transmission at 4-b/s/Hz spectral efficiency", IEEE Photon. Technol. Lett., vol. 21, no. 12, pp. 802–804, Jan. 2006.

[21] X. L. Chandrasekhar, S. B. Z. Winzer, P. J. Gnauck, A. H. Peckham, "448-Gb/s Reduced-Guard-Interval CO-OFDM Transmission Over 2000 km of Ultra-Large-Area Fiber and Five 80-GHz-Grid ROADMs", IEEE J. Lightwave Technol., vol. 29, pp. 483, 2011

[22] A. J. Lowery, "Amplified-spontaneous noise limit of optical OFDM Lightwave systems", Opt. Express, vol.16, no.2, pp.860-865, Jan. 2008.

[23] D. Qian, N. Cvijetic, J. Hu, and T. Wang, "Optical OFDM transmission in metro/access networks," presented at the Optical Fiber Communication

Conf./National Fiber Optic Engineers Conf. (OFC/NFOEC), San Diego, CA, Mar. 2009, Paper OMV1.

[24] G. P. Giddings, X. Q. Jin, H. H. Kee, X. L. Yang, and J. M. Tang, "Real-time implementation of optical OFDM transmitters and receivers for practical end-to-end optical transmission systems", Electron. Lett., vol. 45, no.15, pp. 800-802, 2009.

[25] G. P. Giddings, X. Q. Jin, E. Hugues-Salas, E. Giacoumidis, J. L. Wei, and J. M. Tang, "Experimental demonstration of a record high 11.25Gb/s real-time optical OFDM transceiver supporting 25km SMF end-to-end transmission in simple IMDD systems", Opt. Express, vol. 18, no.6, pp. 5541 – 5555, 2010.

[26] R. P. Giddings, X. Q. Jin, E. Hugues-Salas, E. Giacoumidis, J. M. Tang, "Experimental demonstration of record high 11.25Gb/s real-time end-to-end optical OFDM transceivers for PONs", IEEE Future Network & MobileSummit, Florence, Italy, June 2010.

[27] A. Tsokanos, C. Mouchos, E. Giacoumidis, J. M. Tang, "A Scalable Model for the Performance Evaluation of ROADMs with Generic Switching Capabilities", Journal of Networks (JNW), vol. 5, no. 10, pp. 1215-1220, 2010.

[28] Y. Tang and W. Shieh, "Filter concatenation impact on 107-Gb/s coherent optical OFDM system", OptoElectronics and Communications Conference (OECC), pp. 1-2, 2009.

[29] Y. Tang and W. Shieh, "Transmission of 100 Gbit/s WDM Systems with Coherent Optical OFDM", Electronics Letters, vol. 44, pp. 588-589, 2008.

[30] E. Giacoumidis, A. Kavatzikidis, I. Cano, M. C. Santos, J. M. Tang, J. Prat, and I. Tomkos, "Mitigation techniques for peak-to-average power ratio and optical beat interference in OFDMA-PONs", IEEE International Conference on Transparent Optical Networks (ICTON), Stockholm, Sweden, June 2011 (Invited Paper).

[31] L. Hanzo, S. X. Ng, T. Keller and W. Webb, *Quadrature Amplitude Modulation: From Basics to Adaptive Trellis- Coded, Turbo-Equalised and Space-Time Coded OFDM, CDMA and MC-CDMA Systems* (Wiley, 2004).

[32] E. Giacoumidis, J. L. Wei, X. Q. Jin, and J. M. Tang, "Improved transmission performance of adaptively modulated optical OFDM signals over directly modulated DFB laser-based IMDD links using adaptive cyclic prefix", Optics Express, vol. 16, pp. 9480-9494, 2008.

[33] E. Giacoumidis, J. L. Wei, and J. M. Tang, "Influence of Adaptive Cyclic Prefix on the Transmission Performance of Adaptively Modulated Optical OFDM Signals over Directly Modulated Laser-Based IMDD Links", Semiconductor & Integrated Optoelectronics (SIOE), Cardiff, Wales, April 2008.

[34] E. Giacoumidis, and J. M. Tang, "Improved transmission performance of Adaptively Modulated Optical OFDM signals over MMFs using adaptive cyclic prefix", IEEE OptoElectronics and Communications Conference and the Australian Conference on Optical Fiber Technology (OECC/ACOFT), Sydney Convention & Exhibition Centre, Australia, July 2008.

[35] E. Giacoumidis, X. Q. Jin, A. Tsokanos, and J. M. Tang, "Statistical Performance Comparisons of Optical OFDM Adaptive Loading Algorithms in Multimode Fiber-Based Transmission Systems", IEEE Journal of Photonics, vol. 2, pp. 1051 – 1059, 2010.

[36] E. Giacoumidis and J. M. Tang, "Statistical Investigations of Optical OFDM Adaptive Loading Algorithm over 1000 Worst-Case MMFs", Optical Fiber Communication Conference and Exposition (OFC) and the National Fiber Optic Engineers Conference (NFOEC), Los Angeles, California, USA, March 2011, Paper JWA089.

[37] J. M. Tang, R. P. Giddings, X. Q. Jin, J. L. Wei, X. Zheng, E. Giacoumidis, et al., "Real-Time Optical OFDM Transceivers for PON Applications", Optical Fiber Communication Conference and Exposition (OFC) and the National Fiber Optic Engineers Conference (NFOEC), Los Angeles, California, USA, March 2011 (Invited) Paper OTuK3.

[38] E. Giacoumidis, J. L. Wei, A. Tsokanos, A. Kavatzikidis, E. Hugues-Salas, J. M. Tang, and I. Tomkos, "Performance Optimization of Adaptive Loading Algorithms for SMF-Based Optical OFDM Transceivers", IEEE 16th European Conference on Networks and Optical Communications (NOC) and 6th Conference on Optical Cabling and Infrastructure (OC&I), Northumbria University, Newcastle upon Tyne, UK, July 2011.

[39] E. Giacoumidis, J. L. Wei, E. Hugues Salas, J. M. Tang, and I. Tomkos, "Adaptive Loading Algorithms Evaluations for IMDD SMF System-Based Optical OFDM Transceivers", Progress In Electromagnetics Research Symposium (PIERS), Suzhou, China, Sep 2011.

[40] E. Giacoumidis, J. L. Wei, X. L. Yang, A. Tsokanos, and J. M. Tang, "Adaptive Modulation-Enabled WDM Impairment Reduction in Multi-Channel Optical OFDM Transmission Systems for Next Generation PONs", IEEE Journal of Photonics, vol. 2, pp. 130 – 140, 2010.

[41] E. Giacoumidis, J. L. Wei, and J. M. Tang, "Adaptive Modulation Induced WDM Impairment Reduction in Optical OFDM PONs", IEEE Future Network & MobileSummit, Florence, Italy, June 2010.

[42] E. Giacoumidis, I. Tomkos, and J. M. Tang, "Adaptive Modulation-Induced Reduction in Filter Concatenation Impairment for Optical OFDM Metro/Regional4Systems", J. Opt. Commun. Netw, vol. 3, pp. 587 – 593, 2011.

[43] E. Giacoumidis, I. Tomkos, and J. M. Tang, "Filter Concatenation Impairments Reduction by Adaptively Modulated Optical OFDM Signals for Metro/Regional Networks", IEEE Future Network & MobileSummit, Warsaw, Poland, June 2011.

[44] E. Giacoumidis, I. Tomkos, and J. M. Tang, "Group Delay Ripple Reduction in Cascaded ROADMs by Adaptively Modulated Optical OFDM signals for Metro/Regional Networks", IEEE 16th European Conference on Networks and Optical Communications (NOC) and 6th Conference on Optical Cabling and Infrastructure (OC&I), Northumbria University, Newcastle upon Tyne, UK, July 2011.

CHAPTER 2

Reviews of High-Speed Optical Networks and OOFDM

Contents

2.1 Introduction.....32

2.2 General Network Concepts.....33

2.3 Access Network Technology Evaluations.....36

2.3.1 Digital Subscriber Line (DSL).....37

2.3.2 Hybrid Fibre Coaxial (HFC).....39

2.4 Passive Optical Networks (PONs).....41

2.5 PON Evolution.....45

2.6 NG-PON Evolution.....47

2.6.1 NG-PON General Requirements.....50

2.6.2 Service Requirements.....51

2.6.3 General Requirements on Architecture/Infrastructure.....52

2.7 Promising Technologies for NG-PONs.....53

2.7.1 WDM-PON.....53

2.7.2 Hybrid WDM/TDM-PON.....56

2.8 Optical OFDM technology for Next Generation Optical Networks

2.8.1 OFDM concept and description.....57

2.8.1.1 Bit Encoding.....59

2.8.1.2 IFFT/FFT.....60

2.8.1.3 Cyclic Prefix.....64

2.8.1.4 Serialization.....65

2.8.1.5 DAC/ADC.....66

2.8.1.6 Pilot-Assisted Channel Estimation and Equalization.....68
2.8.1.7 Synchronization.....69
2.8.2 Optical OFDM.....71
2.8.2.1 Coherent OOFDM (CO-OFDM) Transceivers.....71
2.8.2.2 IM/DD OOFDM Transceivers.....73
2.8.2.3 Comparison between CO-OFDM and IM/DD OOFDM.....75
2.8.2.4 AMOOFDM.....77
2.9 OOFDM PON.....80
2.10 Conclusion.....81
References.....83

2.1 Introduction

This century has been identified as the century of information, since our life is being "bombarded" from various types of information such as Internet, Television, Telephony, etc. Moreover, the requirement for installation of telecommunication networks with high capacity to convey legacy real-time traffic with guaranteed Quality of Services (QoS) has become the primary target. This is the main driving force for the current rapid development of high-speed networks in the telecommunication industry. Specifically, the following aspects have played key roles in advancing high-speed networks [1], [2]:

1) The rapid growths of Internet and world-wide-web (www) in accordance with the number of Internet users and the available bandwidth per user.
2) Cost reduction. Such reduction derives from the combination of the advances in telecommunication technology and the collapse of service provider's monopoly.
3) The occurrence of various types of telecommunications traffic. Major telecommunications companies such as MCI, WorldCom and AT&T have reported a significant annual growth of information data while the corresponding annual voice data growth is considerably low to only about 10% [3].
4) The rapid development of wide-zone technologies such as DSL and cable modems [2] can offer signal capacities of a few decades of Mb/s per user. Furthermore, wireless communications are, without a doubt, an important cost-effective and high-speed solution. Unfortunately, in comparison to optical fibres, wireless communications have much smaller bandwidth, greater network latency and less robustness. Moreover, the optical bandwidth of an

optical fibre around the 1.5μm region is up to about 25 THz, implying that much higher bandwidths would be available compared to radio frequencies [1], [4], [5], [6].

From the operator's point of view, cost-effectiveness is the highest priority for the deployment of next generation high-speed networks such as NG-PONs, i.e., keeping the cost per bit as low as possible. Generally speaking, the main costs involved are the costs of the electro-optic converters and other specific components. It is also greatly beneficial if the cost can be shared between subscribers as many as possible.

2.2 General Network Concepts

In this section, a detailed analysis of the current available networks is presented. According to the geographical coverage, telecommunication networks are consisting of three major sub-network types as shown in Figure 2.1.

- *Core Networks*: They are the central part of a telecom network, providing various services to customers who are connected by access networks. Core/backbone network provides paths for exchange of information between different sub-networks. For enterprise networks serving one organization, the term backbone is used very often, while for service providers, the term core network is more often used. The distances indicated below are illustrative and vary widely based on the location of the network, for example, the link length in Europe (typically from 200km – 1000km) is shorter than those in North America (few thousand of kilometres).

- *Metro/Regional Sub-networks:* They are the part of a network that lies within a large city or region. This network collects traffic over a limited area and passes it on to the core networks. The metro network consists of metro core network, which connects a group of central offices (COs) within a city or region.
- *Access networks*: They are the part of a communication network which connects subscribers to their immediate service providers. Contrasted to the core network, an access network may be further divided into a feeder plant and a distribution network, and drop plant or edge network. The main drive behind novel access technology developments is to mitigate from slow traditional telephone lines (64 kb/s) to high signal capacity links, in order to bring high-speed connections for clients while keeping a cost-effective deployment.

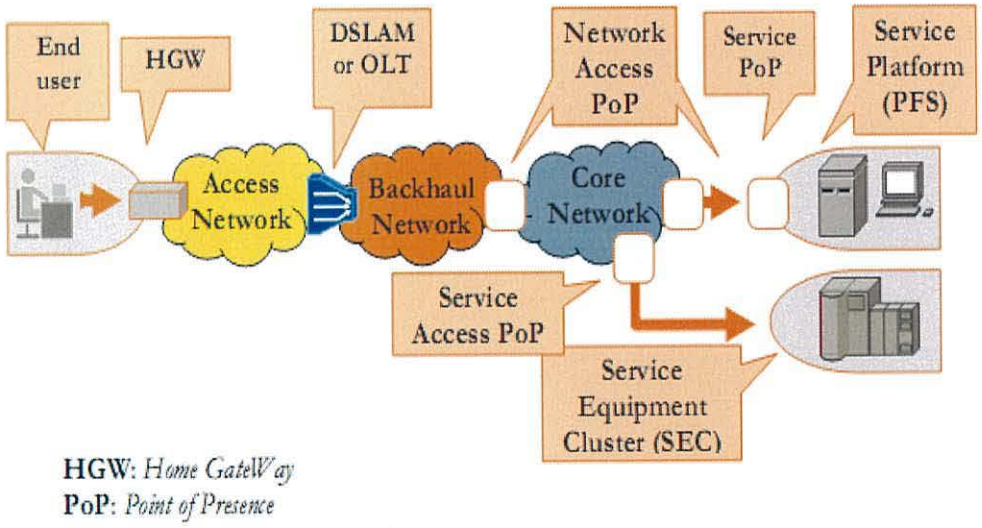

Figure 2.1: Network hierarchy [7].

As the main focus of the thesis is access networks, to gain a deep understanding of such networks, Figure 2.2 is illustrated, which consists of three principal parts including CO, local convergence points and network interface units [7].

- *Central Office (CO):* It is a communication switching facility in a public network. The CO is responsible for transmitting/receiving data from/to subscribers and inserting/extracting these data to a core/metro network. A CO can serve on the order of thousands of subscribers.
- *Local Convergence Points:* Its main target is to distribute downstream signals to the customers or concentrate individual customer information flows and transmit the aggregated traffic upstream to the CO. A remote node can also be placed, where a terminal or computer is located apart from the main network. It may refer to a branch office or a travelling user with a laptop. Access to a company LAN is typically made via an Internet or dial-up connection.
- *Network Interface Units:* They are located at the customer site and enable the users to connect to the network. Depending on the technology used for the access network, this unit may have various names such as ONU or ONT.

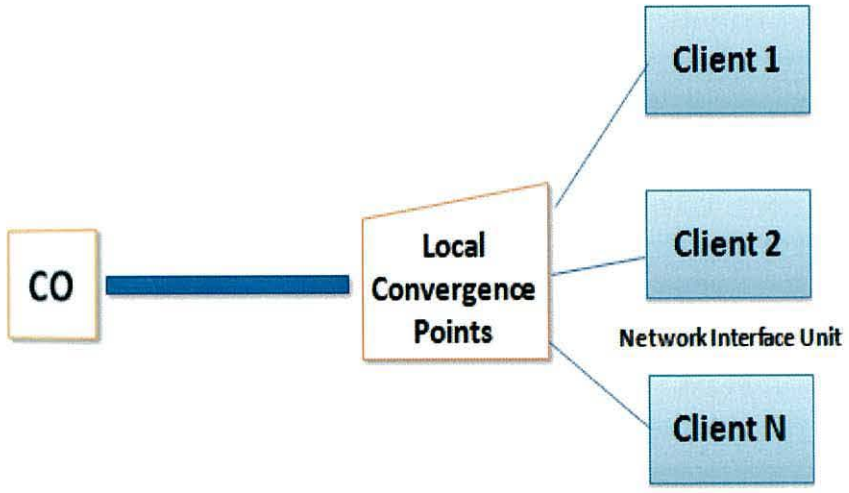

Figure 2.2: Access Network scheme.

With the exponentially increasing end-users' demands for broadband services and the availability of enormous transmission capacities in core networks, the existing access networks have become critical bottlenecks for fully utilizing the core network bandwidths to provide end-users with desired services. To address such a challenge, this thesis is focusing on exploring various techniques for enabling cost-effective, flexible and "future proof" next generation high-speed access networks.

2.3 Access Network Technology Evaluations

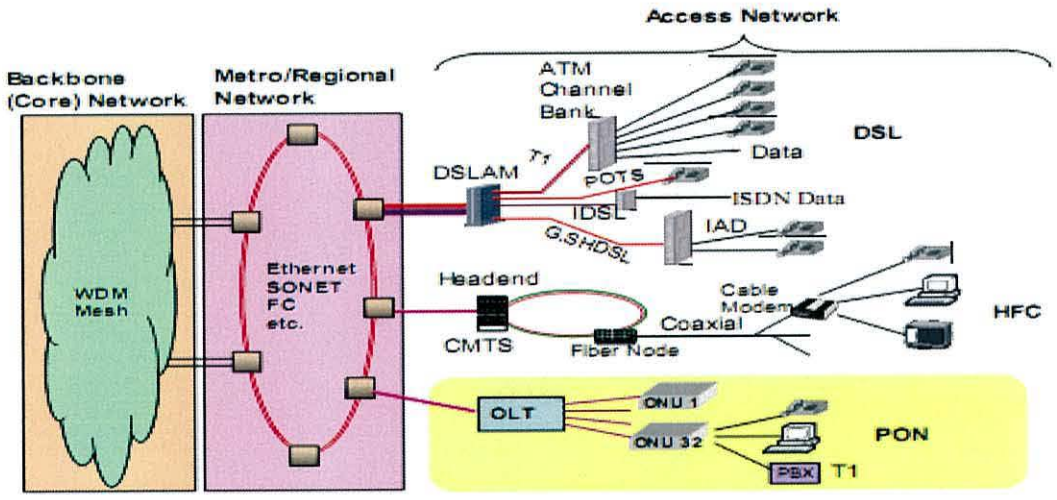

Figure 2.3: Generic structure of a modern telecommunication network [8].

Initially, the most widely deployed transmission media in access networks are twisted-pair copper cables that have been used for telephone lines for more than 100 years. Over a long history, analogue voice services were transmitted over a 4 kHz bandwidth; the voice grade bandwidth was also used to transmit digital Internet signals, however, the best data rate available was only 56 kb/s [8]. In order to deal with the growing bandwidth requirement, solutions including new modulation

techniques for legacy copper cables and deployment of optical fibre were proposed. This leads to the coexistence of today's major wired access network technologies including DSL, HFC, and PONs.

2.3.1 Digital Subscriber Line (DSL)

DSL is a family of technologies that provides digital data transmission over wires of a local telephone network. For the telecommunications marketing, the term DSL is widely understood to mean Asymmetric DSL (ADSL), the most commonly installed technical variety of DSL. The data throughput of consumer DSL services typically ranges from 256 kb/s to 20 Mb/s in the direction to the costumer (downstream), depending on DSL technology, link conditions and service-level implementation. In ADSL, the data throughput in the upstream direction (i.e. in the direction to the service provider) is lower, hence, the designation of *asymmetric* service.

The commercial success of DSL and similar technologies largely reflects the advances made in electronics over the past few decades that have increased performance and reduced costs even while digging trenches in the ground for new cables (copper or fibre optic) remains expensive. Several factors contributed to the popularity of DSL technology:

- Until the late 1990s, the cost of digital signal processors for DSL was prohibitive. All types employ highly complex DSP algorithms to overcome the inherent limitations of the existing twisted pair wires.
- A DSL connection can be deployed over existing cables. Such deployment, even including equipment, is much cheaper than installing a new, high-bandwidth fibre-optic cable over the same route and distance.

- In the case of ADSL, competition in Internet access caused subscription fees to drop significantly over the years, thus making ADSL more economical than dial up access.

A typical set-up and connection is showed in Figure 2.4.

1. The DSL transceiver performs a self-test.
2. The DSL transceiver checks the connection between the DSL transceiver and the computer.
3. The DSL transceiver then attempts to synchronize with the DSL-Access Multiplexer (DSLAM).

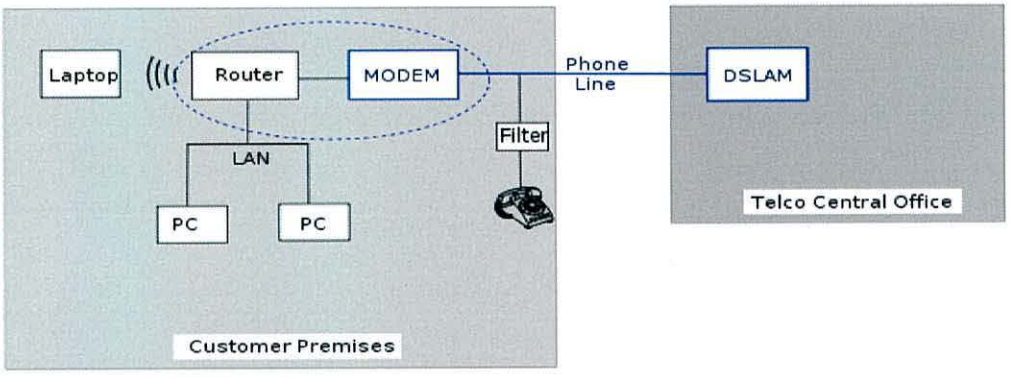

Figure 2.4: Schematic diagram for the DSL Connection [9], [10], [11].

The customer end of the connection consists of a terminal adaptor or in other words "DSL modem", as shown in Figure 2.5.

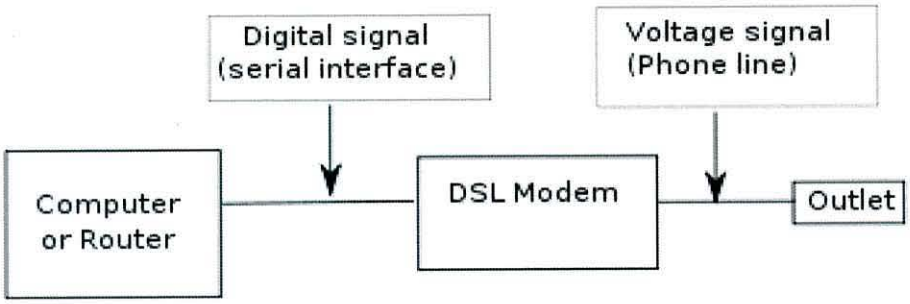

Figure 2.5: DSL modem schematic [9], [10], [11].

In some DSL variations such as High-Bit-Rate DSL (HDSL), the terminal adapter connects directly to the computer via a serial interface, using protocols such as Ethernet. [9], [10], [11]

2.3.2 Hybrid Fibre Coaxial (HFC)

HFC implements a hybrid optical fibre and coaxial copper cable architecture to deliver CATV, voice, and Internet services to end users and transmit aggregated data from users. As shown in Figure 2.3, cable modems at individual households are connected to a Cable Modem Termination System (CMTS) at a head-end office.

Downstream data signals from head ends are transmitted to remote fibre node where they are converted back to the RF domain and broadcast to individual cable modems through the coaxial cable plant. Each individual cable modem recognizes its data by the Identifier (ID) embedded in downstream data. Customer data are multiplexed using TDM. The CMTS acts a Media Access Control (MAC) master which assigns upstream time slots for each cable modem. The downstream and upstream signals are transmitted simultaneously through the same cable between the home and the remote fibre node through FDM. The coaxial cable has a useable frequency range of up to 1

GHz, which is much broader than that corresponding to twisted pairs. Broadcast TV signals normally occupy a frequency band from 50 MHz to 500 MHz or 750 MHz. Each CATV channel occupies a 6 MHz or 8 MHz bandwidth, and 5 MHz to 42 MHz are used for upstream data transmission.

DOCSIS Versions	Downstream		Upstream	
	Modulation format	Max. data rate	Modulation format	Max. data rate
1.0	64-QAM,256-QAM	38Mb/s	QPSK, 16-QAM	10Mb/s
2.0		40Mb/s	QPSK, 16-QAM, 32-QAM, 64-QAM, 128-QAM	30Mb/s
3.0		160Mb/s		120Mb/s

Table 2.1: Summary of DOCSIS modulation format and data rate.

Data over Cable Service Interface Specification (DOCSIS) specifies the modulation formats for both HFC downstream and upstream transmissions. Table 2.1 lists the available downstream/upstream modulation formats, and the corresponding maximum achievable data rate specified by the three versions of DOCSIS. However, such a large bandwidth is shared by hundreds of households per fibre node, the per user bandwidth is only 3 Mb/s to 8 Mb/s downstream and 200 kb/s to 800 kb/s upstream.

2.4 Passive Optical Networks (PONs)

PON systems are promising solutions for access networks. A typical TDM-PON system is illustrated in Figure 2.6, which consists of an Optical Line Terminal (OLT) located in the CO, multiple ONUs, a fibre link and a Power Splitter (PS). The section between OLT and ONUs is referred to as Optical Distribution Network (ODN).

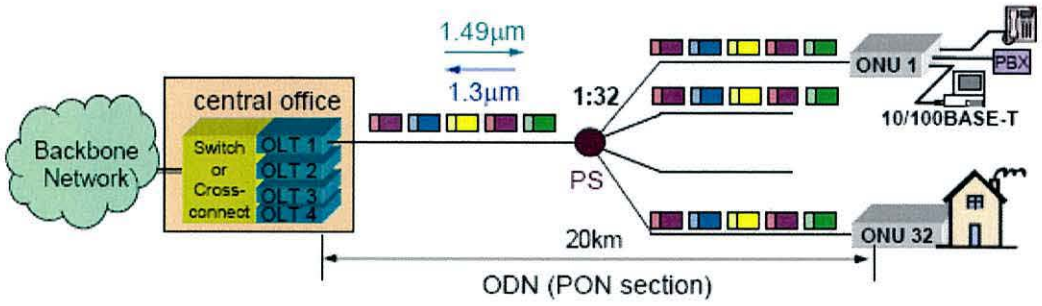

Figure 2.6: A typical TDM-PON architecture [8].

Multiple OLTs in the CO are interconnected with a backbone switch or cross-connect, which provides the cross-connection and switching among different OLTs, ONUs and the backbone network. OLT also provides the translation between the backbone signal formats (e.g. SONET/SDH, or Ethernet) and ODN [8]. Similar to the OLT, the ONU performs translation between ODN signal formats and signal formats used by the end user equipments. The PON architecture generally supports 32 ONUs with a maximum covered transmission distance of usually 10 to 20km [8]. The bidirectional transmission of downstream and upstream signals is realized by Coarse WDM (CWDM) with 1.49μm and 1.3μm wavelengths being assigned to downstream and upstream, respectively.

The PON is a shared network due to the use of the Point-to-Multi-Point (P2MP) topology. In downstream, the OLT broadcasts signals to all ONUs by interleaving frames destined for different ONUs as a continuous stream. Each ONU extracts its own frames based on its own ID. In upstream, since there is only one receiver in the OLT and a single feeder fibre, ONUs take turns to send their data in a TDM schedule. Moreover, when an ONU is not sending data, it has to turn off its laser to avoid interference with other ONUs' upstream transmission. As a result, the use of burst mode ONU transmitters and OLT receivers is critical in PON.

The PON has numerous advantages which are summarized as followings:

- PON eliminates the need for active optoelectronic and electronic devices located in the cabinet in the harsh outside environment. No power consumption equipment leads to low maintenance cost and better system performance stability.
- The system cost including OLT devices, fibre installation and maintenance is shared by a number of customers. This makes PONs cost-effective.
- PON offers topological flexibility by placing the PS anywhere along the fibre link.

Compared to DSL and HFC, PON eliminates the bandwidth "bottleneck" caused by legacy copper cables and thus offers much larger capacity and reach to each individual user. PON systems have been deployed all over the world. In a global view, Asia Pacific gains the most success in PONs. Take Japan for example, the number of PON subscribers has exceeded that of DSL and HFC, thus PON becomes the dominant access network technology [12]. The success of PON relies on not only

the strong user demand of broadband services but also government and regulatory support and competitive market. In Japan, the government set up "e-Japan" plan targeting 30 million PON subscribers by 2010. South Korea government established the "e-Korea" (2002) plan and later "U-Korea" (ubiquitous integration) to build broadband convergence networks as core networks for U-Korea. China also announced to deploy the world's largest PON deployment [13]. It is envisioned that PON will experience a golden time in the next a few decades.

Standardized PON has several variants including ITU-T Asynchronous Transfer Mode (ATM) PON (APON)/Broadband PON (BPON)/GPON and IEEE EPON, as well as NGPONs including IEEE 10G-EPON, ITU-T XG-PON and NG-PON2.

Table 2.2 presents the basic advantages and disadvantages of PON systems. Nowadays, TDM-PON systems are usually designed reaching a maximum signal capacity of 2.5 Gb/s and over maximum transmission distances of up to 20km, with a typical split ratio of 1:32, (standard ITU G.984).

Advantages	Disadvantages
Distanced junctions are non-active	The same bandwidth has to be shared among distinct users
Passive network	The optical power is divided within output ports, degrading the maximum achievable transmission performance
Easy video and data transmission	The same optical signal is received among all ONUs, reducing the network security level
System architecture includes the less possible number of transceivers	The available bandwidth for uploading is not broadcast (less bandwidth from the entire point-to-point)
Low life-circle	Requirement of complicated algorithms for the reception of upstream signals
Short optical fibre length	Complicated transceivers (optical power, possibility for burst mode)

Table 2.2: Advantages and disadvantages of PON systems.

Table 2.3 shows the basic characteristics and specifications for the basic prototype PON networks (ITU-T G.983, G.803.2ah, and G. 984, corresponding to the BPON [14], the EPON [15] and the GPON [16], respectively). The next section reviews the evolution of PON technologies.

	BPON	EPON	GPON
Model	ITU G.983	IEEE 803ah	ITU G.984
Packet Size	53 bits (48 of payload and 5 of overload)	1518 bits	Variable size from 53 to 1518 bits
Maximum Bandwidth	Downstream propagation: 1.2 Gb/s Upstream propagation: 622 Mb/s	Symmetrical propagation until: up to 1.25 Gb/s	Downstream propagation = from 1.25 Gb/s up to 2.5 Gb/s. Upstream propagation = 155 Mb/s, 622 Mb/s, 1.25 Gb/s or 2.5 Gb/s
Wavelength	Downstream propagation = 1480 nm up to 1500 nm Upstream propagation = 1260 nm up to 1360 nm	Downstream propagation =1550 nm Upstream propagation = 1310 nm	Downstream propagation = 1480 nm up to 1500 nm Upstream propagation =1260 nm up to 1360 nm
Maximum Transmission Distance	20 km	20 km	60 km
Propagation	ATM	Ethernet	ATM, Ethernet, TDM
Voice	TDM	VoIP or TDM	TDM
Video	1550 nm overlay	1550 nm overlay	RF or IP
Maximum Number of Wavelengths	32	16	64

Table 2.3: Basic characteristics of PON systems.

2.5 PON Evolution

Figure 2.7 illustrates the evolution of PON technologies together with reference to actual deployments in major global areas. The first generation of PON is ITU-T APON (G.983.1) supporting a data rate from a few tens of Mb/s to hundreds of Mb/s, which gained small scale deployment. Later, ITU-T specified BPON (G.983.3) and further GPON (G.984) which supports data rate of up to 2.5 Gb/s thus were widely deployed over the world. In the meantime, to compete with GPON, IEEE also specified EPON standard (802.3ah) offering 1 Gb/s data rate. To deliver ever increasing broadband services, both ITU-T and IEEE started NG-PON standardization work of 10G-EPON (802.3av) and XG-PON (X is the Rome sign of 10: G.987),

respectively, targeting 10Gb/s data rate. Moreover, ITU-T also considers long-term solutions with even higher data rates, which is referred to NG-PON2. PON standards cover the data link layer (MAC layer) and Physical (PHY) layer of the Open System Interconnect (OSI) reference model.

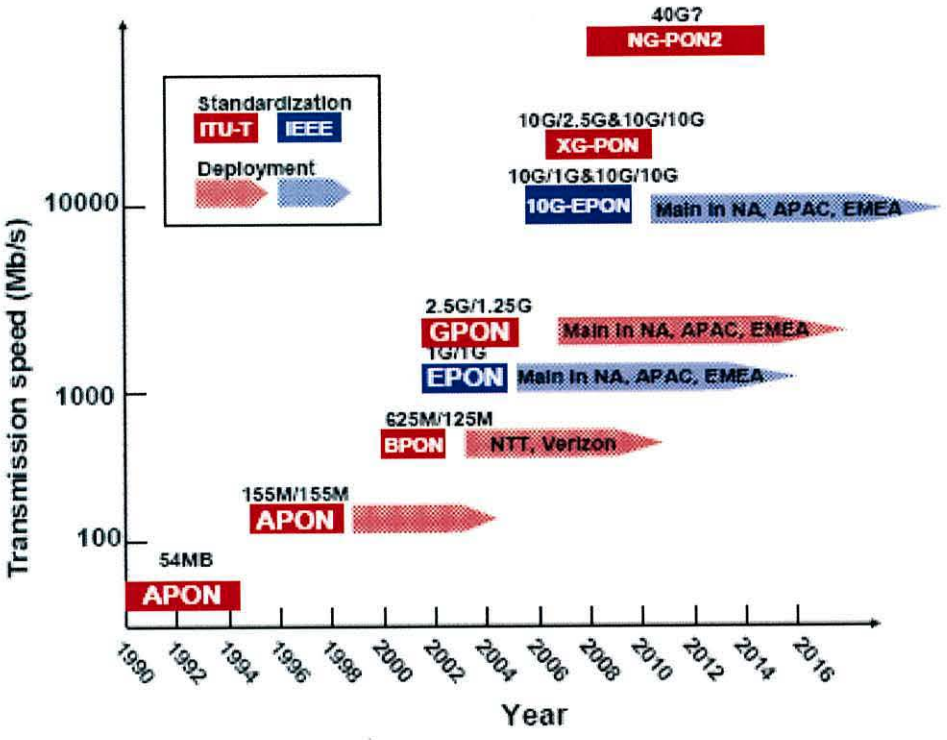

Figure 2.7: History of PON development. [17]

2.6 NG-PONs Evolution

Nowadays, the evolution of "bandwidth-hungry-services" is being witnessed. In all these examples the bandwidth is significantly increased for application involving both customers and businesses reaching the limits of GPON (ITU-T G.984 series) and the 1G-EPON (IEEE 802.3ah). For upgrade of the GPON to higher data rates discussions have been made at FSAN-ITU and the IEEE working groups. In particular, IEEE 802.3 working group is responsible for standardization of NG-PONs, specifically within 802.3av [18], [19]. This IEEE NG-PONs is focusing on 10G-EPON (signal capacity reaching 10 Gb/s), as an evolution upgrade from the 1G-EPON. The target for upstream is 1 Gb/s and 10 Gb/s according to the target application and the mature electronics involved. As an alternative solution for NG-PONs, the FSAN-ITU which includes telecommunication operators and equipment manufacturers such as Orange, Huawei, AT&T, Alcatel-Lucent, Nokia-Siemens and Ericsson, have revealed two categories of NG-PONs. The NG-PON1 and the NG-PON2:

- NG-PON 1 is considered as the first evolution of the GPON. For this solution, the FSAN group is working to develop an NG-PON standard that supports coexistence with current GPON on the same ODN. The coexistence feature enables seamless upgrade of individual customers to future PON on an ODN without disrupting services of other users on the PON. Generally, the coexistence between NG-PON1 and current GPON is enabled through a wavelength band plan enhancements specified in Recommendation G.984.5. The design architecture of NG-PON1 is focused on 10GPON (also known as XG-PON where X is taken as the Latin sign for 10). The mid-term evolution NG-PON1 includes several technology options such as XG-PON; multiple

G/XG-PONs overlay in the fibre though the use of WDM (i.e. WDM1 as specified in G.984.5). Indeed, XG-PON is capable of supporting sign capacity up to 10 Gb/s, at least for the downstream transmission. Different from IEEE focus, the possible signal capacity for the upstream transmission for XG-PON system could be 2.5- and 10 Gb/s depending on the target application as well cost and feasibility of necessary devices. The asymmetric 10G/2.5G-PON is referred to as "XG-PON1" and asymmetric 10G/10G-PON is referred to as "XG-PON2". A typical example of NG-PON1 architecture is illustrated on Figure 2.8.

- For the design architecture regarding NG-PON2, it is considered to be a solution of GPON. The process of NG-PON2 is in parallel to NG-PON1. It is assumed that a completely new outside plant could be deployed for this solution so that there is no need for the requirement in terms of coexistence with current GPON on the same ODN. The working group related to NG-PON2 is investigating alternative solutions such as novel technology of WDM-PON, hybrid WDM/TDM-PON and OFDM. Moreover, the data rates should be up to 40 Gb/s for future access networks. Finally, extensive component research and development is required, in order to make NG-PON2 an innovative and cost-effective solution.

In Figure 2.9, the NG-PON technology evolution pathway is presented, which was proposed by FSAN.

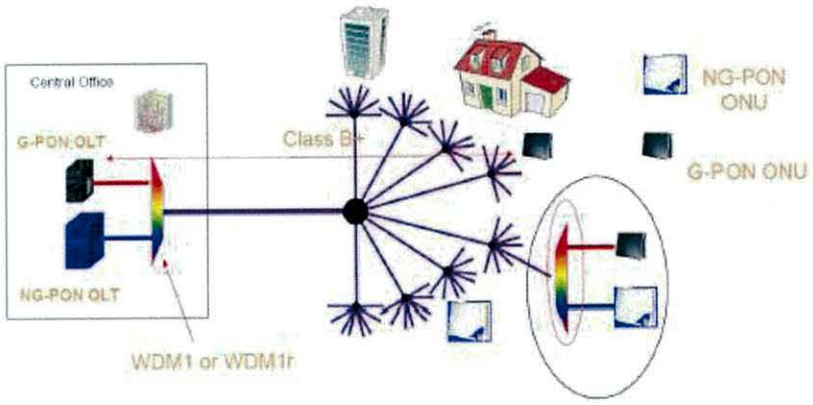

Figure 2.8: An example of migration GPON to XG-PON1 [7].

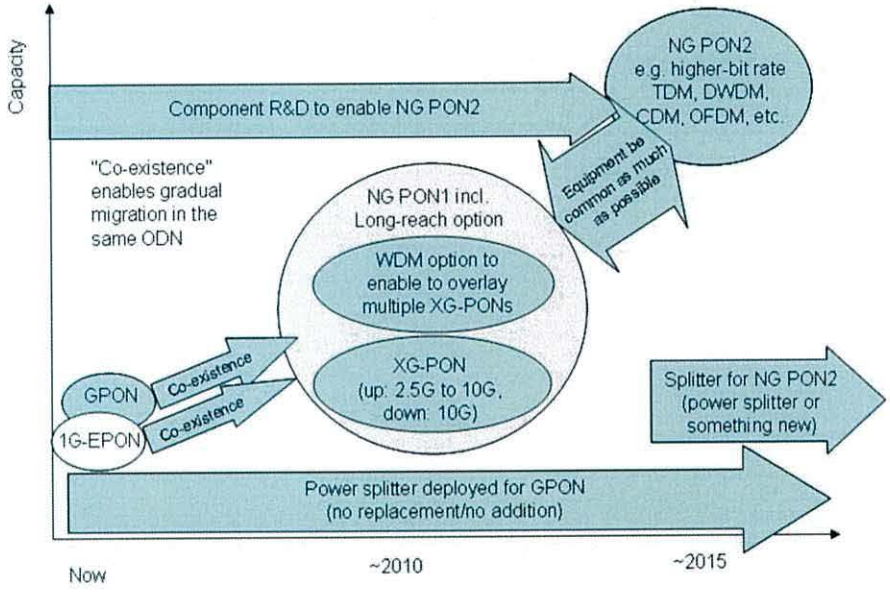

Figure 2.9: NG-PON technology pathway (source from FSAN) [20].

2.6.1 NG-PON General Requirements

The general requirements are analysed here for both NG-PON1 and NG-PON2. For NG-PON1 the specifications as established by FSAN [21] are shown below:

- Increase bandwidth
- Increase the reach and split ratio
- Respect similar ODN
- Respect wavelength allocation for GPON
- Keep changes of Transmission Convergence (TC)/MAC to minimum
- Enable co-existence with GPON
- Reuse equipment management system
- Assure simple reconfiguration of network and services
- Cost reduction

IEEE working group has set similar goals for NG-PONs. Nevertheless, the main focus is on achieving 10 Gb/s over TDM EPON technology.

In comparison with NG-PON1, NG-PON2 does not have to respect the similar ODN as current GPON. NG-PON2 system would not be restricted to G.984.5 enhancement band operation and optical characteristics of embedded ODN components. Consequently, the technology candidates for NG-PON2 will be increased in comparison to NG-PON1. NG-PON2 systems may be focused on a long-term

deployment and hence consider the use of "emerging" technologies, such as colourless WDM-PON, OFDM, (Code Division Multiplexing) CDM and 40 Gb/s TDM. [7]

2.6.2 Service Requirements

NG-PON systems are required to fully support various services from residential subscribers, professional customers to mobile backhaul due to its high quality of service and high rate capability. Furthermore, since telecommunication networks are evolving from the traditional circuit, NG-PON systems should also support legacy narrow band services, such as Plain Old Telephony Service (POTS)/Integrated Services Digital Network (ISDN) and T1/E1. Regarding business applications, G-PON systems provide Ethernet services such as point-to-point, multipoint-to-multipoint, and routed-multipoint Ethernet Virtual Connection (EVC) services. NG-PON systems shall also support accurate frequency/phase/time synchronisation for the mobile backhaul application.

Some examples of NG-PON 1 services are presented in Table 2.4:

No	Service	
1	Telephony	VoIP
2		POTS emulation
3		ISDN emulation
4	TV (real time)	IPTV Digital TV broadcasting
5	Leased line	T1/E1
6	High-speed internet access	
7	Mobile backhaul	
8	L2 VPN services	
9	IP services	

Table 2.4: Examples of NG-PON1 services.

2.6.3 General Requirements on Architecture/Infrastructure

NG-PON should be also able to support business applications, as well as cell site backhaul – FTTCell.

In terms of infrastructure, the NG-PON physical layer shall support the following requirements:

Signal bit rate: The main target of NG-PON is the increase of the signal bit rate, so as the network can provide significantly more bandwidth per user. Groups from both IEEE and FSAN-ITU PON have agreed that 10 Gb/s is the next step, at least for the downstream transmission bit rate, for the first evolution of PON systems.

Loss budget: This is defined as the insertion loss between ONU and OLT. According to FSAN study report, NG-PONs are expected to operate over "class C" (between 28.5 dB and 31 dB) at a *BER* of 10^{-12} without involving any optical post or pre-

amplifiers. For future studies, the loss budget will be extended to operate over "class C++" (>32 dB), including optical post/pre-amplifiers.

Splitting ratio: In a similar way to GPON, which supports 1:32 or 1:64 of split ratio, the minimum requirement for NG-PON1 should be 1:64 of split ratio. In addition, for some applications such as office consolidation, a higher split ratio will be needed and therefore, external amplifiers should be used.

Transmission distance: Since most of operators have constructed their ODN infrastructures with 20km transmission distances, for the case of NG-PON1 this should be the minimum required distance as well. Moreover, at least 60km logical reach is required for NG-PON1.

Co-existence: The NG-PON1 systems have to respect the similar ODN as current GPON which allows a smooth migration between GPON and NG-PON.

2.7 Promising Technologies for NG-PON2

As ITU-T NG-PON2 would not be restricted to the G.984.5 enhancement wavelength band operation and optical characteristics of current ODN system components, it offers opportunity to consider novel technologies. In this section, the potential technologies including WDM-PON and hybrid WDM/TDM-PON are discussed.

2.7.1 WDM-PON

It is agreed that PONs based on pure TDM cannot cope with the requirements of future networks with aggregated bandwidth and the allowable power budget. A promising solution to address this challenge is to adopt WDM-PON. A general

WDM-PON architecture is shown in Figure 2.10. In the downstream direction, OLT uses a mixed wavelength laser array or a Multi-Frequency Laser (MFL) to generate a downstream signal, which is multiplexed to form a WDM signal. An Arrayed Wavelength Grating (AWG) is adopted in the remote node to route the wavelengths to a proper ONU. While in the upstream direction, each ONU uses an individual wavelength to carry its signal and these ONU signals are aggregated into a WDM signal after passing through the AWG. The OLT receiver de-multiplexes the received WDM signal using filters and a photo-detector array. A Band Splitter (BS) or circulator is used in both the OLT and ONU to separate the upstream/downstream signals so that bidirectional transmission is performed.

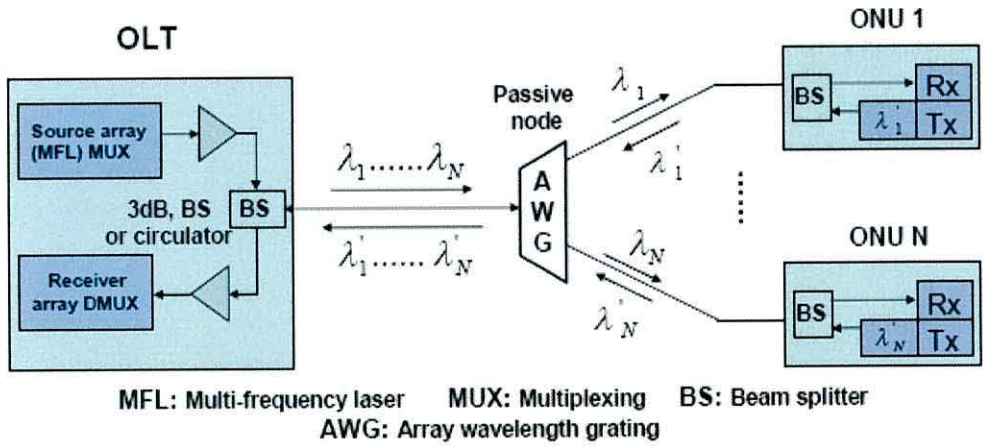

Figure 2.10: A general WDM-PON architecture [17].

WDM-PONs exhibit advantages in many aspects:

- As ONU is assigned with a dedicated wavelength, which provides a tremendous bandwidth and excellent privacy to an individual customer.
- WDM-PONs preserve a passive ODN thus maintenance cost is low.

- Each ONU and OLT has an independent P2P connection thus largely simplifies the MAC layer (no P2MP media access control) and enables the achievement of system protocol transparency.

- Easy to scale. Each wavelength can operate at different data rate and run different protocol so an easy pay-as-you-grow upgrade is possible.

The disadvantages of WDM-PONs are the high cost of WDM components and wavelength specific ONU. This may limit its wide practical applications. Therefore, colourless ONU operation is highly preferred to minimize stock and wavelength management problems and thus the cost for operators. Generally, there are three colourless ONU solutions:

1) Use of a tunable laser and an external modulator in each ONU [22], [23], the approach offers, in the long-term, the highest performance for WDM-PON by allowing the highest potential number of channels. It makes economic sense because of the availability of commercial tunable semiconductor lasers at prices of potentially a few ten U.S. dollars.

2) Broadband Light Source (BLS) from CO and optical injection-locked Laser Diode (LD) such as F-P LDs [24], [25] and VCSELs [22] in each ONU. The BLS can be from Amplified Spontaneous Emission (ASE) generated by an EDFA [26] or Light-Emitting Diodes (LEDs) [27] which is sliced by the AWG and each sliced carrier is fed to an individual ONU for upstream transmission. Although BLS and injection locking F-P have already been commercialized, this scheme is not easy to provide higher

data rates beyond 1 Gb/s due to high power loss in spectrum slicing and the intrinsic noise of F-P LDs [22].

3) Reuse the downstream wavelength. In this approach, the downstream optical signal received by ONU is split into two: one is detected by the ONU receiver and the other is re-modulated by the upstream signal and sent back to OLT receiver. The modulators in ONU can be injection-locked F-Ps [28], EAMs [29], or RSOA/SOA intensity modulators [28], [29]. The major challenge for this scheme is the crosstalk effect between the residual downstream signal and the re-modulated upstream signal. Moreover, Rayleigh Backscattering (RB) noise is also an issue if bi-directional transmission is used in the WDM-PON.

As NG-PONs based on WDM architecture operate at high bit rates (>10 Gb/s) per wavelength, the tunable ONU and the downstream wavelength reuse approaches discussed above seem survive easily in NG-PONs.

2.7.2 Hybrid WDM/TDM-PON

In real cases, WDM-PONs are often combined with TDM-PONs to increase transmission distance, power split ratio and system scalability. A typical example of such hybrid WDM/TDM-PONs is the WDM Ethernet PON (WE-PON), developed by Electronics and Telecommunications Research Institute, Korea (ETRI) and Korea Telecom [30], by combining WDM PON and EPON together.

The hybrid WDM/TDM PON possesses the advantages of both WDM-PON and TDM PON, and also effectively eliminates the limitations of pure TDM-PON. With the increase of number of customers and transmission distance enabled by

WDM/TDM-PON, the number of COs can also be reduced leading to considerable power and maintenance cost savings. Similar to WDM-PONs, colourless ONUs are also preferred in WDM/TDM-PONs.

2.8 Optical OFDM technology for Next Generation Optical Networks

2.8.1 OFDM concept

OFDM began to be considered for practical wireless applications in the mid–1980s. Cimini of Bell Labs [31] published analytical and seminal experimental results on the performance of OFDM modems in mobile communications channels. In 1987, Lassalle and Alard [32] considered the use of OFDM for radio broadcasting. OFDM is now widely applied in radio systems for digital audio and video broadcasts, WLAN, Wireless Wide Area Networks (WWAN, Worldwide Interoperability for Microwave Access, or WiMAX), and wire-line access systems via ADSL.

The concept of OFDM, essentially identical to Coded OFDM (COFDM) and Discrete Multi-Tone modulation (DMT), is a FDM scheme utilized as a digital Multi-Carrier Modulation (MCM) method. The basic idea of OFDM is quite simple [33], [34], [35], [36], [37]: the signal data are transmitted on a number of different frequencies via a large number of closely-spaced orthogonal data-carrying subcarriers, as depicted in Figure 2.11, and as a result the symbol period is much longer than that for a serial

system with the same net data rate. In Figure 2.11 the narrowband overlapped subcarriers are illustrated in both the frequency and time domains.

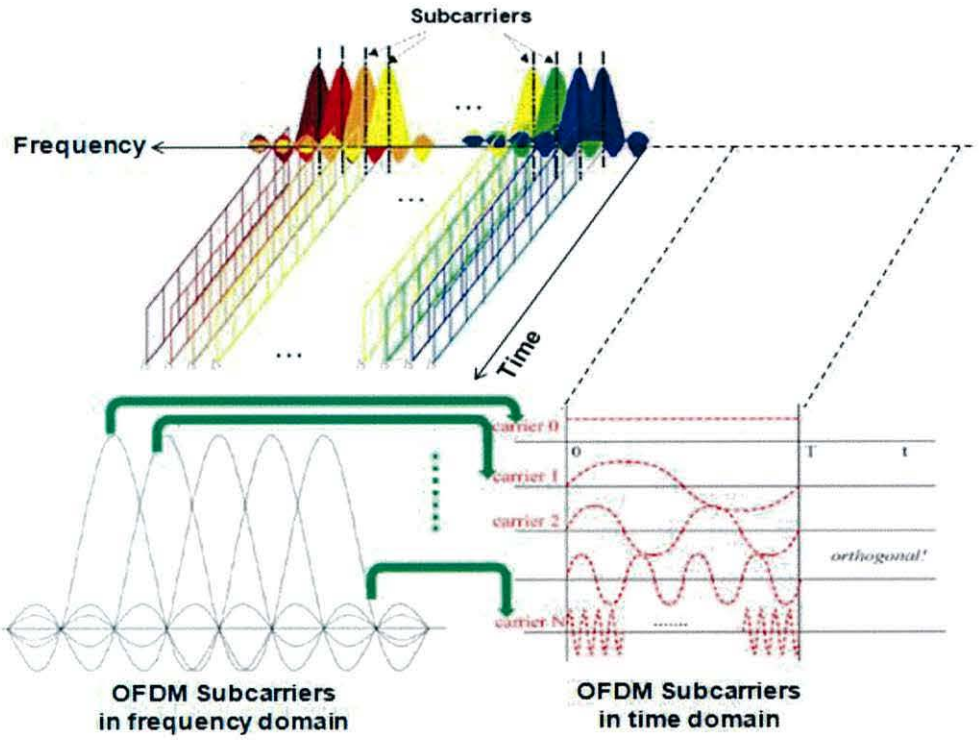

Figure 2.11: Schematic diagram of OFDM technology using subcarriers.

Compared to FDM, OFDM precisely chooses the inter-subcarrier frequency spacing to ensure orthogonality between different subcarriers, as shown in Figure 2.12, so that the demodulator for one subcarrier is independent on others even though spectral overlap occurs between subcarriers. Clearly, OFDM offers significant enhancement in spectral efficiency (at least 50%) compared to FDM. On the other hand, thanks to the advances of DSP technologies, the modulation/multiplexing and de-modulation/de-multiplexing in the OFDM system can be realized by efficient Inverse Fast Fourier Transform (IFFT) and FFT, respectively. Therefore, in comparison with FDM, the OFDM systems are relatively simple, as a large number of modulators, receiver filters

and demodulators required in the FDM system are not necessary. Moreover, OFDM also has an advantage of combating frequency-selective fading effect caused by wireline or wireless channels.

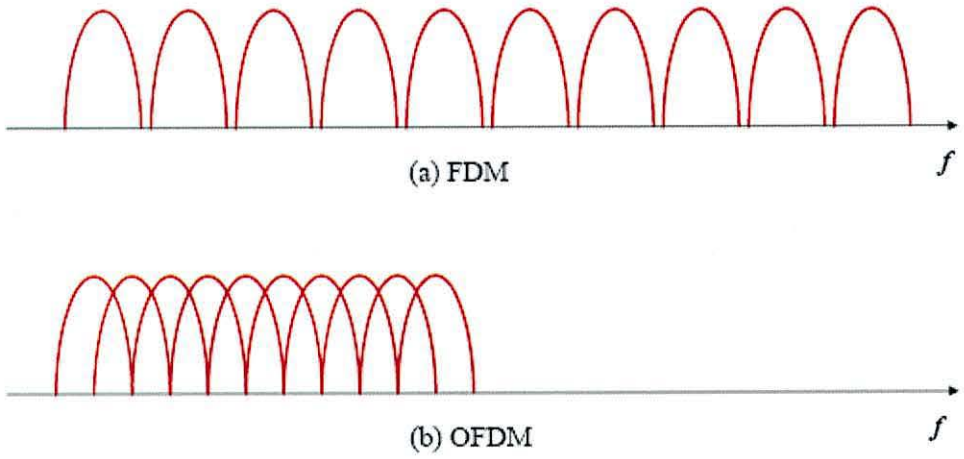

Figure 2.12: Spectra of (a) FDM, and (b) OFDM.

2.8.1.1 Bit Encoding

The bit encoding process is to map information bits into signal constellation points, as illustrated in Figure 2.13. A serial bit stream is first converted into parallel bits corresponding to each subcarrier, and then encoded to complex numbers using a specific signal modulation format. Figure 2.13 (b) shows two examples of multi-level modulation formats namely Quadrature PSK (QPSK) and 16-QAM. In QPSK the signal phase is keyed between four possible values (45°, 135°, 225° and 315°) to represent the four possible variations of a two-bit set. Whilst in 16-QAM both the signal amplitude and phase are keyed to represent the 16 possible variations of a 4 $(\log_2 16)$-bit set. It should be noted that the information bits on different subcarriers may convey information from different sources, thus OFDM can deliver heterogeneous services for different users. Also, the modulation formats taken on

different subcarriers can be different, which improves the OFDM system scalability and flexibility.

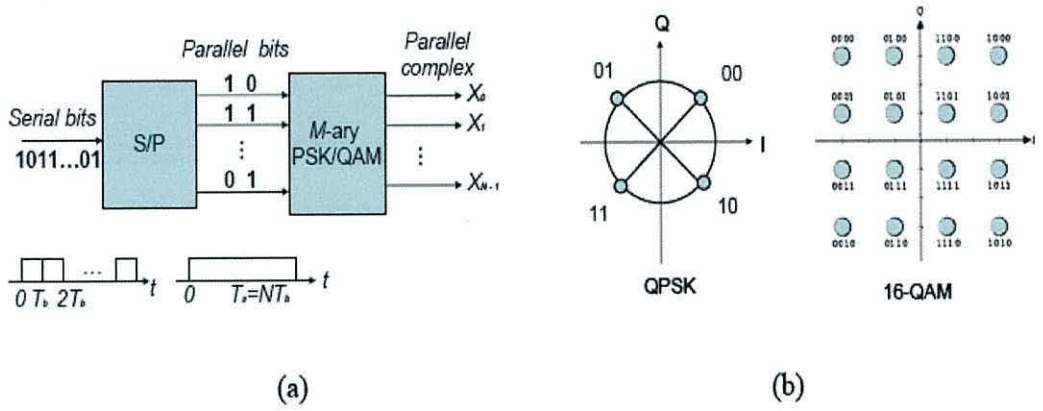

Figure 2.13: (a) Block diagram of bit encoding process, and (b) Constellation examples. [17]

2.8.1.2 IFFT/FFT

The encoded complex number via bit encoding needs to be up-converted to a RF subcarrier frequency and then multiplexed with other subcarriers. Signal modulation and multiplexing are achieved digitally using Inverse Discrete Fourier Transform (IDFT) in the OFDM transmitter and de-modulation and de-multiplexing using DFT in the OFDM receiver. IDFT (DFT) is the core component in the transmitter (receiver) to perform the functionalities of modulation (demodulation) and multiplexing (de-multiplexing). The IDFT is defined by [38]

$$x(l) = \frac{1}{\sqrt{N}} \sum_{k=0}^{N-1} X(k) e^{j2\pi k \frac{l}{N}} \tag{2.1}$$

$$X_{k,n} = A_{k,n} e^{j\theta_{k,n}} \tag{2.2}$$

where $A_{k,n}$, and $\theta_{k,n}$ are the amplitude and phase of the signal constellation points.

$X_{k,n}$, may not necessarily to be user information, it can also represent pilot and

training signals. The k-th subcarrier waveform can be modulated independently with data $X_{k,n}$. The k-th subcarrier waveform within the n-th symbol period can be expressed as

$$x_{k,n}(t) = X_{k,n}\Pi(t - nT_s)e^{j2\pi f_k t}, k = 0,1,2,..., N_s - 1 \tag{2.3}$$

$$\Pi(t) = \begin{cases} 1, t \in [0, T_s] \\ 0, t \notin [0, T_s] \end{cases} \tag{2.4}$$

where N_s is the number of subcarriers, f_k is the k-th RF subcarrier frequency, T_s is the OFDM symbol period, and $\Pi(t)$ has a rectangular pulse shape of unity magnitude over the time duration of T_s. Therefore, each subcarrier spectrum has a sinc form (Figure 2.14). When $X_{k,n}$, is treated as unit for simplicity, the correlation between any two subcarriers in the n-th symbol period is given by

$$\frac{1}{T_s}\int_{(n-1)T_x}^{nT_x} x_{k,n}x_{l,n}^*(t)dt = e^{j2\pi(f_k - f_l)}\frac{\sin(\pi(f_k - f_l)T_s)}{\pi(f_k - f_l)T_s} \tag{2.5}$$

When the subcarrier frequency spacing satisfies

$$\Delta f = f_k - f_{k-1} = \frac{1}{T_s}, k = 1,2,3,..., N_s - 1 \tag{2.6}$$

Equation (2.5) can be further expressed as

$$\frac{1}{T_s}\int_{(n-1)T_x}^{nT_x} x_{k,n}x_{l,n}^*(t)dt = e^{j2\pi(k-l)/T_s}\frac{\sin(\pi(k-l)T_s)}{\pi(k-l)T_s} = \begin{cases} 0, k \neq l \\ 1, k = l \end{cases} \tag{2.7}$$

Equation (2.7) shows that mutual orthogonality between subcarriers is achieved, when subcarrier frequency spacing and symbol period satisfy Equation (2.6). By combining Equations (2.3) – (2.4) and Equation (2.6), the expression of OFDM signal associated with the *k*-th subcarrier within the time duration of is given by

$$X_{k,n} = X_{k,n} e^{j2\pi \frac{k}{T_s} t} \tag{2.8}$$

It shows in Equation (2.8) that each subcarrier waveform has an integer number of cycles within one OFDM symbol period T_s, and the number of cycles grows with the subcarrier index. Figure 2.14 (a) gives an example of the time-domain waveforms containing four subcarriers. Meanwhile, due to the rectangular pulse shape of the encoded subcarrier data $X_{k,n}$, the corresponding subcarrier spectra are sinc functions with a spacing of Δ_f, as shown in Figure 2.14 (b). Orthogonality is also maintained in the frequency domain by the way that the sinc function for one subcarrier has a zero at the centre of others. Thus no Inter-Carrier Interference (ICI) occurs between different subcarriers even when their spectra are overlapped.

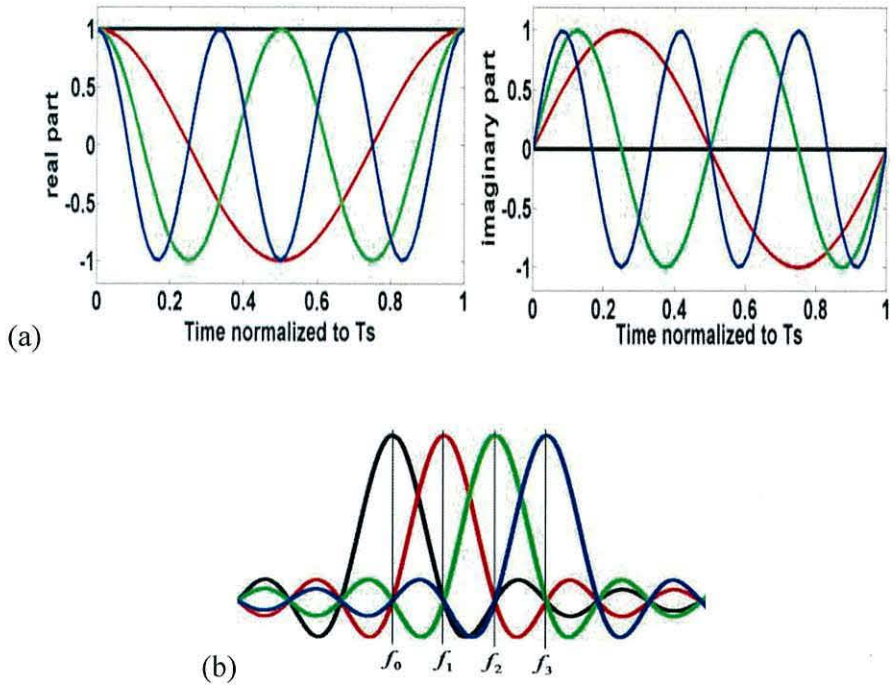

Figure 2.14: The (a) OFDM subcarrier waveforms and (b) spectrum. [17]

The resulting time-domain OFDM signal waveform within the time range [(n-1)T_s, nT_s]

$$x_n(t) = \frac{1}{\sqrt{N_s}} \sum_{k=0}^{N_s-1} X_{k,n} e^{j2\pi \frac{k}{T_s} t} \tag{2.9}$$

When the OFDM signal given in Equation (2.9) is sampled at a speed of $f_s = N_s / T_s$, the resulting sample at the time $t = lT_s / N_s, l = 0,1,2,..., N_s - 1,$ can be expressed as

$$x_n(t) = \frac{1}{\sqrt{N_s}} \sum_{k=0}^{N_s-1} X_{k,n} e^{j2\pi k \frac{l}{N_s} t} \tag{2.10}$$

By comparing Equation (2.10) and Equation (2.1), it is very interesting to note that Equation (2.10) is equivalent to $x_{l,n} = IDFT(X_{k,n})$, which means that the modulation

and multiplexing of a large number of OFDM subcarriers can be achieved by using IDFT. In practice the IDFT is implemented as an IFFT, an equivalent, fast method of calculating the IDFT.

When the impulse response of the transmission channel is *h(t)*, the received signal at the receiver end is given by

$$y(t) = x(t) \otimes h(t) + w(t) \tag{2.11}$$

where *w(t)* is the channel noise and "$\otimes$" represents continuous convolution operation.

In the receiver, assuming ideal synchronization followed by necessary signal processing, when the FFT input sample of the *n*-th received OFDM symbol is $y_{l,n}$, the FFT output is expressed as:

$$Y_{k,n} = \sum_{k=0}^{N_s-1} y_{l,n} e^{j2\pi k \frac{l}{N_s}}, l = 0,1,2,...,N_s - 1 \tag{2.12}$$

For an ideal OFDM system $Y_{k,n}$, is identical to the original data $X_{k,n}$. In a real transmission channel, a simple one-tap equalizer is usually adopted in the OFDM receiver to recover the transmitted signals.

2.8.1.3 Cyclic Prefix

OFDM is widely used in broadband wired and wireless communication systems because it is an effective solution to combat the Inter-Symbol Interference (ISI) effect caused by a dispersive channel. The solution embraced from the introduction of the CP in 1980 [39] in order to reduce the ISI problem and improve the performance robustness to the multipath propagation problem. A CP is a copy of the last fraction of

each OFDM symbol which is added to the front of the symbol, as illustrated in Figure 2.15. The CP duration period depicted in Figure 2.15, can be understood by Equation 2.13,

$$CP = \frac{T_p}{T_b - T_p} \tag{2.13}$$

where T_b is the CP time duration and T_p the OFDM-CP symbol period.

If the CP is longer than the expected largest time delay, the dispersion effect is localized within the CP region only. After removing the CP in the receiver, the received data can be recovered without interference between two adjacent different symbols. The aforementioned key aspects form the basis of most OFDM systems.

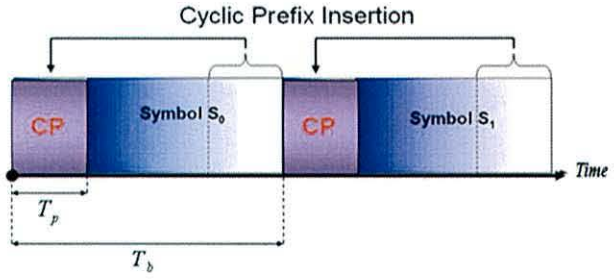

Figure 2.15: Representation diagram of CP insertion in the time OFDM signal.

2.8.1.4 Serialization

After inserting CP into each OFDM symbol, the OFDM signal is serialized through a parallel-to-serial convertor. On serialization, a number of low-speed parallel subcarrier signals are converted into a high-speed serial signal. In the OFDM receiver, an inverse process of performing serial to- parallel conversion is undertaken for data recovery.

2.8.1.5 DAC/ADC

DAC and ADC are two key components limiting the transmission performance of OFDM signals. These components can also introduce distortions to signals due to its signal clipping and quantization effects. As the effects of signal clipping and quantization in DAC are similar as those in an ADC, the following discussions are, therefore, made for an ADC only. As ADCs have limited amplitude ranges, signal clipping occurs when the signal amplitude exceeds the maximal input amplitudes of the ADCs. Signal clipping is closely related to the operating point of the automatic-gain-control unit that precedes the analogue-to-digital stage. In addition, signal clipping can be used for reducing high PAPRs of OFDM signals [32]. On the other hand, the quantization error induced by the finite resolution is generally treated as an additive noise with a white spectrum, which is uniformly distributed and uncorrelated with the input signal.

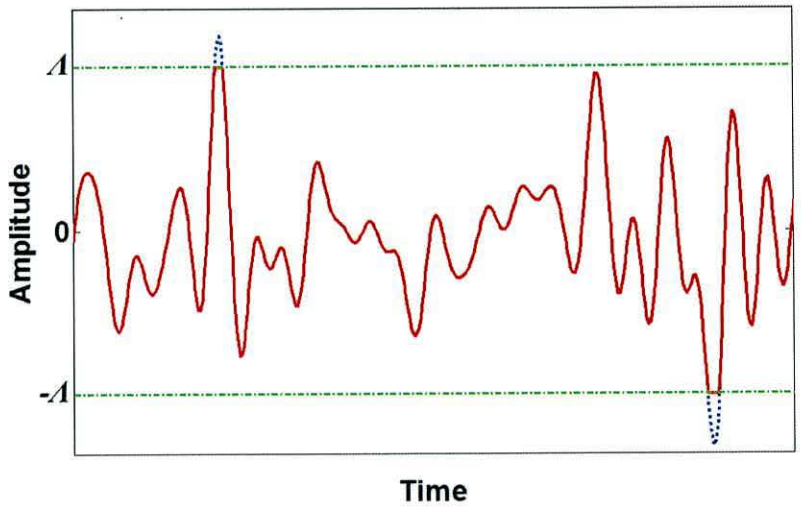

Figure 2.16: Clipping the amplitude of OFDM signals, A is maximal input amplitude of ADCs [32].

The automatic-gain-control unit that precedes the analogue-to-digital stage of an ADC sets a finite dynamic-amplitude range. Amplitude clipping occurs if the input signal, *A(t)*, exceeds the ADC's maximal input amplitude, as seen in Figure 2.16. For a given clipping ratio ζ, the clipped signal has the form

$$A_c = \begin{cases} A(t), & |A(t)| \le \Lambda \\ \Lambda e^{j\arg[A(t)]}, & |A(t)| > \Lambda \end{cases} \tag{2.14}$$

where Λ is the maximal input amplitude of an ADC defined as $\Lambda = \sqrt{\zeta \cdot P_m}$ with ζ being the clipping ratio and P_m being the average signal power [40], [41]. The clipping ratio is defined in Ref. [41]. Clearly, clipping introduces distortions to the input signal.

Sampled continuous-valued amplitude, A_s is linearly quantized into a set of equidistant output values, which span the entire dynamic range of $[-\Lambda, \Lambda]$. The quantization process can be expressed as a generic symmetric-staircase function:

$$Q(A_s) = \sum_{k=-(L/2)+1}^{L/2} \frac{\hat{A}_k + \hat{A}_{k-1}}{2} g(A_s, \hat{A}_k, \hat{A}_{k-1}) \tag{2.15}$$

where $\hat{A}_k$ and $\hat{A}_{k-1}$ represent the *k*-th and *(k-1)*-th quantization threshold values. L is the quantization levels depicted $L = 2^b$ with a number of quantization bits of *b*, *g* is the rectangular function defined as

$$g(x, x_1, x_2) = \begin{cases} 1 & x_1 \le x < x_2 \\ 0 & otherwise \end{cases} \tag{2.16}$$

From the above analysis, it can be seen that ADC errors mainly stem from two sources: 1) Quantization errors due to the finite step size of $2\Lambda / L$ for input-signal

values within the dynamic range of $[-\Lambda, \Lambda]$.and 2) amplitude clipping for input-signal values outside that range. It is necessary to point out that a Low-Pass Filter (LPF) or RF filter is usually inserted before ADC to remove the alias sideband signals [31], [32].

2.8.1.6 Pilot-Assisted Channel Estimation and Equalization

In OFDM systems, channel estimation can be achieved by transmitting known pilot signals that are interspersed with the user data. In the receiver, the system frequency response is estimated by extracting the pilot signals from the received signals, and is used for subsequent channel equalization so that the distortive effects can be largely removed and the transmitted signal can be restored prior to bit decoding. When the *k*-th subcarrier channel impulse response is $h_k(t)$ and corresponding noise is

$w_k(t)$, the received OFDM signal for the *k*-th subcarrier is

$$y_k(t) = x_k(t) \otimes h_k(t) + w_k(t) \tag{2.17}$$

where $x_k(t)$ is the transmitted OFDM signal for the *k*-th subcarrier. The time domain convolution between the transmitted OFDM signal and the channel response is equivalent to the multiplication of the OFDM signal spectrum with the channel frequency response. Assuming ideal synchronization in the receiver, after performing FFT to the received signal, we have the FFT output corresponding to the *k*-th subcarrier

$$Y_k = X_k H_k + W_k \tag{2.18}$$

The estimated system frequency response of the k-th subcarrier can be obtained by channel estimation based on pilot signals

$$Y_k = Y_{p,k} / X_{p,k} \tag{2.19}$$

where $X_{p,k}(t)$, and $Y_{p,k}(t)$, are the transmitted and received pilot signals of the k-th subcarrier. The OFDM receiver restores the transmitted signal by multiplying the received signal with the inverse of the estimated subcarrier channel response H_k^{-1}.

$$\hat{X}_k = X_k H_k^{-1} = X_k + W_k / H_k \tag{2.20}$$

This approach is considered to be simple one-tap equalization. The disadvantage of the one-tap equalizer is that the channel noise cannot be removed. For a channel that has strong attenuation, the noise effect imposed on the received signal is increased upon the equalizer. Practically, such an issue can be resolved efficiently by averaging the subcarrier channel frequency response estimations over long time duration [42].

2.8.1.7 Synchronization

The discussions in all the above subsections are based on an assumption that ideal OFDM symbol synchronization is performed in the receiver. In practical OFDM systems, however, synchronization errors may occur because of the following physical effects [43]:

- Symbol Timing Offset (STO) induced by the time delay of a transmission link.
- Sampling Clock Offset (SCO) induced by the clock mismatch between the transmitter and the receiver.

- Carrier Frequency Offset (CFO) induced by the frequency mismatch between the oscillators involved in the transmitter and receiver.
- Carrier Phase Error (CPEr) induced by the constant phase shift between the transmitter and the receiver, or by the random phase noise in the local oscillators and other components.

All these synchronization errors will degrade system performance. STO-induced synchronization errors may cause a fraction of a FFT window for an OFDM symbol to occur in an extended region of an adjacent symbol, leading to system performance degradation due to the effects of ISI and ICI. SCO brings about the significant ICI effect, as the sampled values do not correspond to the peaks of the sinc [sin(x)/x] waveforms after the FFT in the receiver. CFO also introduces ICI and destroys the orthogonality of OFDM subcarriers. The influence of CPEr is less important compared to the impacts of other three synchronization errors, as CPEr-induced constant phase shift or phase noise can be compensated by channel estimation and equalization. In OFDM transmission systems, there are usually two solutions for synchronization: the first is to use so-called blind approaches [44], [45], which make use of the features of the repeated OFDM symbol pattern with a predetermined time period; the second are non-blind approaches [46], [47], which take advantage of the features of training symbols or pilots that are interspersed with the transmitted user data. For both the abovementioned approaches, correlation calculations of incoming signals are usually performed, i.e., a sequence of samples is multiplied by a time-shifted copy of the same sequence to produce a time-dependent autocorrelation profile, which is then employed for synchronization.

2.8.2 Optical OFDM

For satisfying the rapidly increasing end-users' data traffic, the concept of OFDM was introduced into the optical domain, thus leading to the proposition of the OOFDM concept in 2005 [48]. Soon afterwards, opportunities for employing OOFDM signals converted by Directly Modulated DFB Lasers (DMLs) were theoretically explored over MMF-based LANs [41] and SMF-based optical access networks [49].

2.8.2.1 Coherent OFDM (CO-OFDM) transceivers

A typical CO-OFDM transmission link diagram is shown in Figure 2.18. This includes five basic functional blocks: OFDM transmitter, Electrical-to-Optical (EO) up-converter, optical link, Optical-to-Electrical (OE) down-converter, and OFDM receiver [50], [51]. In this section, as discussions are focused on the signal processing aspect of coherent OOFDM, assumptions of perfect linearity in each functional block are made.

In the OFDM transmitter, a complex baseband OFDM signal, *x(t)*, and subsequently EO up-converter transfers the complex baseband signal to the optical domain using an optical I/Q modulator comprising a pair of MZMs with a 90° phase offset. The baseband OFDM signal is directly up-converted to the optical domain given by,

$$E(t) = x(t)\exp(j\omega_{LD_1}t + \varphi_{LD_1}) \tag{2.21}$$

where $\omega_{LD_1}, \varphi_{LD_2}$ are the angular frequency and phase of the transmitter laser, respectively. The up-converted signal *E(t)* traverses the optical medium with impulse response *h(t)*, and the received optical becomes,

$$E(t) = [x(t)\exp(j\omega_{LD_1}t + \varphi_{LD_1})] \otimes h(t) \tag{2.22}$$

where $\otimes$ stand for convolution. The optical OFDM signal is the fed into the OE down-converter to be converted to an electrical OFDM signal. Figure 2.18 shows the direct down-conversion architecture where the intermediate frequency is near DC. The directly down-converted near-DC signal can be expressed as

$$r(t) = [x(t)\exp(j\Delta\omega t + \Delta\varphi)] \otimes h(t) \tag{2.23}$$

$$\Delta\omega = \omega_{LD_1} + \omega_{LD_2}, \qquad \Delta\varphi = \varphi_{LD_1} + \varphi_{LD_2} \tag{2.24}$$

where $\Delta\omega$ and $\Delta\varphi$ are the angular frequency offset and phase offset between the transmitter and receiver lasers respectively. In the OFDM receiver, the down-converted near-DC OFDM signal is first sampled with ADCs. Then the sampled signal needs to go through sophisticated synchronization and channel estimation before de-mapping can be made. The synchronization includes: 1) FFT window synchronization where the OFDM symbol is properly delineated to avoid ISI; 2) frequency synchronization, namely, the frequency offset $\Delta\omega$ needs to be estimated and compensated. Assuming successful completion of FFT window synchronization and frequency synchronization, the OFDM signal through FFT of the sampled value becomes

$$Y_k = X_k H_k - e^{j\varphi'} + W_k \tag{2.25}$$

where X_k is the transmitted information data, H_k is the CTF in frequency domain, φ' is the common phase error, W_k is the noise. With channel estimation, the CTF X_k and the phase error φ' can be estimated so that an estimated value, X_k', can be obtained with single tap equalizer [31].

$$X_k' = Y_k \frac{\hat{H}_k^*}{\left|\hat{H}_k\right|^2} e^{-j\hat{\phi}} \tag{2.26}$$

where $\hat{H}$ and $\hat{\phi}$ is the estimated CTF and phase error respectively. The estimated value X_k' is then de-mapped back to the original transmitted digital bits.

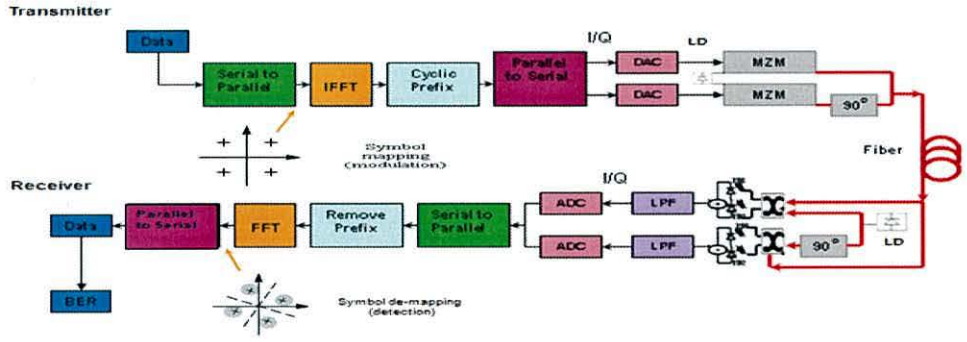

Figure 2.18: Conceptual diagram of a generic CO-OFDM system; LD: Laser Diode; MZM: Mach-Zehnder Modulator.

2.8.2.2 IM/DD OOFDM transceivers

In IM/DD OOFDM systems, OOFDM signals are usually transmitted with intensity modulation or linear field modulation then received with square-law detection. Most recently, 100 Gb/s IM/DD OOFDM signal transmission over 500km standard SMFs with a spectral efficiency of 3.57 bits/s/Hz have been demonstrated in a single-band direct-detection system [5].

Figure 2.19 shows the conceptual diagram of a generic IM/DD OOFDM system [17], which also contains five basic functional blocks: OFDM transmitter, EO up-converter, optical link, OE down-converter, and OFDM receiver. However, for the IM/DD OOFDM system, an intensity modulator such as a DFB laser is used for EO up-converter, while a square-law direct detection photo-diode is used for OE down-

converter. In the OFDM transmitter, due to intensity modulation used for the OE up-converter, real valued OFDM signals are required to drive a DFB-laser. To produce a real valued OFDM signal, the mapper in the OFDM transmitter is modified by creating the truncated original complex parallel data in the positive frequency bins and the complex conjugate of the data in the negative frequency bins. The subcarriers contained in both the positive and negative frequency bins are arranged specially to satisfy Hermitian symmetry, which can be expressed as,

$$X_k = \begin{cases} 0 & k = 0 \\ X_k & k = 1,\ldots,(N/2)-1 \\ 0 & k = N/2 \\ X^*_{N-k} & k = (N/2)+1,\ldots,N-1 \end{cases} \tag{2.27}$$

In the EO up-converter, an intensity modulator is used to transfer the OFDM signal from the electrical domain to the optical domain to create an OOFDM signal $A_o(t)$. After that, the OOFDM signal is coupled into a fibre link. Optical amplification may be used when required to compensate for the link loss.

In the OE down-converter, the transmitted optical signal power emerging from the optical link is coupled into and subsequently detected by a square-law photodiode. The received electrical signal, $A_E(t)$ is given by

$$A_E(t) = |A_o(t)|^2 \otimes h_e(t) + w(t) \tag{2.28}$$

where $h_e(t)$ is the impulse response of the transmission link in the electrical domain; $w(t)$ represents the receiver related noise, which is mainly generated in the electrical front-end of the receiver.

In the OFDM receiver, after passing through a LPF and an ADC, the sampled electrical signal is decoded into the original data sequence by the receiver which is the inverse of the transmitter. The information transmitted in the positive frequency bins is then recovered. In this case, as no local oscillators are required, synchronization only includes FFT window synchronization and simplifies the system complexity as compared with coherent OOFDM cases.

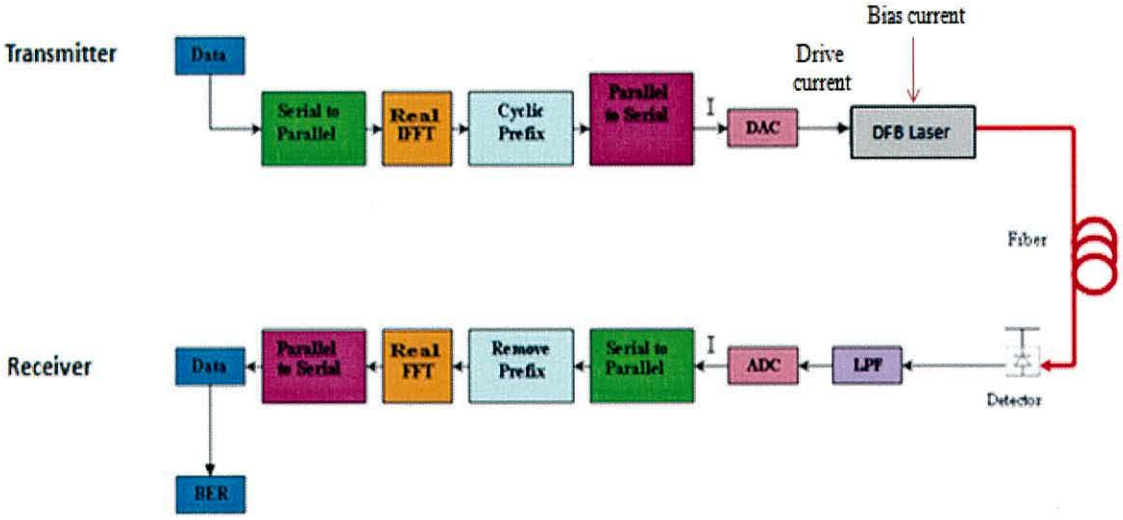

Figure 2.19: Conceptual diagram of a generic IM/DD OOFDM system.

2.8.2.3 Comparison between CO-OFDM and IM/DD OOFDM

CO-OFDM and IMDD OOFDM each have their own strengths and drawbacks. Table 2.5 summarizes the differences between CO-OFDM and IM/DD OOFDM. Generally, CO-OFDM represents the ultimate performance in robustness to CD and PMD, as CD and PMD induced phase shifts can be well preserved upon linear coherent detection. Therefore, theoretically speaking, CO-OFDM is capable of offering virtually unlimited dispersion tolerance. On the other hand, for IM/DD OOFDM, tolerance to

CD and PMD is limited due to nonlinear direct detection. In addition, CO-OFDM also outperforms IM/DD OOFDM on receiver sensitivity.

On the other hand, due to the coherent detection with a local laser, CO-OFDM requires frequency offset compensation, which complicates the receiver synchronization compared to IM/DD OOFDM where frequency offset does not occur. More importantly, the requirements of expensive and bulky equipments for E/O and O/E conversions in CO-OFDM systems limit their applications to long-haul transmission systems. IM/DD OOFDM offers promising solutions for cost-sensitive application scenarios including LAN, access networks and MANs.

	CO-OFDM	IMDD OOFDM
Modulation	Field modulation	Intensity modulation
Detection	Coherent detection	Square-law direct detection
Linearity of E/O and O/E	Linear	Nonlinear
Dispersion tolerance	Unlimited (theoretically)	Limited by direct detection
Synchronization	FFT window; and frequency offset	FFT window
Receiver sensitivity	High	Relatively Low
System complexity and cost	Complex, expensive	Simple, cost-effective
Applications	Long-haul transmissions	MANs, access networks, and LANs

Table 2.5 Comparisons between CO-OFDM and IM/DD OOFDM [17].

2.8.2.4 AMOOFDM

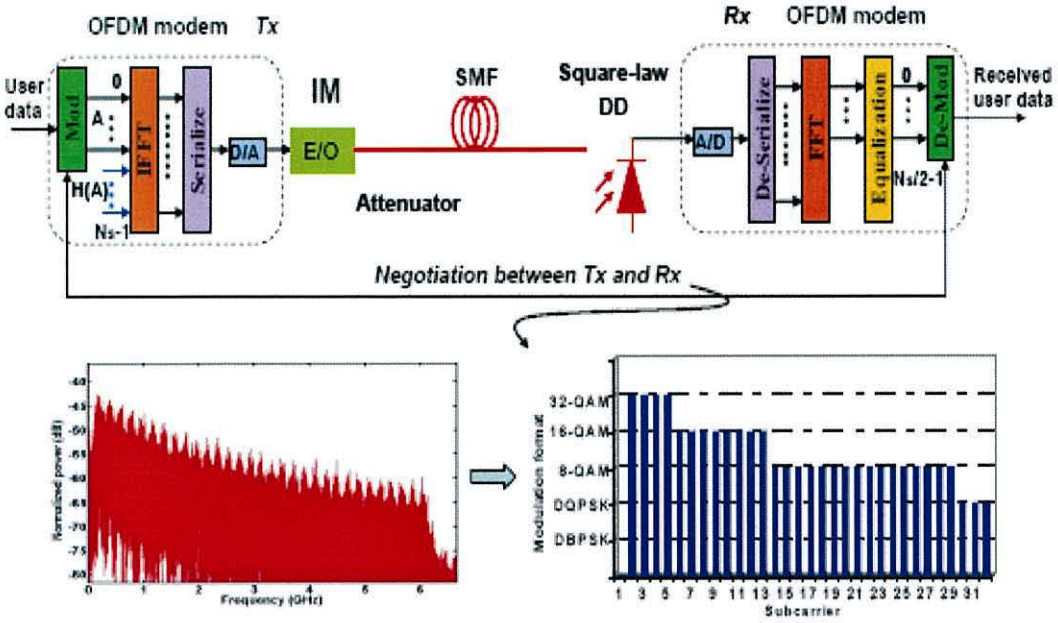

Figure 2.17: AMOOFDM transmission system [17].

In an IM/DD OOFDM system, there is a system frequency response roll-off effect induced by optical and electrical components involved in the transmission system. To compensate this roll-off effect, AMOOFDM [17], [32], [40], [41], [49], [50], in which different signal modulation formats are taken on individual subcarriers which have identical electrical powers while keeping the total *BER* at $\leq 1.0 \times 10^{-3}$, was proposed to adapt channel conditions. Figure 2.17 depicts the AMOOFDM system, where the highest signal modulation format that can be used on each subcarrier is identified by negotiations between the transmitter and the receiver in the initial stage of establishing a connection over the SMF system. The modulation formats vary from Differential Binary PSK (DBPSK), Differential QPSK (DQPSK), 8-QAM, to 256-QAM. Generally speaking, a high (low) signal modulation format is used on a given carrier suffering a low (high) transmission loss. Any subcarrier suffering a very high

loss may be dropped completely to avoid the occurrence of a large number of errors on the subcarrier. A practical way to realize adaptive modulation is to feedback the subcarrier *BERs* and the total channel *BER* to the transmitter so that the optimum modulation format for each subcarrier can be determined. In an AMOOFDM system, the total channel *BER*, BER_T, is

$$BER_T = \sum_{k=2}^{M_s} En_k \Big/ \sum_{k=2}^{M_s} n_k \tag{2.29}$$

where $M_s = N_s/2$ is the number of data-carrying subcarriers in the positive frequency bins, En_k is the total number of detected errors and n_k is the total number of transmitted binary bits. Both En_k and n_k are for the *k*-th subcarrier, whose sub-channel *BER*, BER_k is given by $BER_k = En_k / n_k$. Based on BER_T and BER_k, the maximum modulation format adopted on each of the subcarriers within a symbol can be identified through negotiations between the transmitter and the receiver. Usually, a high signal modulation format is always preferred if BER_T remains at 1.0×10^{-3} or better. Once the link has been established, the modulation format on each subcarrier remains unchanged.

Once an optimum modulation format for each subcarrier is configured, the maximum signal line rate of the AMOOFDM system is obtained, which is calculated using the expression given below:

$$R_{signal} = \sum_{k=2}^{M_{Ss}} S_k = \frac{\sum_{k=2}^{M_S} n_k}{T_S} = \frac{r_S \sum_{k=2}^{M_S} n_k}{2M_S(1+\eta)} \tag{2.30}$$

where S_k is the signal bit rate corresponding to the k-th subcarrier, n_k is the total number of binary bits conveyed by the k-th subcarrier within one symbol period T_S, which is related to the ADC/DAC sampling rate r_s by $T_S = 2N_S(1+\eta)/r_S$ and η is the CP parameter defined previously. It should be noted that Equations (2.29) – (2.30) are not only valid for AMOOFDM systems but also applicable for identically modulated OOFDM systems, where an identical modulation format is adopted across all the subcarriers.

The AMOOFDM technique has many advantages. AMOOFDM supports maximum data rate and improves the system flexibility. Also, compared with identical modulation, adaptive modulation is capable of reducing fibre nonlinearities including Four-Wave Mixing (FWM) and Cross-Phase Modulation (XPM) due to the reduced PAPR of the DWDM AMOOFDM signals [17]. Therefore, AMOOFDM is a cost-effective solution for the delivery of broadband services for subscribers. In this thesis, explorations are also undertaken of the implementation of AMOOFDM in NG-PONs.

2.9 OOFDM PON

As discussed in Chapter 2.8, OOFDM is an advanced signal modulation technique for PONs due to its high spectral efficiency, high chromatic dispersion tolerance, excellent system scalability and flexibility [23], [52], [53], [54]. Integrated circuit implementations of OFDM modems are feasible for affordable mass-produced transmitters and receivers. Apart from these advantages, OOFDM PON also offers, in particular, multiple access capability that allows different OFDM subcarriers to be assigned to different customers/services [54], [55]. Figure 2.18 shows a typical architecture and multiple access strategy of OOFDM PON. For downstream transmission, different services such as Ethernet data, RoF signals share the same laser and downstream wavelength. The signal is broadcast to all ONUs by using a PS. Each ONU recovers its signal at the allocated subcarriers. For upstream transmission, each ONU maps its data and/or signal to the allocated subcarriers, sets all the other subcarriers to zero, and completes the modulation to generate an electrical OFDM frame. The OFDM frame is then converted into OOFDM symbols with low cost DMLs and transmitted over fibre. The OOFDM symbols from multiple ONUs will be combined at the optical coupler, forming a single OOFDM frame, and detected by a single photo-detector at the OLT receiver.

Compared to conventional TDM-PON technologies, OOFDM PON not only provides improved performance but also the possibility of convergence between optical, wireless, and copper access networks.

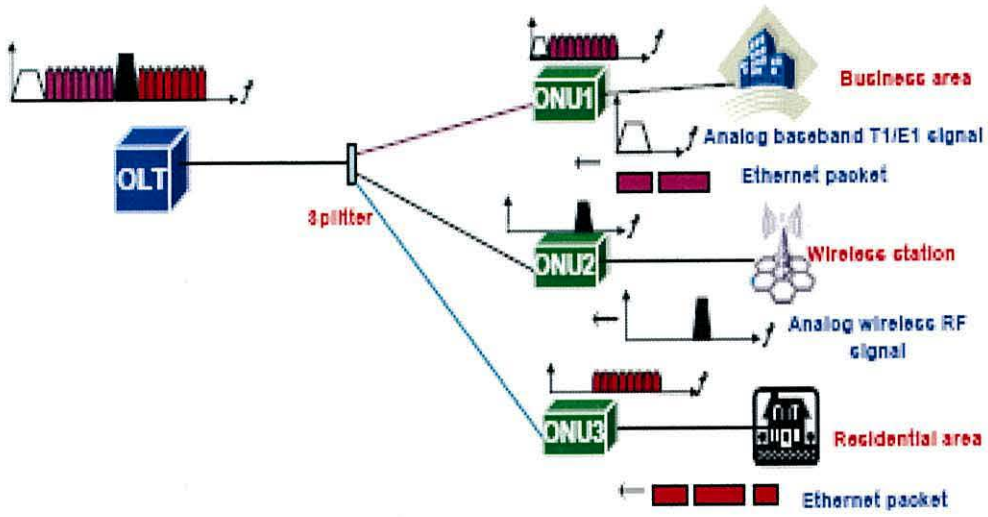

Figure 2.18: A typical architecture and multiple access strategy of OOFDM PON [17].

The OOFDM PON is widely viewed as promising technologies for NG-PONs, together with the WDM-PON, WDM/TDM PON. While WDM-PON is a "future-proof" solution to support the required bandwidth and scalability for NG-PONs due to the mature WDM technology (WDM-PON was also considered as the base technology for NG-PON2 by FSAN group [57]), and WDM/TDM PON provides better flexibility than pure WDM PONs do, allowing delivery of services to more subscribers and the efficient use of bandwidth of each wavelength, OOFDM PON brings about high transmission performance, high spectral efficiency, strong dispersion tolerance as well as flexibility.

2.10 Conclusion

In this Chapter, we have analysed the principles of OFDM and OOFDM. The basic idea of OFDM is to divide the serial bit stream into a number of parallel streams and transmit these low-rate parallel data simultaneously by using classical modulation

formats such as *M*-ary QAM and (D)PSK on each parallel subcarrier. OFDM is therefore resilient to channel frequency-selective fading effects. With the aid of CP, OFDM has significantly improved tolerance to the channel dispersive effects. The efficient implementation of IFFT (FFT) largely reduces the OFDM system complexity. The disadvantages of OFDM are its high PAPR and sensitivity to time and frequency synchronization problems. OOFDM enables excellent robustness against the fibre linear effects such as CD and PMD. Theoretically, CO-OFDM offers virtually unlimited dispersion tolerance. However, CO-OFDM is sensitive to the frequency and phase noise from the LD upon coherent detection. Moreover, the requirement of bulky and expensive equipments limits its applications in long-haul transmission systems. IM/DD OOFDM uses simple intensity-modulation and direct-detection thus outperforms CO-OFDM on cost-sensitive application scenarios such as access networks. In addition, AMOOFDM systems can further improve the system scalability and flexibility. In the meantime, IM/DD OOFDM also brings about important challenges including relatively low OOFDM signal ER induced by intensity-modulation, nonlinear effects from intensity modulators and strong intermixing upon direct detection. Addressing these challenges forms the main task of this Thesis.

References

[1] R. Ramaswami and K. N. Sivarajan, "Optical networks: A practical perspective", Academic Press Inc., NY, 2nd Ed., 2002.

[2] R. W. Smith, "Broadband Internet connections: A user's guide to DSL and cable", Addison-Wesley Pub Co., 1st Edition, 2002.

[3] "The role of ATM in an IP World", RHK Atom. III, Vol. 4.

[4] P. E. Green, "Fiber optic networks", Prentice-Hall Inc., NJ, Translation K. Καroubalos, Ed. A. Papasotiriou & SIA O. E., 1993.

[5] G. P. Agrawal, "Fiber-Optic Communication Systems", 2nd Ed., John Wiley & Sons Inc., NY, 1997.

[6] I. P. Kaminow and T. L. Koch, "Optical fiber telecommunications IIIB", Academic Press Inc., NY, 1997.

[7] T. Nga Duong, "Etude de techniques de modulation multi-porteuse OFDM pour la montee en debit dans le reseau d'acces optique", PhD Thesis Manuscript, University of Rennes, 2010.

[8] C. F. Lam, Passive Optical Networks: Principles and Practice, Academic Press, Oct. 2007.

[8] http://www.cablelabs.com/news/pr/2006/06_pr_docsis30_080706.html

[9] Burstein, Dave (2002). *DSL*, John Wiley and Sons, New York, ISBN 0-471-08390-0, pp. 53-86.

[10] B. Lee, J. Cioffi, et al., Gigabit DSL, IEEE Transactions on Communications, Sep, 2007, pp. 1689-1692.

[11] http://en.wikipedia.org/wiki/DSL

[12] K. Tanaka, A. Agata, and Y. Horiuchi, "IEEE 802.3av 10G-EPON standardization and its research and development status", J. Lightw. Technol., vol. 28, no. 4, pp. 651661, Feb. 2010.

[13] IDATE Consulting & Research, "FTTx market report," July 2009. Available at www.idate.org

[14] ITU-T, "Broadband Optical Access Systems Based on Passive Optical Networks (PON)", ITU-T Recommendation G.983.1, October 1998.

[15] IEEE 802.3ah Ethernet in the First Mile Task Force, "Part 3: Carrier Sense Multiple Access with Collision Detection (CSMA/CD) Access Method and Physical Layer Specifications Amendment: Media Access Control Parameters, Physical Layers, and Management Parameters for Subscriber Access Networks", IEEE Standard 802.3ah-2004, 2004.

[16] ITU-T, "Gigabit-capable Passive Optical Networks (GPON)", ITU-T Recommendations G984.x, March 2003.

[17] J. L. Wei, "Intensity Modulation of Optical OFDM Signals Using Low-Cost Semiconductor Laser Devices for Next-Generation PONs", PhD Thesis Manuscript, Bangor University, 2010.

[18] http://en.wikipedia.org/wiki/10G-EPON

[19] http://www.oeee802.org/3/av/

[20] "Next Generation PON", *IEEE Communication Magazine*, Nov. 2009

[21] ITU-T Recommendation Y.2201, "NGN Release 1 Requirements", April 2007.2

[22] CIP White Paper: WDM-PON Technologies, available at: http://www.ciphotonics.com/New_PDFs/WPON_White_Paper_v1%200.pdf

[23] J. L. Wei, X. L. Yang, R. P. Giddings, J. M. Tang and K. A. Shore, "SOA Intensity Modulator-Enabled Colourless Transmission of Adaptively Modulated

Optical OFDM Signals for WDM-PONs", presented at the 14th OptoElectronics and Communications Conf. (OECC), (Hongkong, China, 2009), Paper ThLP77.

[24] S. L. Woodward, P. P. Iannone, K. C. Reichmann, and N. J. Frigo, "A spectrally sliced PON employing Fabry-Perot lasers", IEEE Photon. Technol. Lett. 10, 1337-1339, 1998.

[25] K. Y. Park and C.H. Lee, "Intensity noise in a wavelength-locked Fabry-Perot laser diode to a spectrum sliced ASE", IEEE J. Quant. Electronics, vol. 44, no. 3, pp. 209-215, March 2008.

[26] D. K. Jung, H. Kim, K. H. Han, and Y. C. Chung, "Spectrum-sliced bidirectional passive optical network for simultaneous transmission of WDM and digital broadcast video signals", Electron. Lett. 37, 308-309, 2001.

[27] K. H. Han, E. S. Son, H. Y. Choi, K. W. Lim, and Y. C. Chung, "Bidirectional WDM PON using light-emitting diodes spectrum-sliced with cyclic arrayed waveguide grating", IEEE Photon. Technol. Letters, vol. 16, no. 10, pp. 2380-2382, Oct. 2004.

[28] C. W. Chow, C. H. Yeh, C. H. Wang, F. Y. Shih, and S. Chi, "Demonstration of signal remodulation long reach carrier distributed passive optical network using OFDM-QAM signal", at the ECOC (Vienna, Austria, 2009), paper 8.5.2.

[29] H. Takesue, and T. Sugie, "Wavelength channel data rewrite using saturated SOA modulator for WDM networks with centralized light sources", J. Lightwave Technol. vol. 21, no. 5, pp. 2546-2556, Mar. 2003.

[30] J. Yoo, H. Yun, T. Kim, K. Lee, M. Park, B. Kim, B. Kim, "A WDM-Ethernet hybrid passive optical network architecture", at the 8th International Conference on Advanced Communication Technology (ICACT), (Korea,2006), Feb 2006.

[31] L. J. Cimini, Jr., "Analysis and simulation of a digital mobile channel using orthogonal frequency division multiplexing", IEEE Trans. Commun., vol. CM-33, pp. 665–675, 1985.

[32] X. Jin, "Theoretical and Experimental Investigations of Optical OFDM for Local and Access Networks", PhD Thesis Manuscript, 2010

[33] J. A. C. Bingham, "Multicarrier modulation for data transmission: An idea whose time has come", IEEE Commun. Mag., Vol. 28, pp. 5–14, 1990.

[34] R. van Nee and R. Prasad, OFDM for Wireless Multimedia Communications. Boston: Artech House, 2000.

[35] W. Y. Zou and Y. Wu, "COFDM: An overview", IEEE Trans. Broadcasting, vol.41, pp. 1–8, 1995.

[36] J. H. Stott, "The how and why of COFDM", EBUTech. Rev., pp. 43–50, 1998.

[37] R. W. Chang, "Orthogonal Frequency Multiplex Data Transmission System", USA U.S. Patent 3,488,445, 1966.

[38] L. Hanzo, S. X. Ng, T. Keller, and W. Webb, Quadrature Amplitude Modulation: From Basics to Adaptive Trellis-Coded, Turbo-Equalised and Space-Time Coded OFDM, CDMA and MC-CDMA Systems. Hoboken, NJ: Wiley, 2004.

[39] A. Peled and A. Ruiz, "Frequency domain data transmission using reduced computational complexity algorithms", in Proc. ICASSP 80, Denver, CO, USA, 1980, vol. III, pp. 964–967, IEEE.

[40] J. M. Tang, P. M. Lane, and K. A. Shore, "High-speed transmission of adaptively modulated optical OFDM signals over multimode fibres using directly modulated DFBs", IEEE J. Lightwave Technol., vol. 24, no. 1, pp. 429–441, Jan. 2006.

[41] J. M. Tang, and K. A. Shore, "Maximizing the transmission performance of adaptively modulated optical OFDM signals in multimode-fiber links by optimizing

analog-to-digital converters", J. Lightwave. Technol., vol. 25, no. 3, pp. 787–798, Mar. 2007.

[42] T.-D. Chiueh and P.-Y. Tsai, OFDM Baseband Receiver Design for Wireless Communications, Wiley, 2007.

[43] R. Prasad, OFDM for Wireless Communications Systems. London: Boston, 2004.

[44] X. Q. Jin, R. P. Giddings, E. Hugues-Salas and J. M. Tang, "Real-time experimental demonstration of optical OFDM symbol synchronization in directly modulated DFB laser-based 25km SMF IMDD systems", Opt. Express, vol.18, no. 20, pp. 21100-21110, Sep. 2010.

[45] M. Sandell, J. J. Van de Beek, and P. O. Börjesson, "Timing and frequency synchronization in OFDM systems using the cyclic prefix", in Int. Symposium Synchronization, (Essen, Germany, 1995), pp. 16–19.

[46] W. Shieh, "Maximum-Likelihood Phase and Channel Estimation for Coherent Optical OFDM", IEEE Photon. Technol. Letters, vol. 20, no. 8, pp. 605-607, Apr. 2008.

[47] W. Shieh, H. Bao, and Y. Tang, "Coherent optical OFDM: theory and design", Opt. Express, vol. 16, no. 2, pp. 841-859, Jan. 2008.

[48] N. E. Jolley, H. Kee, R. Rickard, J. Tang, and K. Cordina, "Generation and propagation of a 1550 nm 10 Gb/s optical orthogonal frequency division multiplexed signal over 1000 m of multimode fibre using a directly modulated DFB", presented at the Optical Fiber Communication Conf./National Fiber Optic Engineers Conf. (OFC/NFOEC), (OSA, 2005), Paper OFP3.

[49] J. M. Tang and K. A. Shore, "30-Gb/s signal transmission over 40-km directly modulated DFB-laser-based single-mode-fibre links without optical amplification and dispersion compensation", IEEE J. Lightwave Technol. 24, 2318–2327, 2006.

[50] X. Q. Jin, J. M. Tang, P. S. Spencer, and K. A. Shore, "Optimization of adaptively modulated optical OFDM modems for multimode fibre-based local area networks [Invited]", J. Optical Netw., vol. 7, no. 3, pp. 198–214, Mar. 2008.

[51] X. J. Gu, W. Mohammed, and P. W. Smith, "Demonstration of all-fiber WDM for multimode fiber local area networks", IEEE Photon. Technol. Lett., vol. 18, no. 1, pp. 244–246, Jan. 2006.

[52] J. Yu, M.-F. Huang, D. Qian, L. Chen, and G.-K. Chang, "Centralized lightwave WDM-PON employing 16-QAM intensity modulated OFDM downstream and OOK modulated upstream signals", IEEE Photon. Technol. Lett. vol. 20, no.18, pp.1545-1547, Sep. 2008.

[53] T. Duong, N. Genay, B. Charbonnier, P. Urvoas, P. Chanclou, and A. Pizzinat, "Experimental demonstration of 10 Gbit/s transmission over 110 km SMF by direct modulation of 2 GHz bandwidth DFB laser using discrete multi-tone modulation for passive optical network", at the OFC/NFOEC, (San Diego, USA, 2008), Paper NMB3.

[54] C.-W. Chow, C.-H. Yeh, C.-H. Wang, F.-Y. Shih, C.-L. Pan, and S. Chi, "WDM extended reach passive optical networks using OFDM-QAM", Opt. Express. vol. 16, no. 16, pp.12096-12101, Aug. 2008.

[55] D. Qian, J. Hu, P. N. Ji and T. Wang, "10Gb/s OFDMA-PON for delivery of heterogeneous services", at the OFC/NFOEC, (San Diego, USA, 2008), Paper OWH4.

[56] N. Cvijetic, D. Qian, J. Hu, and T. Wang, "44-Gb/s/λ upstream OFDMA-PON transmission with polarization-insensitive source-free ONUs", at the OFC/NFOEC (San Diego, US, 2010), Paper OTuO3.

[57] J.-P. Elbers, "Optical access solutions beyond 10G-EPON/XG-PON", at the OFC/NFOEC (San Diego, USA, 2010), Paper OtuO1.

CHAPTER 3

Transmission Performance Improvement of AMOOFDM Signals using Adaptive Cyclic Prefix

Contents

3.1 Introduction

3.1.1 Background....91

3.1.2 Scope....94

3.2 Transmission Link Model, Signal Characteristics and Simulation Parameters....95

3.2.1 Transmission Link Model....96

3.2.2 Signal Characteristics....100

3.2.3 Simulation Parameters....102

3.3 Performance of AMOOFDM-ACP Signals over MMFs

3.3.1 Capacity versus Reach Transmission Performance....107

3.3.2 Link Loss Margin....110

3.4 Performance of AMOOFDM-ACP Signals over SMFs

3.4.1 Capacity versus Reach Transmission Performance....113

3.4.2 Link Loss Margin....116

3.5 ACP-Enabled DFB Bandwidth Relaxation....117

3.6 Conclusions....120

References....121

3.1 Introduction

3.1.1 Background

The scope of this Chapter is to investigate a novel technique for IM/DD OOFDM for applications in LANs, MANs and PONs. In LANs, it is well known [5], [6] that, to upgrade the present 1 Gb/s MMF-based backbones to 10 Gb/s and above with the installed fibre infrastructure being preserved, the primary difficulty is the highly-variable modal dispersion present in the graded index fibre, which, in turn, causes the large bandwidth variation. To address this technical challenge, a wide range of approaches are currently being investigated, including low-cost coarse WDM [9], offset launch [10], multilevel coding [11] and adaptive optics [12].

In MANs and PONs, considerable effort has been expended on exploring low-cost CD compensation schemes for SMF-based transmission systems operating at >10 Gb/s, a number of compensation techniques in the electrical domain have been reported, including, for example, the combination of electrical Feed-Forward Equalizers (FFEs) and Decision Feedback Equalizers (DFEs) [13], as well as nonlinear electrical equalization [14].

The AMOOFDM technique, discussed in Chapter 2, has demonstrated great potential for providing a high-speed, cost-effective solution for practical implementation in both LANs and MANs [5], [6], [15], [16], [17], [18], as it has the unique features listed as followings: a) very high signal capacity versus reach performance. Statistical investigations have shown [17] that the AMOOFDM technique can support >50 Gb/s signal transmission over 300m in 99.5% of already installed MMF links with loss margins of >7dB; b) excellent performance flexibility and robustness to fibre types,

variation in launch conditions and signal bit rates [15], [16], [17], [18]; c) efficient use of link spectral characteristics. AMOOFDM has the salient capability of exploiting the fibre bandwidth to its full potential, instead of using the spectral characteristics in the vicinity of the reference frequency only; d) as already mentioned above, re-utilisation of legacy fibres, and finally, e) cost-effective in system installation and maintenance. The primary reason underpinning the above-mentioned AMOOFDM features is that, individual subcarriers within a symbol can be manipulated in the frequency domain by using different signal modulation formats according to the frequency response of a given transmission link. Such subcarrier modulation manipulation provides AMOOFDM with a unique opportunity for exploiting, in a cost-effective manner, the transmission link bandwidth to its full potential, instead of using the link spectral characteristics in the vicinity of the reference frequency only.

In all the AMOOFDM work reported previously [5], [6], [15], [16], [17], [18], a CP of fixed time duration has been utilised to combat Differential Modal Dispersion (DMDs) occurring in MMFs and CDs associated with SMFs. A CP is essentially a copy of the last fraction of each time domain OFDM symbol and added to the front of the corresponding symbol in the transmitter. This treatment produces quasi-periodically extended time domain OFDM symbols, leading to the maintenance of the orthogonality between subcarriers within the symbol. More importantly, due to the CP insertion, the channel dispersive effect becomes equivalent to a cyclic convolution. If the CP length is larger than the expected maximum delay spread to be encountered, after transmitting through the channel, the dispersive effect is localized within the prefix region only. Prior to performing the FFT in the receiver, the distorted CP is removed, thus the OFDM symbol carrying useful information can be recovered

without interference between different symbols. As the CP duration can be chosen by design, in principle, AMOOFDM can be made free from any arbitrary delay spread. It is worth emphasizing that a CP does not convey any useful information.

From the above analysis, it is clear that, if a CP time duration is smaller than the DMD (CD) associated with a MMF (SMF) link, the imperfectly compensated DMD (CD) effect limits considerably the maximum achievable transmission performance of the AMOOFDM signals [5], [15]. In addition, a small CP may also affect the sub-carrier orthogonality, resulting in a significant increase in the minimum required SNR for a specific signal modulation format being taken on a subcarrier [19]. On the other hand, if the CP is longer than the DMD (CD) of a MMF (SMF) link, for a fixed signal sampling speed, the CP wastes a large percentage of the transmitted signal power, giving rise to a degraded effective signal SNR. Furthermore, an excessive length of CP also prevents us from making full use of the available link bandwidth.

Therefore, it is greatly advantageous if the CP lengths can be made variable, according to the properties of different optical transmission links, to ensure that the selected CP lengths are just sufficiently long to compensate for DMDs (CDs) and other effects in MMF (SMF)-based links. For simplification, here the adjustable CP length technique is referred to as ACP and the AMOOFDM modem using ACP as AMOOFDM-ACP. It should be noted that the concept of ACP was first proposed in Ref. [5] by the same research group of this work. Very recently, for long-haul transmission systems, the transmission link dependent CP length has been shown in a single figure of Ref. [20], in which an incoherent OOFDM modem using an identical modulation format crossing all subcarriers is considered.

3.1.2 Scope

The thrust of this Chapter is to explore thoroughly, for the first time, the impact of ACP on the transmission performance of the AMOOFDM-ACP technique for various application scenarios including MMF-based LANs and SMF-based links for MANs and PONs. It is shown that, in comparison with the conventional AMOOFDM technique, AMOOFDM-ACP can improve the signal transmission capacity versus reach performance by a factor of at least 2 (1.3) for transmission distances of >1000m MMFs (<80km SMFs), together with 1dB enhancements in link loss margin and better performance robustness. In addition, for achieving a specific transmission performance, AMOOFDM-ACP can also relax significantly the requirement on the frequency bandwidth of the DFB lasers (DMLs) employed in the transmitter.

As the other salient feature of this work, three ACP mechanisms are identified, which are referred to, throughout this Chapter, as ACP mechanism I, ACP mechanism II and ACP mechanism III. ACP mechanism I is used to compensate completely any amount of dispersion by adopting sufficiently long CPs required by the link. As demonstrated in sections 3.3 – 3.5, this mechanism is effective for dispersion-limited transmission links; ACP mechanism II is to make efficient use of the OFDM signal powers and the link bandwidths by employing relatively short CP lengths, provided that the link is free from dispersion. This mechanism plays a crucial role in determining the transmission performance of the technique for dispersion-compensated links having spectral bandwidths larger than those corresponding to the transmitted signals. Finally, ACP mechanism III is similar to ACP mechanism II, except that it plays a role when the link spectral bandwidths are comparable to (or smaller than) those corresponding to the transmitted signals, the resulting noise margins are too low to

accommodate the signal SNR growth induced by the short CP lengths. This mechanism sets a minimum CP length that may be adopted for a given transmission system. Clearly, the effectiveness of these mechanisms depends upon the transmission link properties.

3.2 Transmission Link Model, Signal Characteristics and Simulation Parameters

As already addressed in section 3.1, AMOOFDM is a signal modulation technique that enables individual subcarriers within a symbol to be manipulated in the frequency domain by using different signal modulation formats according to the frequency response of a given transmission link. Generally speaking, a high (low) modulation format is used on a subcarrier suffering a low (high) transmission loss. Any subcarrier suffering a very high loss may be dropped completely to avoid the occurrence of a large number of errors on the subcarrier.

It should be noted that, for a commercialized real-case, the AMOOFDM optimization will be done using a control-channel, implemented in a higher-layer function (MAC layer). In particular, one subcarrier will be set as a control-channel (starting at a low signal modulation format) transmitting a training sequence. Afterwards, the receiver will send back to the transmitter the *BER* subcarrier distribution and individual subcarrier SNR information, in order the transmitter to change the signal modulation format in each subcarrier, keeping a total BER_T at $\leq 1.0 \times 10^{-3}$. The time duration of this negotiation between the transmitter and receiver for optimizing the system typically takes a few *msec*, and since the channel is relatively stable, the optimization

process will be repeated every 1 hour for example, without interfering to any real data. This reconfiguration of the hardware is considered to be done very fast (a few *μsec*). Even though AMOOFDM in optical communications has not been commercialized yet, the aforementioned procedure is expected to take place in future AMOOFDM development.

3.2.1 Transmission Link Model

In this Chapter, a typical single-channel, optical amplifier-free, IM/DD transmission link based on a DML operating at 1550nm is considered. The link consists of only the transmitter and the receiver linked by MMFs or SMFs as shown in Figure 3.1. In the transmitter, the generated real-valued AMOOFDM signal in the electrical domain is used to drive directly a DML to produce an optical AMOOFDM waveform, which is then coupled into a transmission link. The transmitted optical signal is detected by a photo-detector, and compared against that in the transmitter, the inverse procedure of electrical signal processing is utilised in the receiver to recover the received data. The detailed link diagrams are similar to those illustrated in Refs. [5], [15]. Numerical simulations are undertaken, based on the comprehensive theoretical AMOOFDM model developed in Refs. [5], [15] for MMF and SMF links.

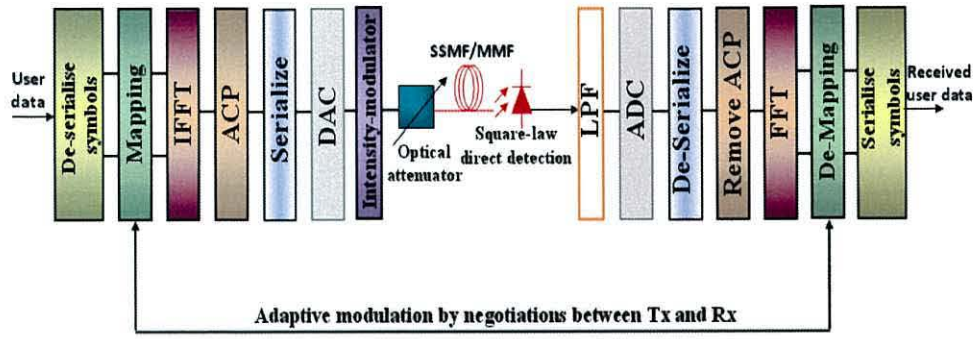

Figure 3.1: Transmission link diagram.

It should be noted that, to produce a real-valued AMOOFDM signal to drive directly the DML in the transmitter, the encoder located at the input of the IFFT is modified by creating the truncated original complex parallel data in the positive frequency bins and the complex conjugate of the data in the negative frequency bins. In addition, no power is contained in the first subcarrier (close to the signal baseband) of the positive frequency bins. The data contained in these two frequency bins are arranged specially to satisfy Hermitian symmetry. Subcarriers in all these frequency bins are able to convey useful information. In this work, information is only transmitted in the positive frequency bins recovered in the receiver.

In the receiver, all the optical signal power emerging from the link is coupled into and subsequently detected by a square-law photo-detector. The received electrical signal, $A_E(t)$, is given by

$$A_E(t) = |A_O(t)^2| \otimes R(t) + v(t) \tag{3.1}$$

where $A_O(t)$ is the optical signal coupled into the link; *R(t)* is the impulse response of the transmission link in the electrical domain; *v(t)* represents the receiver related noise and signal distortions due to intermixing amongst subcarriers and the carrier wave. The noise in the receiver is simulated following procedures similar to those presented in Ref. [21]. Both shot and thermal noises are considered, whilst signal-spontaneous noise and spontaneous-spontaneous beat noise are excluded because of the absence of optical amplifiers in the transmission link. Upon photon detection in the receiver, intermixing takes an effect. It should be noted that, based on the electrical signal waveform in the transmitter, $A_O(t)$ is simulated by using a lump DFB laser model discussed below. Therefore, $A_O(t)$ includes the DML induced nonlinear effects. In

addition, as described below, use is also made of a comprehensive SMF theoretical model to simulate the optical propagation down the SMF transmission links.

The procedures of maximizing signal modulation format levels for individual subcarriers and of choosing appropriate CP lengths are described as followings: In the initial stage of establishing a connection over a link, negotiations between the transmitter and the receiver take place to identify the highest signal modulation format that should be used on each subcarrier, based on a CP length estimated initially by using the DMD or CD value of a given transmission link. The signal modulation format can vary from DBPSK, DQPSK, and 16 to 256-QAM depending upon the frequency response of the link. Generally speaking, a high (low) modulation format is used on a sub-carrier suffering a low (high) transmission loss. The total channel, BER_T is written as

$$BER_T = \frac{\sum_{K=1}^{N_S} En_k}{\sum_{K=1}^{N_S} Bit_k} \tag{3.2}$$

where N_S is the number of subcarriers used in the positive frequency bins; En_k is the number of detected errors and Bit_k is the number of transmitted binary bits. Both En_k and Bit_k are for the k-th subcarrier, whose sub-channel BER_k is defined as $BER_k = En_k / Bit_k$. Based on BER_T and Bit_k, the signal modulation format used on a specific subcarrier can be adjusted through the negotiations. It is worth addressing that, a high signal modulation format is always preferred if BER_T remains at $\leq 1.0 \times 10^{-3}$ or better, and that any subcarrier suffering a very high loss may be

dropped completely if the corresponding BER_k, $k=\{1, 2, \ldots N_S - 1\}$ is still very large even when DBPSK is used.

After completing the first round of signal modulation format manipulation for all the subcarriers, attempts are then made to alter the initially estimated CP length to examine if the previously obtained signal capacity may be increased. The CP length alteration may vary both the signal modulation formats and/or their distribution across the subcarriers, therefore, for any changes made to CP, the aforementioned negotiation procedures are repeated, until a maximum signal transmission capacity is achieved by using a minimum CP length. Once the link has been established, the modulation format on each subcarrier and the selected CP length remain unchanged.

It is well known that direct modulation of a laser drive current introduces a nonlinear frequency chirp to the optical field, which varies with both the drive current and the optical characteristics. To simulate the nonlinear properties of a DFB-based DML, here a lumped DFB laser model developed in Ref. [5] is adopted, taking into account a wide range of nonlinear effects such as longitudinal-mode spatial hole-burning, linear and nonlinear carrier recombination and nonlinear gain. The influence of the laser linewidth on the link performance is negligible because IM/DD transmission is considered in this Chapter. The feasibility of the DFB model has been confirmed by good agreement with experimental measurements [4]. To simulate MMF links, measured impulse responses of an installed worst-case MMF [5] are adopted, whose frequency responses corresponding to a 300m link subject to central launch and small offset launch have been presented in Ref. [5]. It is assumed that the 3dB bandwidth of the link is proportional to the inverse of transmission distance. The impact of modal noise is assumed to be negligible. The validity of such an assumption has been

verified extensively by using a statistical approach developed in Ref. [18]. Here the widely adopted split-step Fourier method is employed to model the propagation of the optical signal down a SMF [22]. It is well known that for a sufficiently small fibre split step length, this theoretical treatment yields an accurate approximation to the real effects. In the SMF model, the effects of loss, CD and optical power dependence of the refractive index are included. The effect of fibre nonlinearity-induced phase noise to intensity noise conversion is also considered upon the photon detection in the receiver. This model has been successfully used in Ref. [15].

3.2.2 Signal Characteristics

To gain a better understanding of the simulated results presented in the following sections of this Chapter, the AMOOFDM-ACP signal characteristics are summarized below. The total transmitted signal bandwidth, BW_T is given by

$$BW_T = \frac{r_s}{2} = \frac{N_s(1+C_P)}{T_b} \tag{3.3}$$

where r_S is the signal sampling speed; T_b is the entire symbol period, and C_p is the ACP parameter, which is defined as

$$C_p = \frac{T_p}{T_b - T_p} \tag{3.4}$$

with T_p being the CP time duration. The symbol period used for carrying real information is $T_b - T_p$. From Equation (3.3), the entire symbol period can be written as

$$T_b = \frac{2N_s(1+C_p)}{r_s} \tag{3.5}$$

It should be pointed out that, due to the use of ADCs in the AMOOFDM transceivers, in practice, the signal sampling speeds are fixed. Therefore, it can be easily understood from Equation (3.5) that T_p increases linearly with C_p.

Due to the insertion of a CP into each symbol, the bandwidth occupied only by the signal, BW_S, is given by

$$BW_S = \frac{BW_T}{1+C_p} = \frac{r_s}{2(1+C_P)} \tag{3.6}$$

Clearly, for a fixed signal sampling speed, an increase in CP length decreases BW_S. In addition, the insertion of a CP can also decrease the effective signal SNR. Considering the noise-like nature of an OFDM signal having a fixed power, the CP-induced SNR reduction, Δ_{SNR} can be expressed as

$$\Delta_{SNR} = \frac{C_p}{1+C_p} S_{nr} \tag{3.7}$$

where S_{nr} is the signal SNR without considering the CP. It should be emphasized that, Equation (3.7) is not valid for very short CP lengths as the strong inter-subcarrier mixing effect brings about significant signal distortions [19]. Considering the operating principles of a CP, and the relationship between the dispersion tolerance of a specific signal and its bandwidth [21], the dispersion tolerance $D_{dispersion}$, of the AMOOFDM-ACP signals is proportional to $\frac{T_P}{BW_T^2}$, which can be expressed as

$$D_{dispersion} \propto \frac{8}{r_s^3} C_p N_s \tag{3.8}$$

It can be found from Equation (3.8) that, for a given r_s parameter, the dispersion tolerance increases linearly with CP length in a dispersion limited system. Finally, the signal line rate, R_b, is calculated by using

$$R_b = \frac{r_s \sum_{k=1}^{N_s-1} n_{kb}}{2N_s(1+C_p)} \tag{3.9}$$

where n_{kb} is the number of binary bits conveyed by the k-th subcarrier within one symbol period. It should be pointed out, in particular, that only when the condition of

$BER_T = 1.0 \times 10^{-3}$ is satisfied, the signal line rate is considered to be valid.

3.2.3 Simulation Parameters

In simulating the AMOOFDM-ACP modem, in the transmitter, $2N_S$ =64 subcarriers are employed, of which 31 carry real information and 1 contains no power. The remaining 32 are the complex conjugate of the aforementioned subcarriers. The powers of all the non-dropped subcarriers are considered to be identical regardless of their signal modulation formats. For QAM signals, gray-coded bit mapping is utilized for enhancing the performance of the AMOOFDM-ACP modem. ADCs are adopted with 7-bit resolution at sampling speeds of 12.5 GS/s. The signal clipping levels are fixed at 13dB. The main purpose of adopting these parameters listed above is to ease the performance comparison made with results published in previously papers [5], [15] to demonstrate the impact of ACP and explore its operation mechanisms. Of course, use can also be made of a set of the optimized modem parameters identified in Ref. [17].

For simulating the performance of the DFB-based DML operating at 1550nm, here all the DFB parameters are adopted from Ref. [5] and shown on Table 3.1, based on which the DFB laser can operate in a typical bias current range of 20-60mA (a threshold bias current of 4.2mA) and a typical peak-to-peak drive current range of 10-30mA, and produces output optical powers in a range of 5-10dBm. If the DFB operating condition of a 30mA bias current and a 15mA peak-to-peak drive current is chosen, the resulting output optical signal has a power of 6.3dBm, a signal extinction ratio of 2dB and an adiabatic frequency chirp of 5 GHz. It should be pointed out, in particular, that under such operating conditions, the DML frequency chirp effect has been found to be negligible (minimum) on the transmission performance of the AMOOFDM signals in MMFs [5] (SMFs [15]). As discussed in Refs. [5], [15], the occurrence of the minimum DML effect on the AMOOFDM transmission performance is because of the coexistence of the AMOOFDM dispersion tolerance for a specific CP, the DML operating condition dependent frequency chirp effect and the DML operating condition dependent-signal extinction ratio. In the following sections, the 30mA bias current and the 15mA peak-to-peak drive current are treated as optimum operating conditions.

Cavity length	300μm
Cross-sectional area of the active region	$0.066\mu m^2$
Photon lifetime	3.6ps
Nonlinear gain coefficient	$7.4\times10^{-23}m^3$
Linewidth enhancement factor	3
Transparency carrier density	$1.5\times10^{24}m^{-3}$
Carrier lifetime	10ns
Bimolecular recombination coefficient	$1.0\times10^{-16}m^3/s$
Auger recombination coefficient	$6.5\times10^{-41}m^6/s$
Linear gain coefficient	$7.5\times10^{-20}m^2$

Optical width (vertical)	0.47μm
Optical width (horizontal)	1.80μm
Confinement factor	0.007
Group refractive index	3.7
Phase refractive index	3.2203
Coupling efficiency from the laser chip to the SMF	38%

Table 3.1: DFB-laser parameters [5].

The feasibility of the developed DFB model is also verified by good agreement with experimental measurements [5]. The time-varying response of the laser depends on interactions within the laser cavity between the carrier densities and the photons. This process is described by the coupled ordinary differential equations given as

$$\frac{dN}{dt}=\frac{I_d}{edwl}-\frac{N}{\tau_c}-BN^2-CN^3-G\frac{(N-N_t)}{1+\varepsilon\phi}\phi \tag{3.10}$$

$$\frac{d\phi}{dt}=\frac{\Gamma G(N-N_t)}{1+\varepsilon\phi}\phi+\varsigma BN^2-\frac{\phi}{\tau_P} \tag{3.11}$$

where N and φ are the carrier density and the photon density, respectively, I_d is the current drive into the active region of the laser with length l, width w, and thickness d, e is the electronic charge, τ_c is the carrier linear recombination lifetime, representing non-radiative loss mechanisms, B is the bimolecular carrier recombination coefficient, representing the rate at which electrons and holes recombine with spontaneous emission of radiation, C is the Auger carrier recombination coefficient, which is a non-radiative loss mechanism, G is the linear gain coefficient, which describes the absorption and stimulated emission of photons, N_t is the transparency carrier density,

ε is the nonlinear gain coefficient, which describes a reduction in the gain mechanism at high photon densities because of ultrafast carrier processes such as carrier heating and spectral hole burning, Γ is the mode confinement factor, which describes the vertical overlap between the confined carrier region and the optical region, τ_p is the photon lifetime, which is closely related to the round trip time within the cavity and depends on cavity length, waveguide loss, grating, and facet reflectivities, and ς describes the fraction of spontaneous emission that is emitted into the fundamental mode of the laser, which will be negligible under normal operating conditions but determines the laser turn-on delay when driven from close to or below threshold.

It is assumed that all photons reaching the exit facet are emitted, so the output optical power is

$$P = w_v w_h h\nu \frac{\phi c}{2n_g} \tag{3.12}$$

where w_v are the vertical and horizontal widths of the guided mode power distributions, h is the Planck's constant, c is the velocity of light in vacuum, $h\nu$ is the photon energy, n_g is the group index, and the factor of 2 in accounts for bidirectional propagation of photons in the cavity.

If the optical frequency tracks the resonant frequency of the DFB cavity, the evolution of optical phase is governed by

$$\frac{d\Phi}{dt} = -\frac{\Gamma a(N - N_t)}{n_p} \tag{3.13}$$

where Φ is the optical phase, α is the linewidth enhancement factor, and n is the phase refractive index. The optical frequency is given by

$$\omega = \omega_0 \left[1 - \frac{\Gamma a (N - N_t)}{n_p} \right]. \tag{3.14}$$

Equations (3.10) — (3.14) are the final equations for simulating the performance of the DFB laser involved in the transmission link. Because there is no attempt to model input parasitic components that will modify the electrical drive current waveform, a low-bandpass filter with 7.5 GHz roll-off frequency is inserted between the DAC and the DFB laser. The following five parameters are obtained by fitting theoretical results with experimental measurements for a commercially available DFB laser. These parameters are the coupling coefficient from the laser chip to the SMF, the cavity length, the photon lifetime, the nonlinear gain coefficient, and the linewidth enhancement factor.

In the receiver, a PIN photo-detector is used, which has a quantum efficiency of 0.8 and a sensitivity of -19dBm (corresponding to a 10 Gb/s Non-Return to Zero [NRZ] with a *BER* of 1.0×10^{-9}).

The 3dB bandwidths (DMDs) of the adopted MMF link are of 202.5 MHz·km (2.0 ns/km) and 241.5 MHz·km (1.3 ns/km) for central and small offset launch, respectively [5]. For simulating SMF links, Non-Dispersion Shifted Fibres (NDSFs) are considered whose parameters are the following: effective area of $80\mu\, m^2$, dispersion parameter of 17.0 ps/(km $\cdot$ nm^2), dispersion slope of 0.07 ps/(km $\cdot$ nm), and fibre loss of 0.20 dB/km.

It should be emphasized that all the above-mentioned parameters are treated as default ones, unless addressed explicitly in the corresponding text when necessary.

3.3 Performance of AMOOFDM-ACP Signals over MMFs

3.3.1 Capacity versus Reach Transmission Performance

The AMOOFDM-ACP transmission performance subject to central and small offset launch [10] is shown in Figure 3.2 and Figure 3.3, respectively, together with the minimum CP length required for achieving the signal transmission capacity. For performance comparison, the transmission performance supported by the conventional AMOOFDM modem using a fixed CP parameter of C_p =25% is also plotted in the same figures. In obtaining these two Figures, the DMLs are set to operate at the optimum conditions discussed in section 3.2.3, and optical attenuators inserted between the DMLs and the transmission links are adjusted to ensure that the optical powers coupled into the MMF links are fixed at 0dBm.

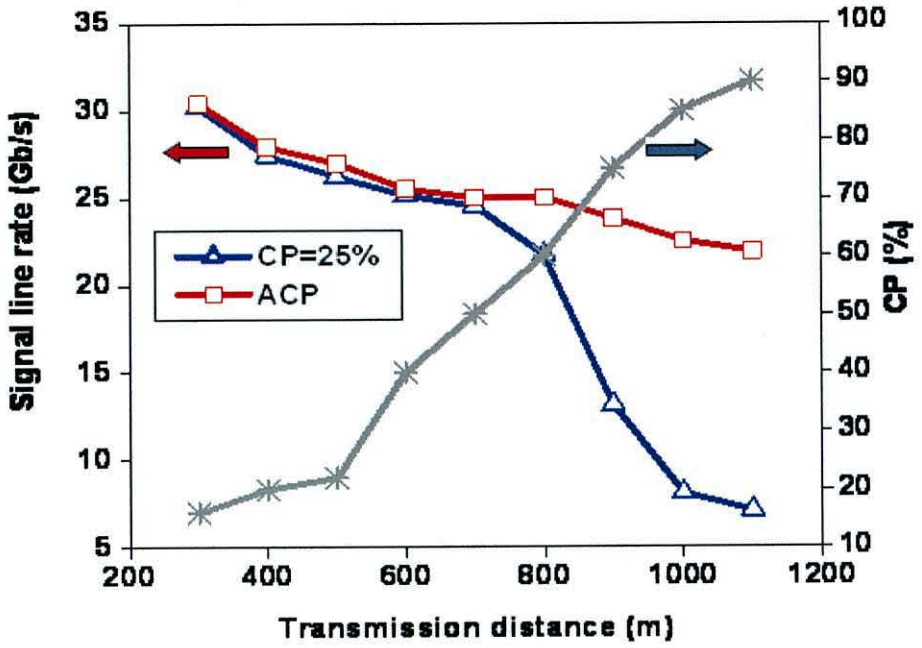

Figure 3.2: Transmission capacity (left) and minimum required CP (right) versus transmission distance over the MMF link subject to central launch.

As expected from Equation (3.8), Figure 3.2 and Figure 3.3 show that the minimum CP lengths required for completely compensating the DMDs of the MMF links increase linearly with transmission distance. In particular, in comparison with the case where AMOOFDM is considered, AMOOFDM-ACP can improve the signal transmission capacity by a factor of at least 2 for transmission distances of >1000m, over which the link DMDs are the dominant factor limiting the maximum achievable transmission performance of the technique [15]. This operation scenario can be regarded as a typical example of how ACP affects the transmission performance through ACP mechanism I.

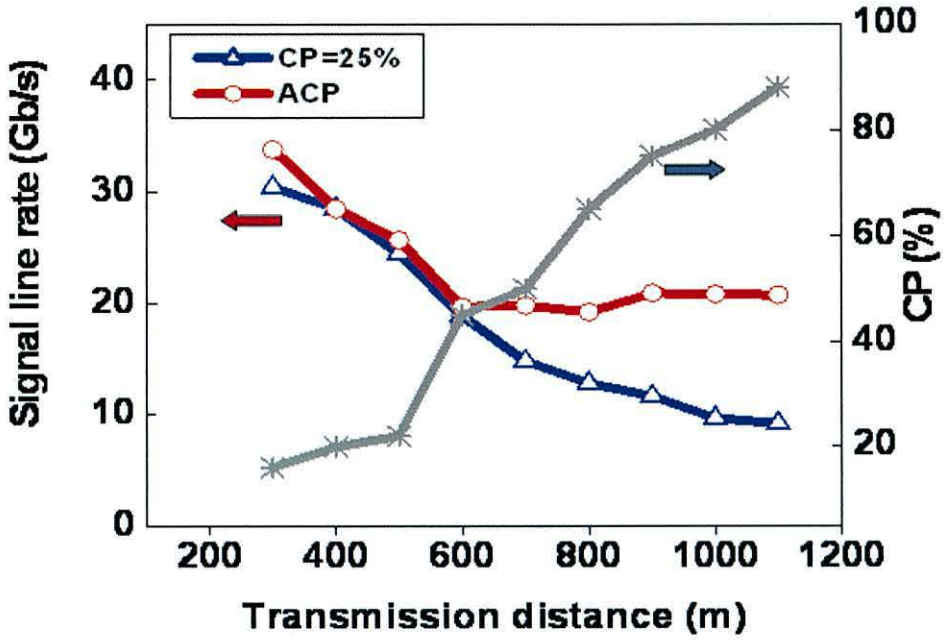

Figure 3.3: Transmission capacity (left) and minimum required CP (right) versus transmission distance over the MMF link subject to small offset launch.

As observed in Figure 3.2 and Figure 3.3, within the above-mentioned transmission distance region, the existence of the slow decay of the AMOOFDM-ACP transmission performance with increasing transmission distance is because a long CP length associated with a long transmission distance decreases the signal power used for conveying useful information. This leads to a reduced effective signal SNR and subsequently low signal modulation formats taken on subcarriers. In addition, the long distance-induced increase in link transmission loss also contributes to the decay [5].

As illustrated in Figure 3.2 and Figure 3.3, for transmission distances of <600m, the minimum required CP parameter is smaller than C_p=25%, implying that the DMDs are compensated completely by the AMOOFDM modems, and that ACP mechanism I does not contribute to the transmission performance observed in this region. Within

such a transmission distance region, the transmission performance of the AMOOFDM-ACP modems is almost identical to that achieved by the conventional AMOOFDM modems, suggesting that ACP mechanism II does not play a role for this case either. This can be explained by considering ACP mechanism III. To maintain a sufficient noise margin before the transmitted data is corrupted, due to the dependence of signal modulation format on CP length [19], a short CP length allows relatively low signal modulation formats to be taken on subcarriers. This constraint is very strong for MMF links (or long SMF links, as discussed in section 3.4, as the majority of subcarriers locating at the flat passband region of the MMF frequency responses, suffer large transmission losses of approximately 10dB below the reference frequency point [17], [18]. By considering Equation (3.9), it can be understood that the small CP length-induced short symbol time duration, together with the simultaneous reduction in the number of the binary bits contained in the symbol, gives rise to the almost identical transmission performance for both the AMOOFDM-ACP and AMOOFDM modems.

By comparing the ACP-enabled transmission performances shown in Figure 3.2 and Figure 3.3, it is very interesting to note that, the use of AMOOFDM-ACP can also improve the performance robustness to different launch conditions over the entire transmission range.

3.3.2 Link Loss Margin

Another very prominent feature of AMOOFDM-ACP is its ability to enhance the link loss margin, as demonstrated in Figure 3.4 and Figure 3.5 for different launch conditions. The link loss margin is defined as the variation range of the optical signal

power, corresponding to which a $BER_T = 1.0 \times 10^{-3}$ can be maintained without varying the adopted signal modulation formats [5], [15]. In order to alter the optical power coupled into the link, an optical attenuator is inserted between the DML and the MMF links. All other parameters are identical to those employed in simulating Figure 3.2 and Figure 3.3, except that the transmission distances are fixed at 1000m and 1100m for Figure 3.4 and Figure 3.5, respectively.

As seen in Figure 3.4 and Figure 3.5, in comparison with AMOOFDM, apart from the abovementioned significant improvement in signal transmission capacity, AMOOFDM-ACP can also enhance the link loss margin by about 1dB, which is independent upon different launch conditions. This is a direct result of ACP mechanism I, which ensures that all types of the MMF links are DMD free, regardless of different launch conditions.

It should be emphasized, in particular, that the performances similar to those shown in Figure 3.2 – Figure 3.5 are also observed in a large number of MMF links having impulse responses constructed statistically by using an approach developed in Ref. [17]. This indicates that AMOOFDM-ACP is very effective not only for the MMF link considered here, but also for the vast majority of MMF links. The detailed statistical evaluation of the effectiveness of the AMOOFDM-ACP technique will be reported elsewhere in due course.

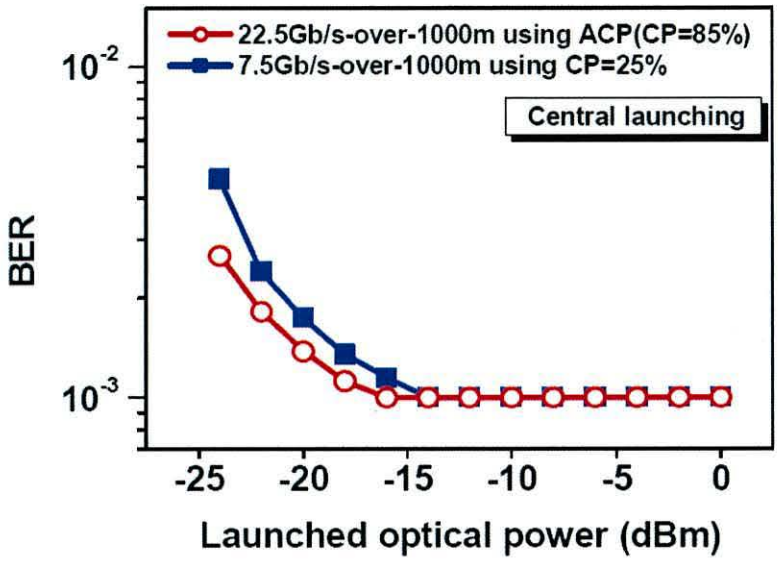

Figure 3.4: Total channel *BER* as a function of optical power launched into the 1000m MMF link subject to central launch for the cases of using CP=25% and ACP.

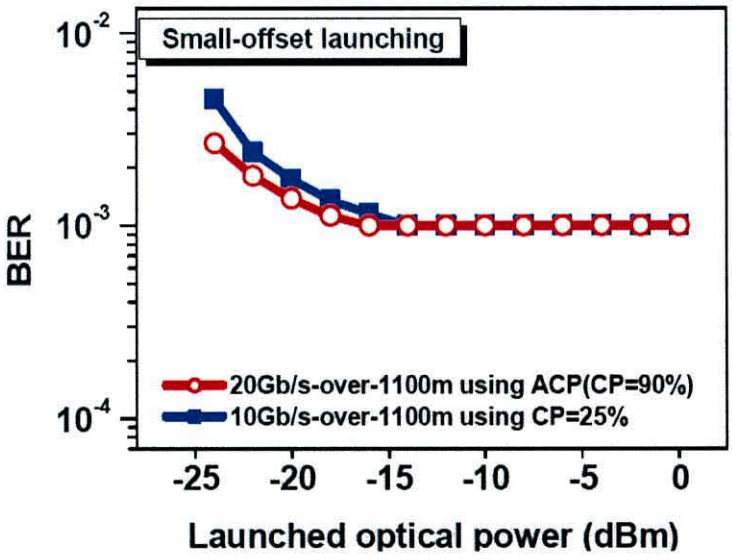

Figure 3.5: Total channel *BER* as a function of optical power launched into the 1100m MMF link subject to small offset launch for the cases of using CP=25% and ACP.

3.4 Performance of AMOOFDM-ACP Signals over SMFs

3.4.1 Capacity versus Reach Transmission Performance

Similar to those illustrated in Figure 3.2 and Figure 3.3, the signal line rate, the minimum required CP length and the corresponding transmission performance supported by the conventional AMOOFDM technique for SMF links are shown in Figure 3.6, where a DML and an ideal-intensity modulator are considered. The inclusion of the DML is because the DML-induced nonlinear effects are no longer negligible for SMF links [15]. In simulating Figure 3.6, an optical power of 6.3dBm is assumed to be coupled into the SMF link.

For the case where the DML model is considered, Figure 3.6 shows that, compared to that achieved by AMOOFDM, AMOOFDM-ACP is capable of improving the transmission performance by a factor of approximately 1.3 for transmission distances of <80km. Over such a transmission distance region, the minimum required CP length grows linearly with transmission distance. This agrees very well with the results obtained in Refs. [15], [20]. The minimum required CP lengths are smaller than the fixed CP value of 25%, indicating that the present systems are free from the ACP mechanism I effect.

The observed signal transmission capacity improvement results from ACP mechanism II. Since the SMF frequency response for <80km is broad, which is capable of providing the majority of subcarriers with relatively low transmission losses. Sufficiently large noise margins are, therefore, available to enable that individual

subcarriers can accommodate a SNR growth caused by the reduced CP length, causing that the signal modulation formats are independent of the variation in the CP length. On the other hand, a small CP length produces a short OFDM symbol period. As a direct result of the co-existence of these two processes, the improvement in signal transmission capacity occurs, as shown in Figure 3.6.

It can also be seen in Figure 3.6 that, the transmission performance of the AMOOFDM-ACP signals using the DML model is very similar to that achieved by the AMOOFDM signals for transmission distances of >80km, over which the link loss and the receiver noise dominate the transmission performance [15]. To partially overcome the noise effect, use can be made of a relatively small CP length to increase the effective signal SNR. This is verified in Figure 3.6, where a slight increase in signal capacity occurs for a reduced CP length in a transmission distance range of 80 – 100km. However, such a capacity improvement is considerably low, compared to that observed for <80km. ACP mechanism III is responsible for such a signal transmission capacity developing trend, because the SMF frequency response becomes narrow with increasing transmission distance, and deep frequency response nulls occur in the signal spectral region. From the above analysis, it is clear that ACP mechanism III sets a minimum CP length for a given transmission link, as shown in Figure 3.6.

For the case where an ideal-intensity modulator is considered, Figure 3.6 shows that, over the entire transmission distance range, the transmission performance of the AMOOFDM-ACP signals is increased by a factor of about 1.2, compared against that achieved by AMOOFDM. ACP mechanism II is the physical reason behind such behaviors. However, this improvement is not as significant as that observed for the

DML case for <80km. This can be explained by considering the processes described as follows: The ideal-intensity modulator produces a double sideband optical signal in the transmitter, upon the photon detection in the receiver, intermixing between the carrier wave and each of these sidebands distort severely the received signal, giving rise to the observed transmission performance degradation. On the other hand, the performance improvement for transmission distances beyond this region is mainly due to an increase in the effective signal SNR. The transmission link loss and the receiver noise play key roles in determining the transmission performance for >80km. The signal extinction ratio corresponding to the ideal-intensity modulator is much higher than that corresponding to the DML. For a fixed input optical power, the signal produced by the ideal-intensity modulator has a high effective signal SNR, which enhances the tolerance to the link loss and the receiver noise, as well as the reduced bandwidth of the SMF frequency response for long transmission distances.

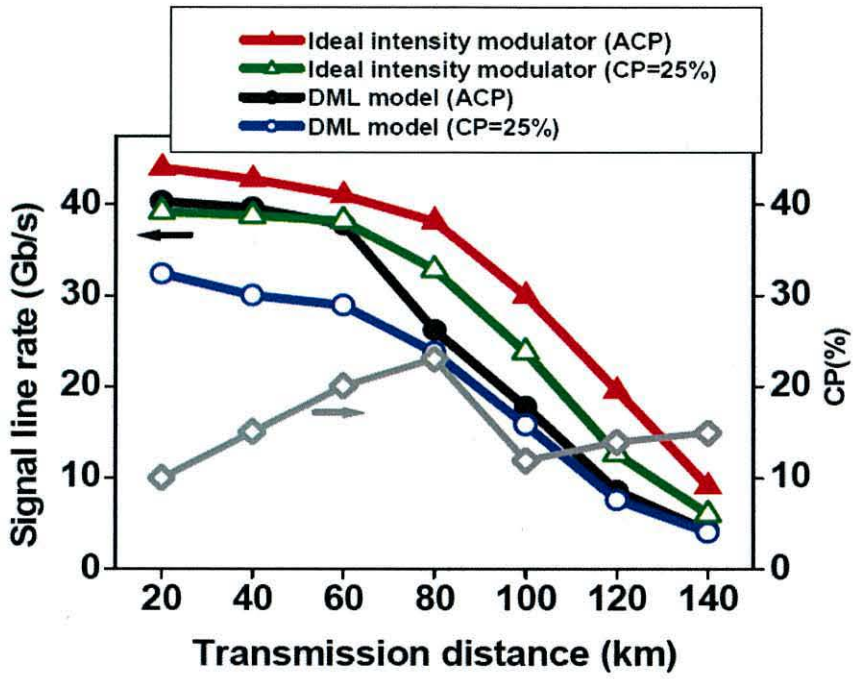

Figure 3.6: Transmission capacity (left) and CP (right) versus transmission distance in the SMF link including and excluding the DML model.

3.4.2 Link Loss Margin

In Figure 3.7, the link loss margin is plotted as a function of transmission distance. Here numerical simulations are undertaken for a SMF link involving the DML operating at optimum conditions. It can be found from Figure 3.7 that, for transmission distances of <80km, apart from the significant signal capacity improvement discussed previously, AMOOFDM-ACP can also increase the link loss margin by about 1dB, compared to that achieved by AMOOFDM. As already discussed in Figure 3.6 the observed link loss margin improvement mainly results from ACP mechanism II. Whilst for transmission distances beyond 80km, the obtained link loss margins are almost identical to those offered by AMOOFDM, because the transmission links are transmission loss-limited.

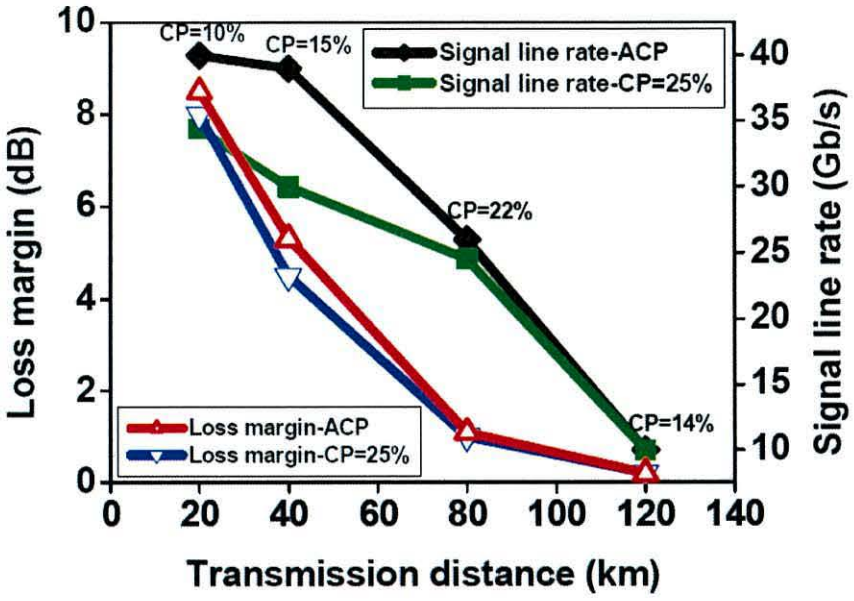

Figure 3.7: Link loss margin and signal line rate as a function of transmission distance in a SMF link for the AMOOFDM-ACP and AMOOFDM modems.

3.5 ACP-Enabled DFB Bandwidth Relaxation

Given the fact that the frequency chirp induced by a DFB laser-based DML is closely related to the DFB bandwidth, a large DFB bandwidth is thus preferred in practical system design. However, a commercially available DFB laser has a bandwidth of typically 10 GHz, which is comparable to the transmitted signal bandwidth. Therefore, it is greatly advantageous if a simple and cost-effective approach can be identified to relax the requirement on the DFB bandwidth without compromising the transmission performance. Fortunately, the use of ACP can fulfill this goal.

The signal line rate as a function of DFB bandwidth for different CP lengths is shown in Figure 3.8 for a 1000m MMF link subject to central launch condition. Since a large bias current gives a high DFB bandwidth, the variation in DFB bandwidth is obtained

by altering the bias current with a peak-to-peak drive current being fixed at 15mA. All other parameters are the same as those adopted in Figure 3.2.

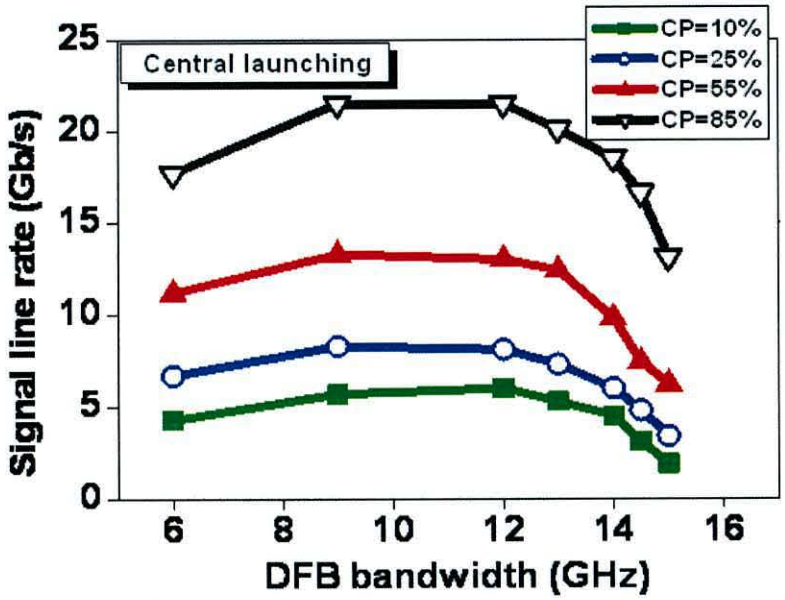

Figure 3.8: Signal line rate as a function of DFB bandwidth for different CP lengths over a 1000m MMF link subject to central launch.

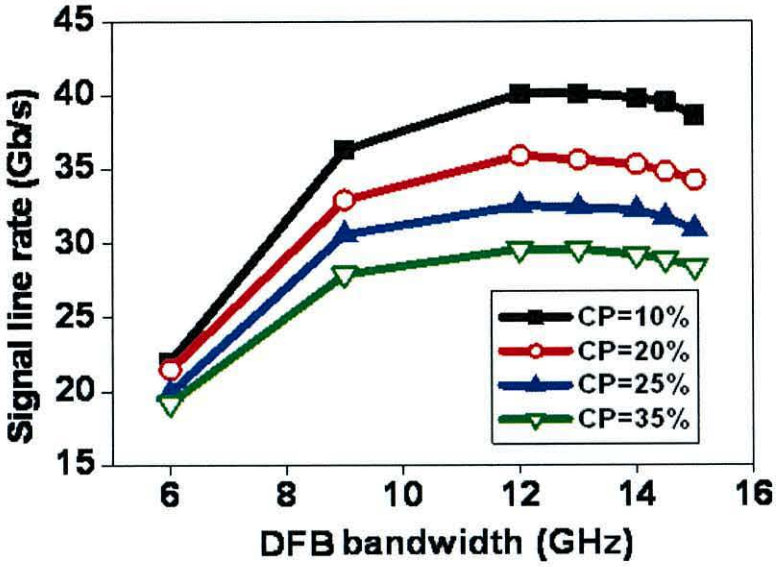

Figure 3.9: Signal line rate as a function of DFB bandwidth for different CP lengths over a 20km SMF link.

It can be seen from Figure 3.8 that, for achieving a specific signal transmission capacity, ACP can significantly relax the requirement on the DFB bandwidth, ACP can always compensate completely for the DMDs associated with the link. It is interesting to note that, for a given CP length, there exists an optimum DFB bandwidth, corresponding to which a maximum signal transmission capacity can be found. For DFB bandwidths smaller than the optimum value, the signal capacity reduction shown in Figure 3.8 is due to the imperfect DMD compensation for the adopted CP length; whilst for DFB bandwidths larger than the optimum value, the decreased signal extinction ratio contributes to the sharp fall in signal transmission capacity, as shown in Figure 3.8. In addition, with shortening the CP length, a high DFB bandwidth is necessary to compensate completely for the DMD, resulting in the optimum DFB bandwidth shifting towards the high bandwidth region, as illustrated in Figure 3.8.

As seen from Figure 3.9, ACP is also very effective for relaxing the requirement on the DFB bandwidth for SMF links. In calculating Figure 3.9, a 20km SMF link is utilized and all other parameters are identical to those adopted in Figure 3.7. Since ACP mechanism II is responsible for the transmission performance improvement over this transmission distance region, a short CP length in Figure 3.9 is, on the contrary to Figure 3.8, preferable to effectively lower the DFB bandwidth requirement for achieving a given signal transmission performance. Furthermore, compared with Figure 3.8, the signal line rate shown in Figure 3.9 drops sharply with decreasing the DFB bandwidth, this is because the small DFB bandwidth enhances the DFB-induced frequency chirp effect.

3.6 Conclusions

By introducing ACP into the conventional AMOOFDM technique, a new AMOOFDM-ACP technique has been proposed. Detailed investigations of the impact of ACP on the transmission performance of the AMOOFDM-ACP technique have been undertaken in a single channel, DML-based, IM/DD MMF and SMF links without optical amplification and dispersion compensation. It has been shown that, in comparison with AMOOFDM having a fixed CP parameter of 25%, AMOOFDM-ACP can improve the signal transmission capacity by a factor of at least 2 (1.3) for transmission distances of >1000m MMFs (<80km SMFs), together with 1dB improvement in link loss margin. Furthermore, ACP can also enhance the flexibility and robustness of the systems. Finally, numerical simulations have also shown that

the AMOOFDM-ACP technique can significantly relax the requirement on the DFB bandwidth for achieving a specific signal transmission capacity. It is also worth mentioning that the experimental verification of the effectiveness of the proposed ACP technique is currently being undertaken, and results will be reported elsewhere in due course.

Three mechanisms have been identified, through which ACP affects significantly the transmission performance of the technique. The effectiveness of these mechanisms depends upon the transmission link properties. It is expected that both ACP mechanism I and ACP mechanism II are also effective for coherent OOFDM systems, in which, however, the ACP mechanism III effect is negligible because of the existence of flat SMF frequency responses.

References

[1] M. Franceschini, G. Bongiorni, G. Ferrari, R. Raheli, F. Meli, and A. Castoldi, "Fundamental limits of electronics signal processing in direct-detection optical communications", IEEE J. Lightwave Technol., vol. 25, pp. 1742–1753, 2007.

[2] P. Watts, R. Waegemans, M. Glick, P. Bayvel, and R. Killey, "An FPGA-based optical transmitter design using real-time DSP for advanced signal formats and electronic predistortion," IEEE J. Lightwave Technol., vol. 25, pp. 3089–3099, 2007.

[3] J. Heiskala and J. Terry, OFDM Wireless LANs: a Theoretical and Practical Guide (Indianapolis, IN: Sams 2002).

[4] N. E. Jolley, H. Kee, R. Rickard, J. M. Tang, and K. Cordina, "Generation and propagation of a 1550 nm 10 Gb/s optical orthogonal frequency division multiplexed signal over 1000m of multimode fibre using a directly modulated DFB", Optical Fiber Communication Conf./National Fiber Optic Engineers Conf. (OFC/NFOEC), (Anaheim, CA, 2005), Paper OFP3.

[5] J. M. Tang, P. M. Lane, and K. A. Shore, "High-speed transmission of adaptively modulated optical OFDM signals over multimode fibers using directly modulated DFBs", IEEE J. Lightwave Technol., vol. 24, pp. 429-441, 2006.

[6] J. M. Tang, and K. A. Shore, "Maximizing the transmission performance of adaptively modulated optical OFDM signals in multimode-fiber links by optimizing analog-to-digital converters", IEEE J. Lightwave Technol., vol. 25, pp. 787-798, 2007.

[7] W. Shieh, H. Bao, and Y. Tang, "Coherent optical OFDM: theory and design", Opt. Express, vol. 16, pp. 841-859, 2008.

[8] A. J. Lowery, "Amplified-spontaneous noise limit of optical OFDM lightwave systems", Opt. Express, vol. 16, pp. 860-865, 2008.

[9] L A. Buckman, B. E. Lemoff, A. J. Schmit, R. P. Tella, and W. Gong, "Demonstration of a small-form-factor WWDM transceiver module for 10-Gb/s local area networks," IEEE Photon. Technol. Lett., vol. 14, pp. 702-704, 2002.

[10] L. Raddatz, I. H. White, D. G. Cunningham, and M. C. Nowell, "An experimental and theoretical study of the offset launch technique for the enhancement of the bandwidth of multimode fiber links", IEEE J. Lightwave Technol., vol. 16, pp. 324–331, 1998.

[11] M. Webster, E. J. Tyler, A. Wonfor, R.V. Penty, and I. H. White, "Novel cascaded optical coding schemes for bandwidth efficient systems applications", Proc. Optical Fiber Communication Conf. and Exhibit (OFC), vol. 3, (Anaheim, CA, 2001), pp. WDD47-1–WDD47-3.

[12] R. A. Panicker, J. P. Wilde, J. M. Kahn, D. F. Welch, and I. Lyubomirsky "10×10Gb/s DWDM transmission through 2.2-km multimode fiber using adaptive optics", IEEE Photon. Technol. Lett., vol. 19, pp. 1154–1156, 2007.

[13] P. M. Watts, V. Mikhailov, S. Savory, P. Bayvel, M. Glick, M. Lobel, B. Christensen, P. Kirkpatrick, S. Shang, and R. I. Killey, "Performance of single mode fiber links using electronic feed-forward and decision feedback equalizers", IEEE Photon. Technol. Lett., vol. 17, pp. 2206–2208, 2005.

[14] M. Cavalari, C. R. S. Fludger, and P. Anslow, "Electronic signal processing for differential phase modulation formats", presented at the OFC, (Los Angeles, CA, 2004), Paper TuG2.

[15] J. M. Tang, K. A. Shore, "30-Gb/s signal transmission over 40-km directly modulated DFB-laser-based single-mode-fiber links without optical amplification and dispersion compensation", IEEE J. Lightwave Technol., vol. 24, pp. 2318-2327, 2006.

[16] J. M. Tang, P. M. Lane, and K. A. Shore, "Transmission performance of adaptively modulated optical OFDM signals in multimode fiber links", IEEE Photon. Technol. Lett., vol. 18, pp. 205-207, 2006.

[17] X. Q. Jin, J. M. Tang, P. S. Spencer, and K. A. Shore, "Optimization of adaptively modulated optical OFDM modems for multimode fiber-based local area

networks", IEEE J. Opt. Netw., vol. 7, pp. 198-214, 2008. http://www.opticsinfobase.org/abstract.cfm?URI=JON-7-3-198

[18] X. Q. Jin, J. M. Tang, K. Qiu and P. S. Spencer, "Statistical investigations of the transmission performance of adaptively modulated optical OFDM signals in multimode fibre links", IEEE J. Lightwave Technol., vol. 26, 2008 (accepted for publication).

[19] L. Hanzo, S. X. Ng, T. Keller, and W. Webb, Quadrature Amplitude Modulation: From Basics to Adaptive Trellis- Coded, Turbo-Equalised and Space-Time Coded OFDM, CDMA and MC-CDMA Systems (Wiley, 2004).

[20] B. J. C. Schmidt, A. J. Lowery, and J. Armstrong, "Experimental demonstrations of electronic Dispersion compensation for long-haul transmission using direct-detection optical OFDM," IEEE J. Lightwave Technol., vol. 26, pp. 196 – 203. 2008.

[21] G. P. Agrawal, *Fibre-Optic Communication Systems*, (Wiley, 1997).

[22] G. P. Agrawal, *Nonlinear Fibre Optics*, (Academic, 1995).

CHAPTER 4

Adaptive Loading Algorithms

Contents

4.1 Introduction.....126
4.2 Theoretical OOFDM SMF/MMF-Based Model, Statistical Construction of Worst-Case MMF links, and Simulation Parameters.....129
4.2.1 Statistical Construction of Worst-Case MMF links.....130
4.2.2 Simulation Parameters for SMF/MMF-based links.....132
4.3 Implementation of Adaptive Loading Algorithms.....133
4.4 Statistical Performance of Adaptive Loading Algorithms over MMF links.....138
4.4.1 Impact of Transmission Distance on Adaptive Loading Algorithms.....138
4.4.2 Impact of Subcarrier Number and Sampling Speeds 141
4.5 Adaptive Loading Algorithm Performance over SMF links.....144
4.5.1 Impact of Transmission Distance and Launched Optical Power.....144
4.5.2 Impact of Subcarrier Number and Sampling Speeds.....149
4.6 Conclusions.....152
References.....154

4.1 Introduction

OOFDM offers great potential for providing a cost-effective, high-speed, "future-proof" technical solution, due to full utilization of the rapid advances in modern DSP technology [1]. To maximize the OOFDM transmission performance and simultaneously improve the system flexibility and performance robustness, full use can be made of orthogonality among different subcarriers within an OOFDM symbol by applying various adaptive loading algorithms on each individual subcarrier, according to the SNR experienced by the subcarrier [2]. The widely adopted adaptive loading algorithms include BL, PL, and BPL, all of which can be implemented using the well-known "water-filling" approach. In the BL algorithm [3], [4], different signal modulation formats are taken on individual subcarriers which have identical electrical powers. In the PL algorithm [1], [5], [6], electrical subcarrier powers are manipulated with the same signal modulation format being taken on all those subcarriers. Finally, in the BPL algorithm [7], [8], [9], [10], both the power and signal modulation format of each individual subcarrier are adjusted independently. Each of these adaptive loading algorithms can be utilized to maximize the signal bit rate for a given *BER* and a fixed power constraint or to minimize the *BER* for a given signal bit rate in order to increase the system power budget. Throughout this Chapter, the option of employing the adaptive loading algorithms to increase the signal bit rate is considered.

Of these three adaptive loading algorithms, the BPL algorithm has the ability of achieving the largest signal bit rate [7], [8], [9], [10] but it suffers from the highest level of computational complexity and requires sophisticated OOFDM transceiver designs to accommodate the variations in both the number of bits per symbol and the selective signal modulation formats [1]. On the other hand, as a direct result of the

least computational complexity and the simplest OOFDM transceiver architecture, the PL algorithm has been experimentally implemented successfully in end-to-end real-time OOFDM transceivers at 11.25 Gb/s, using low-cost, off-the-shelf electrical and optical components [1]. In addition, the effectiveness of the PL algorithm has been experimentally confirmed recently, showing in end-to-end real-time IM/DD OOFDM transceivers over < 35km [10] that it offers transmission capacity degradation of maximum at only about 7% compared to the sophisticated BPL algorithm.

As the statement that different adaptive loading algorithms offer similar transmission performances, may have huge potential for practical cost-effective OOFDM SMF/MMF-based transceiver architecture for various applications scenarios including LANs and PONs which have become very popular recently due to the unstoppable bandwidth demand. Detailed explorations of the validity of the above statement in MMF/SMF-based transmission links are of great importance. Considering the fact, that, the IM/DD SMF links employed in Refs. [1], [10], have very simple system frequency responses with approximately Gaussian profiles, the employment of legacy MMFs with more complicated system frequency responses are therefore essential.

As different MMF links reveal large variations in both the 3dB bandwidths and the system frequency responses [11], [12], any explorations of the topic of interest of the present work over a specific MMF link are not adequate. Hence, statistical investigations of the performance of these three algorithms are undertaken over 1000 statistically constructed worst-case MMF links. The use of the worst-case MMF links is due to the fact that their corresponding frequency responses have more unpredictable peaks and nulls occurring within the signal spectral region. This

Chapter tenders for the first time a complete study of adaptive loading algorithms evaluations over OOFDM MMF/SMF-based transceivers for LANs and PONs.

It was shown that, firstly, for both worst-case and normal-case MMF links of < 300m, in comparison with the most sophisticated BPL algorithm, the simplest PL algorithm is sufficiently effective in escalating the OOFDM MMF links performance to its maximum potential. The effectiveness of the PL algorithm was further improved when a large number of OOFDM subcarriers were utilized. On the other hand, for relatively long MMF links with their 3dB bandwidths being much less than the transmitted OOFDM signal spectrum, the sophisticated BPL algorithm has to be adopted. Secondly, for the case when SMF links are employed, it is shown that over transmission distances of < 100km, and over a wide range of launched optical powers, in comparison with the most sophisticated BPL algorithm, the simplest PL algorithm is effective in escalating the OOFDM SMF links performance to its maximum potential. On the other hand, when employing a large number of subcarriers and a high DAC/ADC sampling speed, the sophisticated BPL algorithm has to be adopted. It should be noted that results agree very well with the real-time experimental IM/DD OOFDM SMF-based measurements.

4.2 Theoretical OOFDM SMF/MMF-Based Model, Statistical Construction of Worst-Case MMF links, and Simulation Parameters

A representative single-channel DML-based OOFDM IM/DD transmission system considered in this Chapter is illustrated in Figure 4.1, where the PL, BL, and BPL algorithms are conducted via negotiations between the corresponding elements of the transmitter and receiver, as indicated in Figure 4.1. It should also be noted that inline optical amplification and CD compensation is not included.

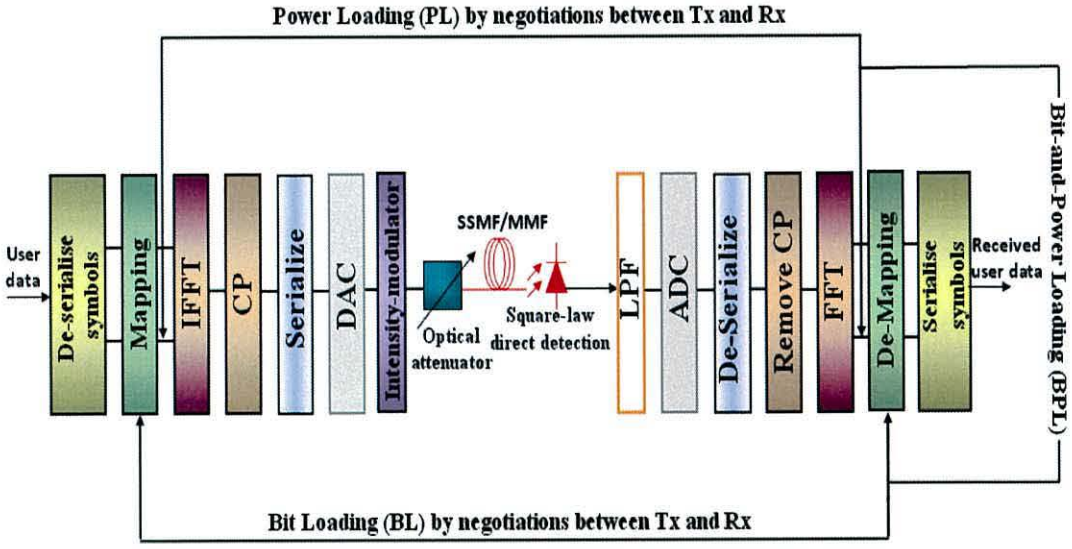

Figure 4.1: IM/DD SMF and MMF-based systems showing the PL, BL, and BPL algorithms.

In simulating the OOFDM transceivers, the signal generation, transmission, and detection procedures similar to those reported in Refs. [4], [11], [12] are adopted. Here, 64 subcarriers are employed, of which 31 carry real user information, and one contains no power, and the remaining 32 are the complex conjugate of all the aforementioned subcarriers. The DAC/ADC operates at optimum 7-bit resolution and

12.5 GS/s sampling speeds. The signal clipping levels are fixed at 13dB, and the CP parameter is taken to be 25% [4]. It should be noted that a boundary condition for the current optical variable data rate manipulation is that the electrical and optical bandwidth for the signal is constant. This is desirable as no hardware adjustment is required, namely, no filter bandwidth adjustment is required.

4.2.1 Statistical Construction of Worst-Case MMF links

By using the approach presented in Ref. [11], the impulse response of a MMF link can be constructed by

$$h(t) = \sum_{m=1}^{M} \beta_m \cdot g(t - \tau_m) \tag{4.1}$$

where *g(t)* is the optical pulse, which corresponds to an excited optical mode; *M* is the total number of the optical modes propagating simultaneously through the link; and τ_m and β_m are the time delay and the amplitude of the *m*-th optical mode. In order to statistically construct 1000 worst-case MMF impulse responses, the following assumptions are considered [11]:

- A Gaussian pulse shape for each optical mode;
- A uniform optical mode time delay distribution with respect to an average time delay with a maximum time deviation being half of the maximum DMDs of 2ns/km. Such a DMD value can represent the worst 5% of all MMF links operating at long wavelengths [11];
- An identical optical mode power distribution across all the excited optical modes.

The adoption of the aforementioned three assumptions results in that the 3dB optical bandwidths of all the constructed worst-case MMF links are much smaller than the standard bandwidth-length production of 500 MHz·km. It should be pointed out that the worst-case MMF impulse responses are constructed under a specific transmission distance of, say, 300m; then, these impulse responses are scaled linearly using the transmission distance required by assuming that the 3dB link bandwidth is proportional to the inverse of transmission distance. When 80 optical modes with their corresponding optical pulse widths being fixed at 10 ps are used [11], the constructed 1000 worst-case MMF links have 3dB bandwidths varying in a range of 220–490 MHz·km. A linear fibre loss of 1 dB/km is also assumed. The validity of the statistical worst-case MMF impulse response construction approach has been verified in Ref. [11].

In this work, the impact of MMF modal noise is assumed to be negligible for the following three reasons:

1) All the transmitted light emerging from the output facet of the MMF transmission link is assumed to be coupled into the photodiode;
2) No mode filtering components are utilized in the entire transmission link;
3) Mode Selective Loss (MSL) is relatively low for restricted launching conditions. The validity of such an assumption has been verified statistically in Refs. [11], [12]. More importantly, experimental measurements have also suggested [13] that, for a typical 500m OOFDM MMF system, the power penalty induced by modal noise is about 1dB, which, from a practical link design point of view, is much smaller than the typical system power budget of > 20dB.

4.2.2 Simulation Parameters for SMF/MMF-based links

Since the influence of optical nonlinearities induced by DMLs under optimum operating conditions is negligible on the transmission performance of OOFDM signals over MMF links [11], for simplicity without losing generality, an ideal optical intensity modulator at 1550nm is thus considered which produces a 5dBm optical power coupled into the MMF links.

For the case of SMF links, a comprehensive SSMF model used successfully in Chapter 3 is adopted using the split-step Fourier method to model the propagation of the optical signal [4]. It is well known that for a sufficiently small fibre split-step length, this theoretical treatment yields an accurate approximation to the real effects. In the SSMF model, the effects of fibre loss, CD, polarization dependence of Kerr nonlinearity and optical power dependence of the refractive index are included. The effect of fibre nonlinearity-induced phase noise to intensity noise conversion is also considered. To simulate the nonlinear properties of DFB laser-based DML for SSMF links, a lumped DFB laser model developed successfully in Chapter 3 and Ref. [4] is adopted, taking into account a wide range of nonlinear effects such as longitudinal-mode spatial hole burning, linear and nonlinear carrier recombination and ultrafast nonlinear gain compression.

In the OOFDM MMF/SMF-based receivers, a square-law photo-detector is employed, having a quantum efficiency of 0.8 and a sensitivity of -19 dBm (corresponding to a 10 Gb/s NRZ with a *BER* of 1.0×10^{-9}).

4.3 Implementation of Adaptive Loading Algorithms

Given the central role of adaptive loading algorithms and the large number of statistically constructed worst-case MMFs utilized, it is necessary to discuss the implementation of these algorithms in our numerical simulations. The adaptive allocation of bit and/or power on each individual OOFDM subcarrier is justified as optical transmission channels remain relatively stable in time. Such adaptive allocation processes also require the knowledge of the Channel State Information (CSI), which can be easily obtained, both theoretically [4], [11], [12] and experimentally [1], [10], [13], using pilot signals implemented in the OOFDM transceiver design. Through negotiations between the transmitter and the receiver, as illustrated in Figure 4.1, all the adaptive loading algorithms can thus be implemented according to the total channel BER_T and each individual subcarrier BER from Equation (3.4) (see Chapter 3). The descriptions of the implementation of these adaptive loading algorithms are detailed below:

- ***Power Loading (PL)***

  According to the system frequency response of a specific transmission link, a maximum possible signal modulation format is taken on all the subcarriers within an OOFDM symbol, and each individual subcarrier power is optimized to ensure that the individual subcarrier $BERs$ detected in the receiver are almost uniformly distributed among all the subcarriers and that the corresponding total channel BER_T is $< 1.0\times10^{-3}$.

- ***Bit Loading (BL)***

  Depending upon the system frequency response, the BL algorithm enables the signal modulation format taken on each individual subcarrier within an

OOFDM symbol to vary with the non-dropped subcarrier having identical powers. Generally speaking, a high (low) signal modulation format is used on a subcarrier experiencing a high (low) SNR. The detailed BL implementation procedures adopted here are similar to those presented in Refs. [4], [11], [12].

- ***Bit-and-Power Loading (BPL)***

  There is a wealth of literature on practical implementation of the BPL algorithm in OOFDM/OFDM systems [7], [8], [9], [14], [15]. For the present case where 1000 statistically constructed worst-case MMF links are considered, the following BPL implementation approach is proved to be very effective, which is thus adopted in our numerical simulations. The descriptions of the approach are given below:

1) For a specific MMF link, by assigning identical powers for individual subcarriers regardless of their signal modulation formats, the BL algorithm is first applied with the highest possible signal modulation format (256-QAM) being taken on each individual subcarrier.
2) The generated OOFDM signal is transmitted through the MMF link. After transmission, the total channel BER_T and the individual subcarrier BER are calculated in the receiver. If the total channel BER_T is $< 1.0\times10^{-3}$, then the signal line rate R, which is calculated using the equation given below, is considered to be the final result, and the simulation process for the MMF link stops.

$$R = \sum_{k=1}^{N_s-1} R_{bk} = \frac{r_s \sum_{k=1}^{N_s-1} n_k}{2N_s\left(1+C_p\right)} \tag{4.2}$$

where R_{bk} is the signal bit rate transmitted by the k-th subcarrier, n_k is the total number of binary bits conveyed by the k-th subcarrier within one symbol period, N_S is the total number of data-carrying subcarriers in the positive frequency bins, r_s is the sampling speeds of the DAC/ADC, and C_P is the CP parameter [4].

If the total channel BER_T is > 1.0×10^{-3}, then the PL algorithm is applied, as described in Step 3.

For an OOFDM system with a new MMF link, during Step 2, the SNR of the k-*th* subcarrier, i.e., SNR_k , is also calculated using pilot signals and the thermal and shot noise associated with the PIN-detector involved in the receiver [11], [12]. As SNR_k includes the channel attenuation, linear, and nonlinear system impairments and receiver noise [16], SNR_k, represents the quality of the sub-channel.

3) The purpose of Step 3 is to make use of the signal modulation format distribution assigned in Step 2 to minimize the *BER* performance using the PL algorithm based on the well-known "water filling" method. Taking into account the SNR_k obtained in Step 2, the optimum electrical power P_{Ok} that is allocated on the k-th subcarrier in the transmitter is computed by [17],

$$P_{Ok} = C_\lambda - \frac{\Gamma_k}{SNR_k} \tag{4.3}$$

where Γ_k is the SNR gap between the SNR required to achieve the Shannon capacity and the SNR required to achieve the present capacity, R_{bk}, at a given

BER. Since the subcarrier bandwidth BW_k and the subcarrier capacity, R_{bk} are made known, Γ_k can be estimated by

$$\frac{R_{bk}}{BW_k} = \log_2\left(1+\frac{SNR_k}{\Gamma_k}\right) \tag{4.4}$$

C_λ is the constant governed by

$$C_\lambda = \frac{1}{N_s}\left(\rho + \sum_{k=1}^{N_s-1}\frac{\Gamma_k}{SNR_k}\right) \tag{4.5}$$

where ρ is the fixed total power budget.

4) Having indentified an optimum electrical power for each individual subcarrier, an updated OOFDM signal is generated, transmitted through the same MMF link and detected in the receiver. If total channel $BER_T < 1.0\times10^{-3}$, the signal line rate calculated in Step 2 is considered to be the final result, and the simulation process for the MMF link stops. On the other hand, if the total channel BER_T is still $> 1.0\times10^{-3}$, the signal modulation format taken on each subcarrier with a subcarrier *BER* of $> 1.0\times10^{-3}$ is reduced to its adjacent low level. After that, a new OOFDM signal is generated and Steps 2-4 are repeated.

A diagram displaying the procedure of the BPL algorithm calculation is depicted below in Figure 4.2:

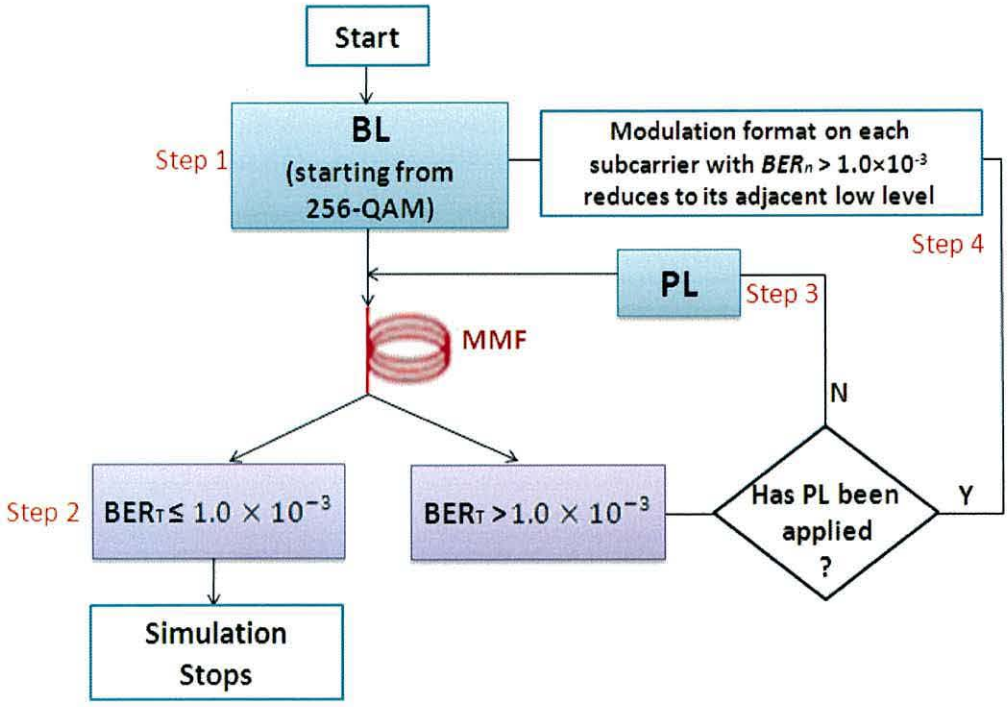

Figure 4.2: BPL algorithm calculation procedure.

For the case of SMF links all aforementioned adaptive loading algorithms procedures described are adopted in a similar manner.

For fair comparisons between the adaptively loading algorithms for both SMF/MMF links, it is worth highlighting the following aspects:

1) For a given transmission system, the total electrical signal powers generated by all the algorithms are set to be identical, and comparisons of maximum achievable transmission capacity at a $BER_T = 1.0\times10^{-3}$ are made;
2) Signal modulation formats vary from DBPSK, DQPSK, and 8-QAM up to 256-QAM;
3) Any subcarrier suffering a very low SNR may be dropped completely if the following condition is met: for the PL algorithm only, the detected errors are too large to achieve the required total channel BER_T; for the BL and BPL

algorithms, the detected errors are too large to achieve the required total channel BER_T even when the lowest signal modulation format is employed.

Finally, it should be noted that for the sophisticated BPL algorithm the minimum number of iterations in optimizing was 2 and the maximum was 50.

4.4 Statistical Performance of Adaptive Loading Algorithms over MMF links

Due to the statistical nature of the numerical results presented in this section, the Cumulative Density Function (CDF) is thus utilized to describe the performance of various adaptive loading algorithms for different MMF link conditions and OOFDM transceiver parameters.

4.4.1 Impact of Transmission Distance on Adaptive Loading Algorithms

For different adaptive loading algorithms, Figure 4.3 (a)-(c) shows the CDF versus signal line rate for worst-case MMF links of lengths of 300m, 800m and 1500m, respectively. In obtaining Figure 4.3, all the parameters listed in section 4.2 are adopted including $N_s = 32$. In Figure 4.3 (d), a typical example of a MMF link frequency response plot together with the signal modulation format allocation on subcarriers is illustrated when the BL algorithm is applied over 800m MMF link transmission distance. For this simple example it is observed that at lower power peaks on the MMF spectrum low signal modulation formats can be used, while higher signal modulation formats over higher power regions are taken. For all the MMF

links, Figure 4.3 shows that the BPL (PL) algorithm always offers the best (worst) transmission performance. Similar behaviours can also be found in Figure 4.4 and Figure 4.5. The worst performance associated with the PL algorithm is due to the fact that, compared to the BL and BPL algorithms, the PL algorithm leads to the largest number of subcarriers being dropped, on which the detected errors are too large to achieve an acceptable total channel BER_T.

It can also be seen in Figure 4.3 that the signal transmission capacity differences between the BPL and PL algorithms are independent of signal bit rate, and such differences become slightly larger for longer transmission distances, for example, 1.8 Gb/s for 300m, 2.1 Gb/s for 800 m and 2.5 Gb/s for 1500m. More importantly, along with the long transmission distance-induced reduction in signal transmission capacity, the relative transmission capacity difference between the BPL and PL algorithms increases from ~7% to ~35% when the MMF lengths are extended from 300m to 1500m, as seen in Figure 4.3. This implies that, for a fixed OOFDM signal spectral width, a reduction in 3dB link bandwidth plays an important role in determining the effectiveness of these adaptive loading algorithms.

The results presented in Figure 4.3 indicate that, for both worst-case and normal-case MMF links of < 300m, the simplest PL algorithm can be considered to be an effective means of escalating the OOFDM MMF system performance to its maximum potential; whilst for MMF links of > 800m, it is worth considering the sophisticated BPL algorithm.

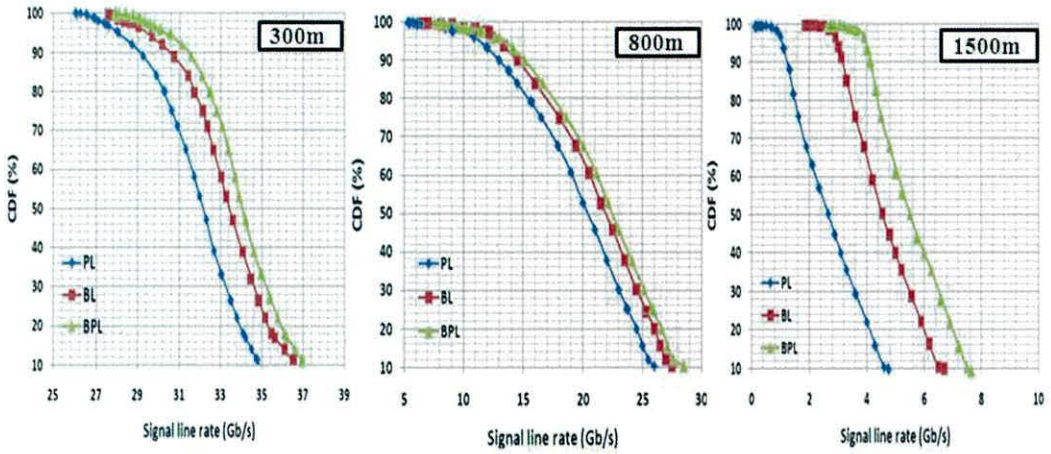

(a) (b) (c)

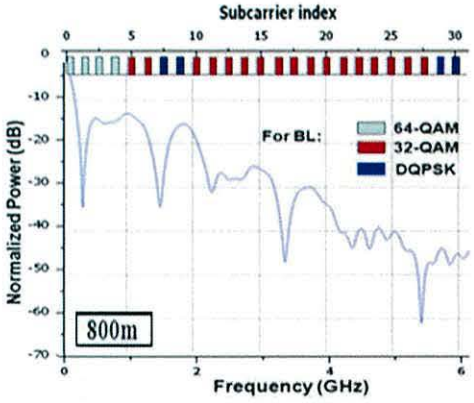

(d)

Figure 4.3: CDF of signal transmission capacity employing 32 subcarriers for the PL, BL and BPL algorithms over 1000 statistically constructed worst-case MMF links of different transmission distances: (a) 300m, (b) 800m, and (c) 1500m. In (d), an example of a MMF link frequency response plot together with the signal modulation format allocation on subcarriers is illustrated, when BL algorithm is applied over 800m.

4.4.2 Impact of Subcarrier Number and Sampling Speeds

Having examined the influence of the transmission distance on the performance of these three algorithms, in Figures 4.4 – 4.5 the impacts of OOFDM transceiver parameters are explored.

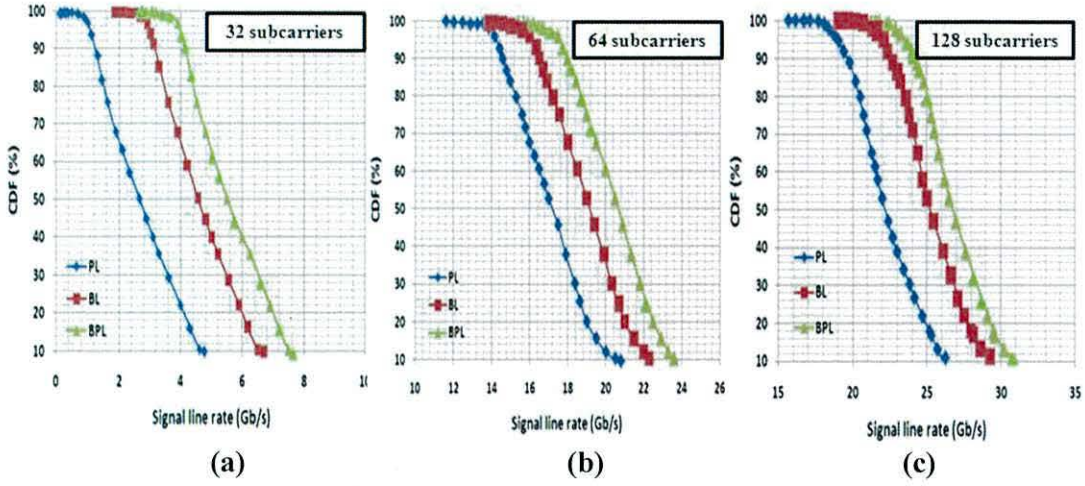

Figure 4.4: CDF of signal transmission capacity at 1500m for the PL, BL and BPL algorithms in 1000 statistically constructed worst-case MMF links for different subcarrier numbers: (a) 32, (b) 64, and (c) 128.

Here special attention is focussed on exploring two crucial parameters namely the number of subcarriers in the positive frequency bins, N_s , and the DAC/ADC sampling speed, r_s . For the systems illustrated in Figure 4.1, the relationships between the OOFDM signal bandwidth, N_s and r_s can be expressed as [11]:

$$B_s = \frac{r_s}{2} = N_s BW_k \left(1 + C_p\right) = \frac{N_s}{T_b}\left(1 + C_p\right) \tag{4.6}$$

where B_s is the OOFDM signal bandwidth, T_b is the OOFDM symbol period. It can be easily understood from Equation (4.6) that r_s determines B_s, and for a fixed r_s, a large N_s value produces a small BW_k value.

For different adaptive loading algorithms and $r_s = 12.5GS/s$, the CDF as a function of signal line rate is plotted in Figure 4.4 for different N_s: Figure 4.4 (a) for $N_s = 32$, Figure 4.4 (b) for $N_s = 64$, and Figure 4.4 (c) for $N_s = 128$. In computing Figure 4.3, the transmission distances are taken to be 1500m to reveal large transmission capacity differences between these algorithms. It is shown in Figure 4.3 that, with increasing N_s from 32 to 128, a five-fold increase in achievable transmission capacity occurs. The large N_s -induced transmission capacity enhancement is a direct result of an increased CP duration [12]: for a fixed sampling speed, a larger number of subcarriers results in a long CP, thus leading to the enhanced OOFDM capability of combating the DMD effect. In addition, it is also very interesting to note that, with increasing N_s from 32 to 128, the transmission capacity difference between the BPL (best) and PL (worst) algorithms decreases from 35% to 17%. This indicates that, compared to the BPL algorithm, a large number of subcarriers can improve the effectiveness of the PL algorithm.

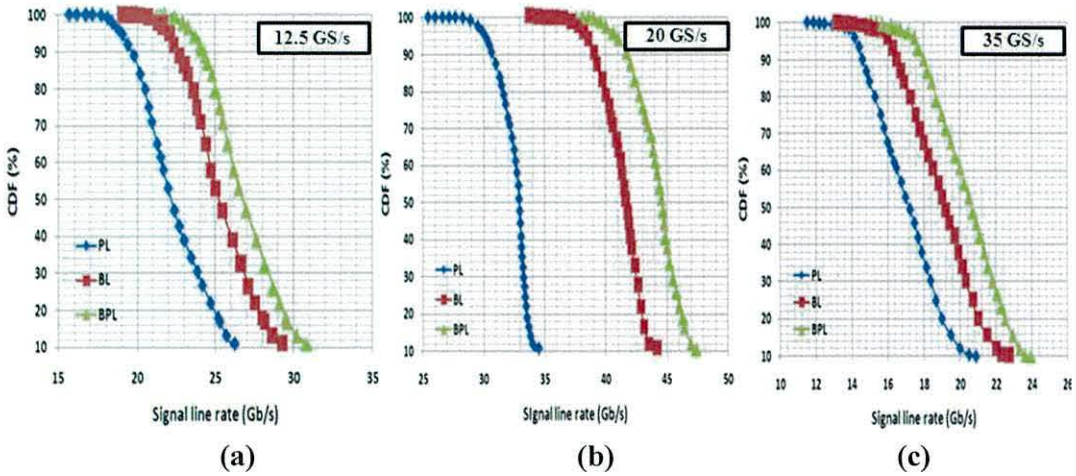

Figure 4.5: CDF of signal transmission capacity employing 128 subcarriers at 1500m for the PL, BL and BPL algorithms in 1000 statistically constructed worst-case MMF links for different sampling speeds: (a) 12.5 GS/s, (b) 20 GS/s, and (c) 35 GS/s.

The impacts of DAC/ADC sampling speed on the performance of these algorithms are presented in Figure 4.5, in which $N_s = 128$ and worst-case MMF lengths of 1500m are adopted. It can be seen in Figure 4.5 that, as the sampling speed increases from 12.5 GS/s to 20 GS/s, the transmission capacity difference between the PL (worst) and BPL (best) algorithms grows from 4 Gb/s to 11.5 Gb/s, giving rise to an 12% enlarged relative transmission capacity difference between the two algorithms. This can be understood by the following phenomenon: a high sampling speed-induced wider signal spectral width allows low signal modulation formats to be taken on high frequency subcarriers when the PL algorithm is applied. Clearly, a large sampling speed degrades the performance of the PL algorithm. Moreover, for MMF links capable of supporting the BL-enabled signal bit rates of 40 Gb/s at a DAC/ADC sampling speed of 20 GS/s, their corresponding averaged 3dB MMF bandwidths are roughly 0.5 GHz [18]. This implies that the use of the BPL algorithm is essential when the 3dB link bandwidths are less than 5% of the OOFDM signal spectrum.

In addition, Figure 4.5 also shows that, for very high sampling speeds of > 35 GS/s, both the signal transmission capacities for all these three algorithms and the relative transmission capacity differences between them are reduced significantly. The physical mechanisms underpinning such behaviours are: firstly, the rapid decay of the MMF frequency response at high frequencies gives rise to large losses for subcarriers located at the high frequency edge of the broad OOFDM signal spectrum, and hence low signal modulation formats and/or subcarrier dropping have to be applied on these subcarriers. Secondly, a fast sampling speed corresponds to a short CP duration, thus weakens the OOFDM capability of combating the DMD effect.

4.5 Adaptive Loading Algorithm Performance over SMF links

The transmission performance of OOFDM signals over SMF links using the three adaptive loading algorithms with procedures and specifications discussed in section 4.4.2 and 4.3.2, respectively, is depicted in Figures 4.6 – 4.11. A comprehensive theoretical OOFDM system model developed in Chapter 3 is also considered here, which includes OOFDM transceivers, DMLs, SSMFs and square-law photo-detectors.

4.5.1 Impact of Transmission Distance and Launched Optical Power

Figure 4.6 presents signal capacities versus transmission distance for a launched optical power of 5dBm, and Figure 4.7 presents signal capacities versus launched optical power over a 40km SMF link. Additionally, as a typical example for performance comparisons between the three adaptive loading algorithms in Figures 4.8 – 4.9, the *BER* and bit distribution over all subcarriers are presented using PL (21.875 Gb/s), BL (22.5 Gb/s), and BPL (22.656 Gb/s) when the transmission distance is set to 80km. It should be noted that for the case of the PL over 80km, 3 subcarriers are dropped due to a large number of detected errors. Moreover, in Figure 4.8, the error-free subcarriers are not showed.

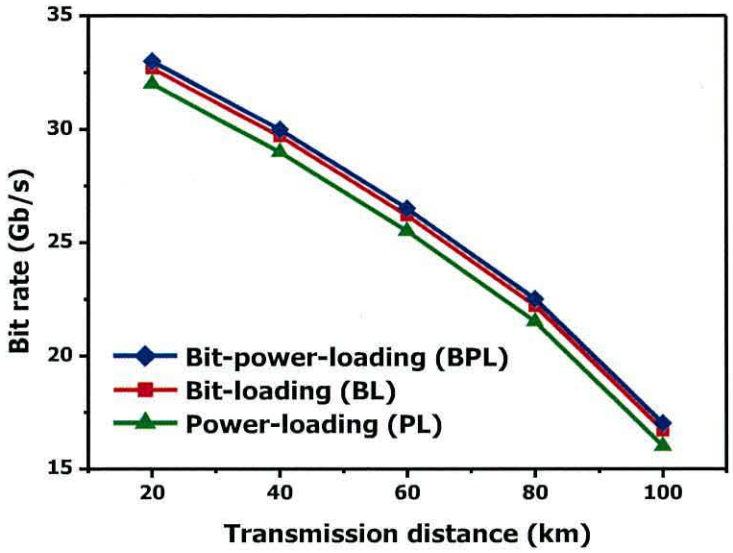

Figure 4.6: Signal bit rate versus transmission distance over a SMF link at 5 dBm launched optical power for PL, BL, and BPL.

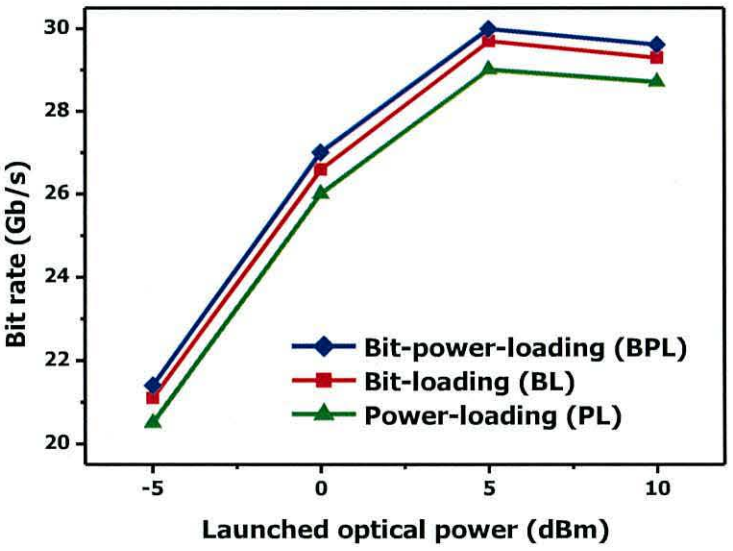

Figure 4.7: Signal bit rate versus launched optical power over a 40km SMF link for PL, BL and BPL.

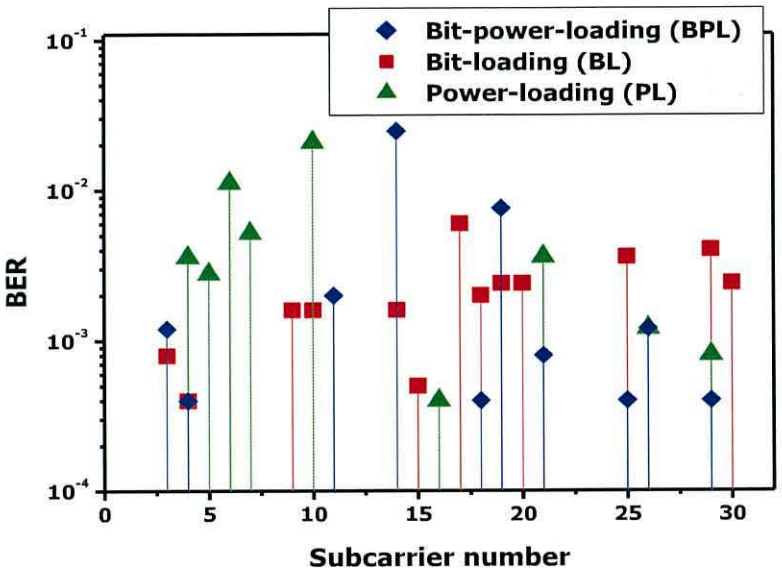

Figure 4.8: *BER* distribution versus number of subcarriers over an 80km SMF link at 5 dBm launched optical power for PL (21.875 Gb/s), BL (22.5 Gb/s), BPL (22.656 Gb/s).

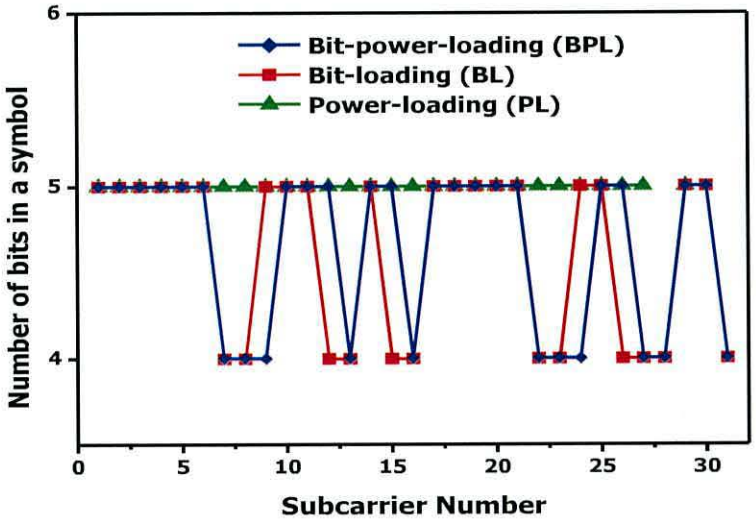

Figure 4.9: Bit distribution versus number of subcarriers over an 80km SMF link at 5 dBm launched optical power for PL (21.875 Gb/s), BL (22.5 Gb/s), BPL (22.656 Gb/s).

It is shown, from Figures 4.6 – 4.9, that a small signal capacity difference of up to about 7% is observed between the BPL (best) and PL (worst) algorithms. The results agree very well with the real-time experimental IM/DD OOFDM SMF-based results

reported in Refs. [1], [10]. This confirms that in comparison with the most sophisticated BPL algorithm, the simplest PL algorithm is effective in escalating the OOFDM SMF links performance to its maximum potential. It is also shown that the signal capacity difference between BPL (best) and PL (worst) is independent of both transmission distance and launched optical power. This occurs, because in contrast to the case of MMF links, where complicated frequency responses with many low power peaks and unpredictable nulls appear, the almost flat response of the SMF bandwidth offers similar characteristics for all subcarriers.

4.5.2 Impact of Subcarrier Number and Sampling Speeds

The impact of the number of subcarriers and the DAC/ADC sampling speed on the transmission performance of the three adaptive loading algorithms discussed in section 4.3.2 is presented in Figures 4.10 – 4.11, where the signal capacities are plotted as a function of subcarrier number and DAC/ADC sampling speed, respectively. It should be noted that, in calculating Figures 4.10 – 4.11, use is made of a 40km transmission system subject to an input optical power of 5 dBm.

From Figure 4.10, it is revealed that the signal capacity difference between the BPL (best) and PL (worst) algorithms increases with the number of subcarriers. In particular, the signal capacity difference between the BPL (best) and PL (worst) increases up to about 10% when 64 subcarriers are employed, while for the case where 15 or 32 subcarriers are considered, the signal capacity difference is decreased to about 5%. This can be explained by considering the following phenomenon: For a small number of subcarriers the CP length is short, which produces short OFDM symbol durations, which plays a dominant role in determining the system performance. This causes the observed small signal capacity difference. On the other

hand, for a large number of subcarriers the CP length increases, which combat completely the CD effect, thus the SNR variations between subcarriers are important, leading to almost doubled (10%) signal capacity difference. This indicates that a large number of subcarriers can improve the effectiveness of the adaptive loading algorithms.

Having identified the maximum signal capacity difference between the BPL (best) and PL (worst) algorithms, when 64 subcarriers are employed further investigations into the impact of DAC/ADC sampling speed are undertaken. In Figure 4.11 the signal capacity versus sampling speed is depicted, revealing that, for high sampling speeds (35 GS/s), the signal capacity difference between BPL (best) and PL (worst) is increased to about 12.4%. On the other hand, for low sampling speeds (12.5 GS/s) the signal capacity difference drops to about 7%. This can be explained by considering the following phenomenon: a high sampling speed-induced wider signal spectral bandwidth allows low signal modulation formats to be taken on high frequency subcarriers when the PL algorithm is applied, and hence, a large sampling speed degrades the PL transmission performance. Numerical investigations also reveal that over a large number of subcarriers and sampling speeds, the sophisticated BPL algorithm should be adopted for IM/DD OOFDM SMF-based systems for distances of < 40km. Finally, it should be noted that, in contrast to Figure 4.5 (c) which corresponds to the case of MMF links for a sampling speed of 35GS/s, here the SMF takes advantage of its wide bandwidth, and thus, higher signal modulation formats on subcarriers can be taken for all adaptive loading algorithms leading to higher signal capacities.

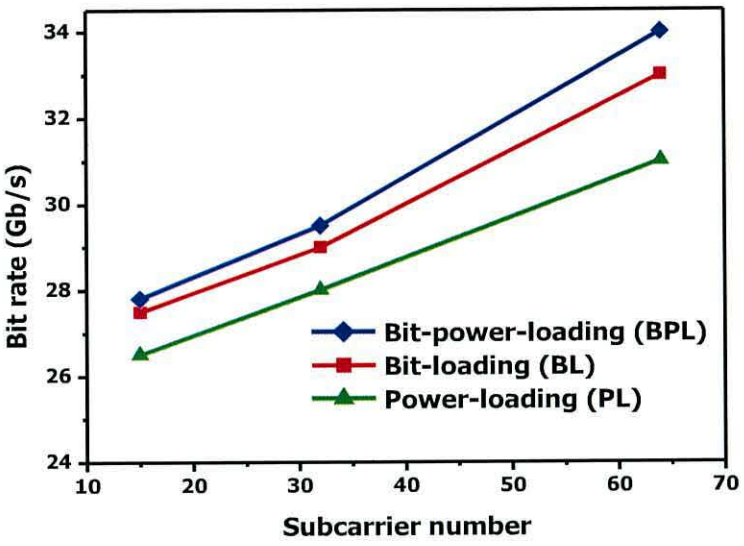

Figure 4.10: Signal bit rate versus number of subcarriers over a 40km SMF link for PL, BL, and BPL.

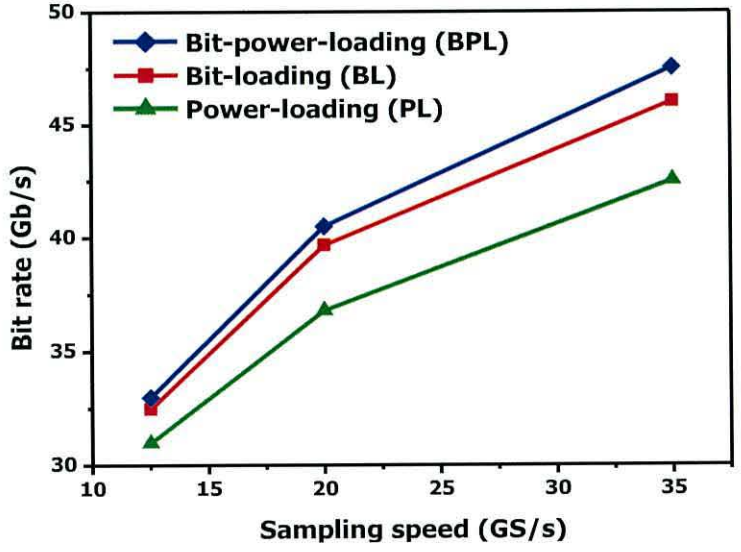

Figure 4.11: Signal bit rate versus sampling speed, employing 64 subcarriers over a 40 km SMF link for PL, BL, and BPL.

4.6 Theoretical and Experimental Results Comparisons

Having explored thoroughly the transmission performance of the three well-used adaptively loading algorithms in IM/DD OOFDM MMF/SMF-based systems, numerical investigations are undertaken in this section to compare theoretical results with experimental measurements.

Numerical results and experimental measurements are presented based on the work reported in Ref. [1], where end-to-end real-time adaptive bit and/or power loading enabled optical Field Programmable Gate Array (FPGA)-based OOFDM transceivers were successfully implemented over IM/DD SMF systems using DML (DFB) lasers. The OOFDM parameters adopted in this section are illustrated on Table 4.1. To conduct numerical explorations on the three adaptive loading algorithms for Figure 4.12, the adopted procedures described in section 4.4 and a comprehensive theoretical OOFDM system model developed in section 4.5 are considered here, including also the following consideration: A DAC roll-off is taking into account which is approximately 11dB (due to the extra 3dB from the DML positive frequency transient chirp) similarly to that reported in Ref. [1]. This consideration in the simulations is necessary since an actual DAC output is a "zero-order hold" that holds the voltage constant for an update period of 1/fs. In the frequency domain, this zero-order hold introduces sin(x)/x distortion (also called aperture distortion) which acts like a LPF attenuating frequencies and in-band signals.

For fair comparisons between the adaptive loading algorithms, the three aspects considered in section 4.2 are also considered here.

All the device and system parameters used in the numerical simulations are identical to those adopted in the experiments reported in Ref. [1], and all other parameters are taken from section 4.6.

Parameter	*Value*
Total points of IFFT/FFT points	32
Data-carrying subcarrier	15
n-subcarrier frequency	n×125 MHz
DAC/ADC sampling speed	4 GS/s
DAC/ADC resolution	8-bits
DFB-laser modulation bandwidth	10 GHz
DFB-laser bias current	36 mA
DFB-laser driving voltage	400 mVpp
PIN-detector bandwidth	12 GHz
PIN-detector sensitivity	-17dBm [a]
SSMF dispersion parameter at 1550nm	18ps/(nm·km)
MetroCor dispersion parameter at 1550nm	-7.6 ps/(nm· km)

[a] Corresponding to 10 Gb/s NRZ data at a *BER* of 1.0×10^{-9}

Table 4.1: Transceiver parameters of IM/DD OOFDM modem, based on the experimental OOFDM demonstration reported in Refs. [1], [10].

The IM/DD OOFDM transmission performance of the adaptive loading algorithms is shown in Figure 4.12. The adopted loading algorithms are constituted of experimental case of PL (from Ref. [1]), theoretical PL, BL, and BPL. It can be seen from Figure 4.12 that the experimental case of PL has identical transmission performance with the theoretical PL, confirming the validity of the adopted IM/DD OOFDM modem. Moreover, theoretical PL, BL, and BPL can support almost identical signal capacities for SMF links of up to 100km. In particular, at 25km SMF transmission, the PL algorithm can achieve raw data rate of 11.25 Gb/s compared to 12.25 Gb/s supported by the BPL algorithm. Numerical simulations are also performed for MetroCor SMFs and a transmission performance very similar (<1% deviation) to that observed in Figure 4.12 is obtained. In comparison with the sophisticated BPL algorithm, the simplest PL algorithm can be considered as an effective means of escalating the

OOFDM SMF link performance to its maximum potential for transmission distances < 100km. This statement and the aforementioned evolution trends in IM/DD SMF systems obtained from Figure 4.12 agree very well with the theoretical results conducted in section 4.5.1, where simulations were undertaken over 40km of SMFs.

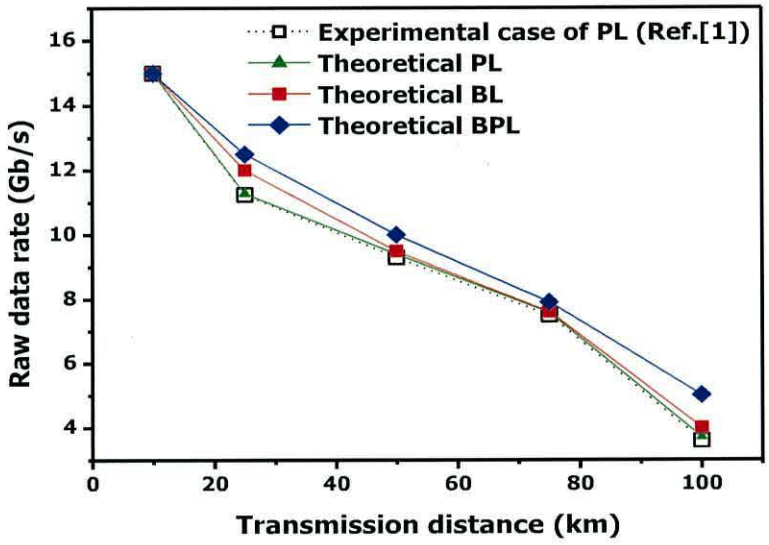

Figure 4.12: Raw signal line rate versus reach performance of IM/DD OOFDM system for experimental case of PL based on Ref. [1] and theoretical PL, BL, and BPL.

4.7 Conclusions

Detailed analytical and numerical investigations over IM/DD SMF links, and over 1000 statistically constructed worst-case IM/DD MMF links without incorporating in-line optical amplification and CD compensation, have been undertaken, for the first time, of the effectiveness of three widely adopted OOFDM adaptive loading algorithms including PL, BL, and BPL. It has been shown that the BPL (PL) algorithm always offers the best (worst) transmission performance.

The absolute transmission capacity differences between these algorithms are independent of signal bit rate and increase with transmission distance and the

DAC/ADC sampling speed when MMF links are employed. On the other hand, the relative transmission capacity difference between the BPL (best) and PL (worst) algorithms significantly decreases for short MMF lengths, large number of subcarriers and low DAC/ADC sampling speeds. In addition, numerical results have also indicated that, for both worst-case and normal-case MMF links of < 300m, in comparison with the sophisticated BPL algorithm, the simplest PL algorithm can be considered as an effective means of escalating the OOFDM MMF link performance to its maximum potential; the effectiveness of the PL algorithm can be further improved when a large number of subcarriers are used. Whilst for relatively long MMF links with 3dB bandwidths are much less than the transmitted OOFDM signal spectrum, the BPL algorithm has to be adopted.

For the case when SMF links are employed, the absolute transmission capacity difference between BPL (best) and PL (worst) algorithms is independent from signal bit rate, transmission distance and launched optical power. Numerical results have revealed that, for SMF links <100km, in comparison with the sophisticated BPL algorithm, the simplest PL algorithm can be considered as an effective means of escalating the OOFDM SMF link performance to its maximum potential. On the other hand, when both the number of subcarriers and the DAC/ADC sampling speed increase, the sophisticated BPL should be adopted. Given the importance of the aforementioned statements for practical cost-effective OOFDM transceiver architecture design for PONs, experimental verifications of the statements in end-to-end real-time OOFDM-PONs have been pledged. Finally, it should be addressed, that, all of the experimental results have shown very good agreements with the theoretical predictions.

References

[1] R. P. Giddings, X. Q. Jin, E. Hugues-Salas, E. Giacoumidis, J. L. Wei, and J. M. Tang, "Experimental demonstration of a record high 11.25Gb/s real-time optical OFDM transceiver supporting 25km SMF end-to-end transmission in simple IMDD systems", Optics Express, vol. 18, no. 6 , pp. 5541-5555, 2010.

[2] Y. Li and W. E. Ryan, "Mutual-Information-Based Adaptive Bit-Loading Algorithms for LDPC-Coded OFDM", Wireless Commun., vol. 6, no. 5, May 2007.

[3] Y. George and O. Armani, "Bit loading algorithms for OFDM", in *ISIT 2004*, Chicago, IL, 2004, p. 388.

[4] E. Giacoumidis, J. L. Wei, X. Q. Jin, and J. M. Tang, "Improved transmission performance of adaptively modulated optical OFDM signals over directly modulated DFB laser-based IMDD links using adaptive cyclic prefix", Opt. Express, vol. 16, pp. 9480-9494, 2008.

[5] C. S. Park and K. B. Lee, "Transmit Power Allocation for BER Performance Improvement in Multicarrier Systems", IEEE Transc. on Commun., vol. 52, no. 10, 2004.

[6] B. S. Krongold, K. Ramchandran, and D. L. Jones, "Computationally efficient optimal power allocation algorithms for multicarrier communication systems", IEEE Transactions on Communications, vol. 48, no. 1, pp. 23-27, 2000.

[7] H. Yang, S. C. J. Lee, E. Tangdiongga, C. Okonkow, H. P. A van den Boom, F. Breyer, S. Randel, A. M. J. Koonen, "47.4 Gb/s Transmission over 100 m Graded-

Index Plastic Optical Fibre based on Rate-adaptive Discrete Multitone Modulation", IEEE J. Lightw. Technol., vol. 28, no. 4, pp. 352-359, 2010.

[8] S. C. J. Lee, F. Breyer, S. Randel, D. Cárdenas, H. P. A. van den Boom, A. M. J. Koonen, "Discrete Multitone Modulation for High-Speed Data Transmission over Multimode Fibres using 850-nm VCSEL", OSA/OFC/NFOEC, 2009.

[9] T-N. Duong, N. Genay, M. Ouzzif, J. Le Masson, B. Charbonnier, P. Chanclou, and J.C Simon, Adaptive Loading Algorithm Implemented in AMOOFDM for NG-PON System Integrating Cost-Effective and Low-Bandwidth Optical Devices," IEEE Photon. Technol. Lett., vol. 21, pp. 790, 2009.

[10] X. Q. Jin, R. P. Giddings and J. M. Tang, "Experimental Demonstration of Adaptive Bit and/or Power Loading for Maximising Real-Time End-to-End Optical OFDM Transmission Performance", Proc. OFC/NFOEC, (OSA, 2011), paper JWA029.

[11] X. Q. Jin, J. M. Tang, K. Qiu, and Paul S. Spencer, "Statistical Investigations of the Transmission Performance of Adaptively Modulated Optical OFDM Signals in Multimode Fibre Links", IEEE J. Lightw. Technol., vol. 26, no. 18, 2008.

[12] X. Q. Jin, J. M. Tang, P. S. Spencer and K. A. Shore, "Optimization of adaptively modulated optical OFDM modems for multi-mode fibre-based local area networks", Journal of Optical Networking, vol.7, no.3, pp.198-214, 2008.

[13] R. P. Giddings, E. Hugues-Salas, B. Charbonnier and J. M. Tang, "Experimental Demonstration of Real-Time Optical OFDM Transmission at 11.25 Gb/s over 500m MMFs Employing Directly Modulated DFB Lasers," IEEE Photon. Technol. Lett., vol. 23, pp. 51-53, 2010

[14] J. M. Cioffi. (2008, Jun. 1). *Advanced Digital Communication, Course Reader* [Online]. Available: http://www.standford.edu/class/ee379c

[15] A. Garcia-Armada, "SNR gap approximation for M-PSK-based bit-loading", IEEE Transactions on Wireless Communications, vol. 5, pp. 57–60, 2006.

[16] E. Giacoumidis, J. L. Wei, X. L. Yang, A. Tsokanos, J. M. Tang, "Adaptive-Modulation-Enabled WDM Impairment Reduction in Multichannel Optical OFDM Transmission Systems for Next-Generation PONs", IEEE Photonics Journal, vol. 2, no. 2, pp. 130-140, 2010.

[17] C. M. Akujuobi and J. Shen, "Efficient Multi-User Parallel Greedy Bit-Loading Algorithm with Fairness Control for DMT Systems", the Centre of Excellence for Communication Systems Technology Research (CECSTR), Prairie View A&M University, Prairie View, Texas 77446, USA.

[18] X. Q. Jin and J. M. Tang, "Effectiveness of the use of 3-dB bandwidths of multimode fibres for estimating the transmission performance of adaptively modulated optical OFDM signals over IMDD links", IEEE Journal of Lightwave Technology, vol. 27, no. 18, pp. 3992-3998, 2009.

CHAPTER 5

WDM Impairment Reduction using Adaptive Modulation in Multi-channel OOFDM Transmission Systems for NG-PONs

Contents

5.1 Introduction 158

5.2 WDM AMOOFDM Transmission System

5.2.1 WDM AMOOFDM Transmission System Models 161

5.2.2 WDM Channel-Bit-Loading Algorithm 163

5.2.3 Simulation Parameters 167

5.3 Cross-Channel Complementary Modulation Format Mapping 168

5.4 Adaptive-Modulation-Induced Reduction in WDM Impairments 171

5.5 DML Frequency Chirp Compensation 175

5.6 Conclusion 177

References 178

5.1 Introduction

In recent years, WDM-PONs have gained overwhelming research and development interests, as WDM-PONs are capable of offering a large number of excellent features including, for example, high-quality data service with guaranteed wide bandwidth, large split ratio, aggregated traffic backhauling, simplified network architecture, and enhanced end user privacy [1], [2]. Of various proposed WDM-PON architectures, Extended-Reach Dense WDM-PONs (ER-DWDM-PONs) have been regarded as a promising strategy for high-capacity NG-PONs, since ER-DWDM-PONs not only preserve all the aforementioned key features associated with conventional WDM-PONs but also enable the convergence of optical access networks and MANs [3], thus resulting in a significant reduction in the number of equipment interfaces and network elements. For practical deployment of ER-DWDM-PONs, the most critical challenges are cost-effectiveness and flexibility [4].

To achieve cost-effective ER-DWDM-PONs, IM/DD has been adopted as one of the most important technical solutions due to its great network simplicity and low installation and maintenance cost. In particular, a further considerable cost reduction can also be made if DFB lasers (DMLs) are employed, because, in comparison with external modulators, the DMLs have salient advantages such as low component cost, compactness, relatively small driving voltage required, and high optical output power. On the other hand, to enhance the transmission capacity and system flexibility of ER-DWDM-PONs with their compatibility with existing TDM-PONs still being preserved to transparently support legacy services, OOFDM [4], [5] has been considered to be one of the strongest contenders, since OOFDM has unique and inherent capabilities of realizing high spectral efficiency [6] and providing, in both the

frequency and time domains, dynamic allocation of broad bandwidth among various end users, as well as reducing network complexity due to its resistance to linear dispersion impairments and full use of mature DSP [7].

Compared with conventional OOFDM, which employs an identical signal modulation format across all the subcarriers, the use of AMOOFDM can further improve, in a cost-effective manner, signal transmission capacity, network flexibility, and performance robustness [8]. These properties are extremely valuable for ER-DWDM-PONs. In AMOOFDM, the signal modulation format taken on a subcarrier within a symbol can be adjusted according to the characteristics of a given transmission system, i.e., a high (low) modulation format is used on a subcarrier experiencing a high (low) SNR. Any subcarriers suffering very low SNRs may be dropped completely to avoid the occurrence of a large number of errors on these subcarriers [8].

Therefore, it is greatly beneficial if use is made of the advanced AMOOFDM technique in DML-based IM/DD ER-DWDM-PONs without incorporating expensive in-line optical amplification and CD compensation. Unfortunately, to the best of our knowledge, no work has been published that explores such a research topic of great importance. Although the WDM OOFDM transmission performance has been reported in Refs. [9], [10], these works have, however, been focused on long-haul IM/DD transmission systems consisting of both external modulators and in-line optical amplifiers. In an IM/DD ER-PON architecture involving a DML, the OOFDM transmission performance has been presented in [3]. However, nonlinear WDM impairments have not been addressed, as a single signal channel is considered, and a Variable Optical Attenuator (VOA) is introduced to emulate the possible link loss in

ER-WDM-PONs. The utilization of VOAs has been considered to be a fairly common practice for examining the feasibility of implementing a specific transmission technique in conventional low-capacity WDM-PONs with transmission distances of approximately 20km over SSMFs, as for such application scenarios, the CD and nonlinear WDM impairments are negligible.

For DML-based IM/DD AMOOFDM ER-DWDM-PONs operating at signal bit rates of > 20 Gb/s over > 40km SSMFs, the above analyses bring up two very interesting open questions, i.e., a) under what conditions do the aforementioned common practice still hold, and b) for cases where the nonlinear WDM impairments are dominant, can an effective technical approach be identified to reduce such impairments? From the practical network design point of view, the provision of answers to these two open questions is very crucial, as these answers may have great potential for offering simple, cost-effective, and accurate solutions for evaluating rigorously the feasibility of implementing the AMOOFDM technique in ER-DWDM-PONs.

This Chapter is dedicated to explore theoretically, for the first time, the multi-channel AMOOFDM transmission performance in DML-based IM/DD ER-DWDM-PONs. In comparison with the conventional OOFDM technique, detailed numerical investigations of the effectiveness of utilizing AMOOFDM in minimizing the nonlinear WDM impairments induced by XPM and FWM are undertaken. In addition, the validity of the aforementioned common network evaluation practice is also examined.

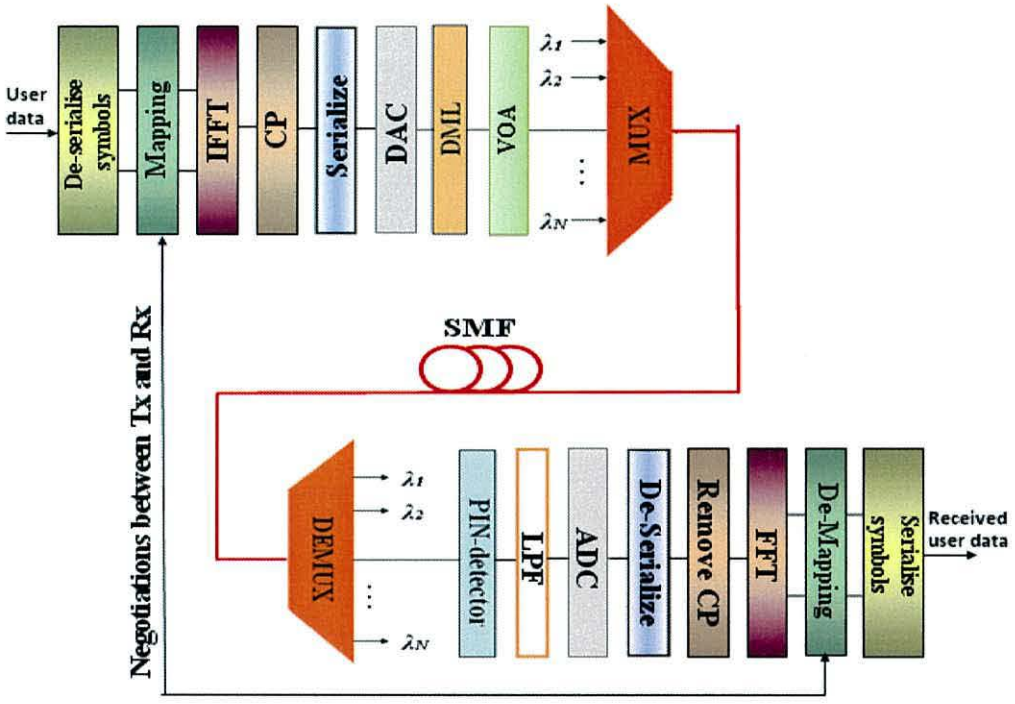

Figure 5.1: DML-based IM/DD WDM AMOOFDM transmission systems.

5.2 WDM AMOOFDM Transmission System

5.2.1 WDM AMOOFDM Transmission System Models

The DML-based IM/DD WDM AMOOFDM transmission system considered in this Chapter is illustrated in Figure 5.1, where both in-line optical amplification and chromatic dispersion compensation are not incorporated. In the transmitter, procedures presented in Ref. [8] are adopted to simulate the generation of a real-valued baseband OFDM signal in the electrical domain. Combined with a proper DC bias current, the electrical signal having a positive sign is employed to directly drive a DML, from which an AMOOFDM signal is produced at a specific optical wavelength. After the DML, a VOA is employed to adjust the optical signal power at a required level. Making use of different incoming random data sequences, the

aforementioned procedures are repeated to generate new WDM channels of different optical wavelengths spaced at a desired frequency interval. All the WDM signals are then aggregated using a Multiplexer (MUX), and the combined WDM AMOOFDM signals are finally launched into a simple IM/DD SSMF transmission system.

After transmitting through the SSMF, in the receiver, the received WDM signals are separated by a De-Multiplexer (DEMUX) with a spectral bandwidth being half of the channel spacing. Each separated WDM channel is detected using a square-law photon detector, in which both shot noise and thermal noise are computed following procedures similar to those presented in Refs. [8], [11]. The down-converted electrical signal is processed using an inverse procedure compared with that adopted in the corresponding transmitter, and data is finally recovered for each WDM channel.

To simulate the nonlinear optical properties of a DFB-laser-based DML, here, a lumped DFB laser model developed in Ref. [11] is adopted, taking into account a wide range of nonlinear effects such as longitudinal-mode spatial hole burning, linear and nonlinear carrier recombination, and ultrafast nonlinear gain compression. The theoretical DML model also includes the transient frequency chirp effect, which originates from the variation of refractive index with carrier density set by the applied electrical driving current. Both theoretical and experimental investigations [6], [8], [12] have shown that such a frequency chirp plays a dominant role in determining the DML-induced transmission performance degradation. On the other hand, in the theoretical DML model, the DFB adiabatic frequency chirp arising due to the static electrical power dependence of refractive index is not considered, as such a chirp effect is negligible due to the fact that the time-domain electrical driving current is continuous and noise-like and has a relatively small signal extinction ratio [13]. The

validity of the theoretical DML model has been confirmed by excellent agreements with experimental measurements [5], [6]. In addition, the theoretical DML model has also been used successfully in both MMF- and SSMF-based transmission systems of various architectures [8], [11], [14], [15].

In this Chapter, a comprehensive SSMF model used successfully in Ref. [8] and [13], [14], [15], [16] is also employed, taking into account the effects of fibre loss, CD, and polarization dependence of Kerr nonlinearity. In particular, the SSMF model includes Self-Phase Modulation (SPM) in each of two orthogonal linear polarization states: XPM between the two polarization states and polarization-dependent FWM terms [17]. Clearly, for one or more optical signals split into two polarization states, the magnitudes of the XPM and FWM terms also vary with the polarization states of the signals.

5.2.2 WDM Channel-Bit-Loading Algorithm

As already mentioned in section 5.1, AMOOFDM enables the signal modulation format taken on each subcarrier within a symbol to vary, depending upon the characteristics (such as frequency response) of a specific transmission system. Throughout this Chapter, for each WDM channel, a wide range of signal modulation formats may be utilized, which includes DBPSK, DQPSK, and 16-QAM up to 256-QAM. Signal modulation formats taken on individual subcarriers within an AMOOFDM symbol for a specific wavelength channel determine the signal line rate of the wavelength channel. The signal line rate of each WDM channel is computed by

$$R_j = \frac{r_{sj} \sum_{K=1}^{N_{SJ}-1} En_{kj}}{2N_{si}(1+C_{pj})} \tag{5.1}$$

where j is the index of the WDM channel. N_{sj} is the total number of data-bearing subcarriers in the positive frequency bins, n_{kj} is the total number of binary bits conveyed by the k-th subcarrier within one symbol period, r_{sj} is the sampling rate of an ADC/DAC employed in the j-th WDM channel, and C_{pj} is the CP parameter defined in Refs. [8], [11]. Through negotiations between the transmitter and the receiver in the initial stage of establishing a transmission link, the signal capacity of the j-th WDM channel can be maximized by assigning the highest possible signal-modulation format on each subcarrier. This operation is conducted by monitoring the total *BER* of the j-th WDM channel, i.e., BER_{Tj} and its corresponding subcarrier *BER*, i.e., BER_{kj}, both of which are defined as

$$BER_{Tj} = \frac{\sum_{K=1}^{N_{SJ}-1} En_{kj}}{\sum_{k=1}^{N_{sj}-1} Bit_{kj}} \tag{5.2}$$

$$BER_{kj} = \frac{En_{kj}}{Bit_{kj}} \tag{5.3}$$

where En_{kj} is the total number of errors detected over the entire data sequence adopted in the j-th WDM channel, and Bit_{kj} is the total number of transmitted binary bits of the data sequence adopted in the j-th WDM channel. Both En_{kj} and Bit_{kj} are for the k-th subcarrier. It should be noted that the signal line rate computed using Equation

(5.1) is considered to be valid only when the corresponding $BER_{Tj} = 1.0 \times 10^{-3}$ is satisfied.

For a given WDM AMOOFDM transmission system, the WDM channel-bit-loading algorithm adopted in numerical simulations is described as followings:

1) A single channel located in the centre of the WDM window is first transmitted through the system. Through negotiations between the transmitter and the receiver according to the total channel BER_T and the corresponding subcarrier *BER*, the highest signal modulation format taken on each subcarrier within a symbol is identified. Any subcarriers suffering very low SNRs may be dropped completely if the corresponding *BERs* are still very large, even if they are encoded using DBPSK. Such negotiations are essential for the following two reasons: i) An IM/DD SSMF transmission system has a Gaussian-shaped frequency response profile, which narrows rapidly with increasing transmission distance [6], [13], [14], [15], [16]; and ii) the DFB frequency chirp considerably distorts the system frequency-response profile [6], [8].

2) The signal-modulation formats identified above are applied on the corresponding subcarriers of each of the remaining WDM channels. A combined WDM signal is thus produced and then transmitted through the transmission system.

3) After transmission, for each of the WDM channels, the signal-modulation formats are adjusted independently according to their individual total channel BER_T and subcarrier *BER*. These WDM signals are then recombined and transmitted over the same system.

4) Step 3 repeats until a maximum signal capacity at $BER_T \cong 1.0 \times 10^{-3}$ is achieved for each individual WDM channel.

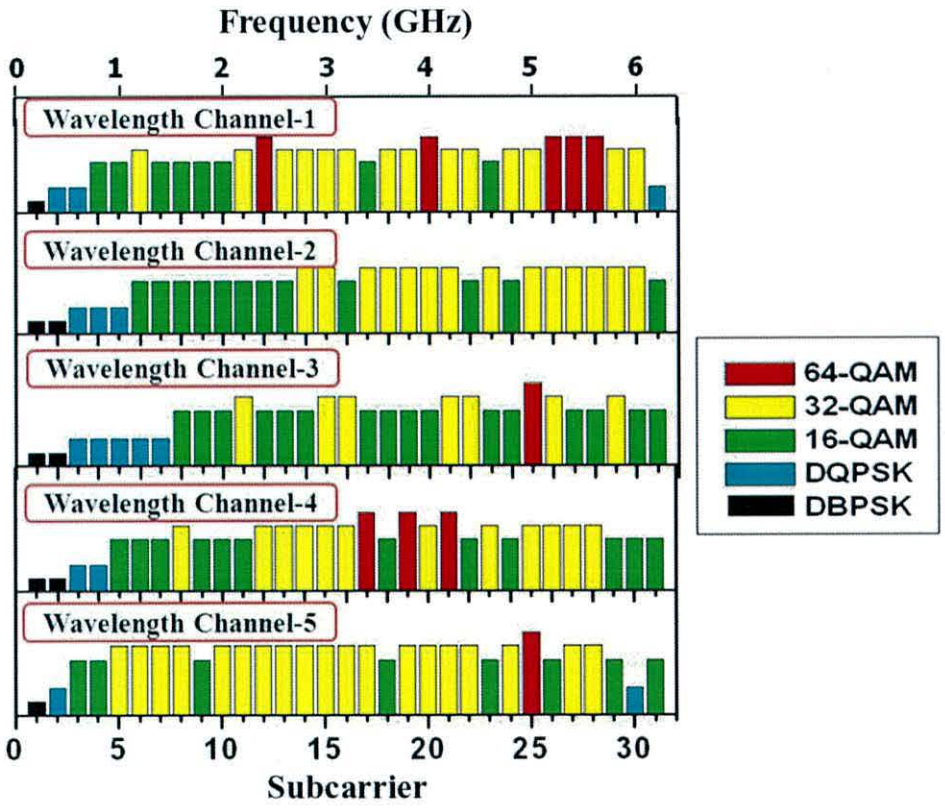

Figure 5.2: Signal modulation format distribution across all the subcarriers of five WDM channels over 40km with the same polarization states. Cross-channel complementary modulation format mapping is shown.

As discussed in sections 5.3 – 5.5, the joint manipulation of signal modulation format taken on different subcarriers for all the WDM channels is to effectively reduce the FWM-induced WDM impairments, thus leading to a considerably increased transmission capacity for each WDM channel, compared with that obtained using the conventional OOFDM technique.

It is also worth pointing out that, in the WDM channel bit-loading algorithm, an identical electrical power for each non-dropped subcarrier is adopted, regardless of

the signal modulation format used. In comparison with a complex BPL algorithm widely used in DSL systems [18], the present algorithm gives rise to a very similar signal capacity and, more importantly, significantly reduces the execution time. The reduction in execution time is of great importance, owing to the extremely complexity of the simultaneous maximization of signal modulation formats over several WDM channels.

As an example, a representative signal modulation format distribution across all the subcarriers is illustrated in Figure 5.2 for five WDM AMOOFDM channels after passing through a DML-based IM/DD 40km SSMF transmission system.

In sections 5.4 and 5.5, to demonstrate the effectiveness of AMOOFDM in IM/DD WDM systems, the transmission performance of the conventional OOFDM technique is also presented, in which an identical signal modulation format is taken on each subcarrier within a symbol for each individual WDM channel. The selected signal modulation format is at the highest possible level to ensure that the BER_T better than 1.0×10^{-3} is still satisfied.

5.2.3 Simulation Parameters

Five 50 GHz equally spaced WDM channels are considered with the central channel being positioned at 1550nm. These channels have identical optical powers launched into the SSMF systems. For each individual WDM channel, a total number of 64 (2 Ns) subcarriers are utilized, of which 31 subcarriers carry real data, and 1 contains no power. The remaining 32 subcarriers are the complex conjugate of the aforementioned 32 subcarriers to enforce Hermitian symmetry in the input facet of the IFFT. The CP parameter is taken to be 25% [8]. The ADC/DAC operates at a 12.5 GS/s sampling

rate [8], which gives rise to a sampling time duration of 80 ps. Detailed explorations of the influence of quantization and clipping noise on the transmission performance of the AMOOFDM signals have been undertaken in Ref. [19], in which an optimum 7-bit resolution and an optimum clipping ratio of 13dB are identified for signal-modulation formats up to 256-QAM. Therefore, these identified optimum parameter values are adopted in this Chapter.

All the parameters adopted for both the SSMFs and DFBs can be found in Refs. [8], [11], respectively. In particular, the DFB operating conditions of a 30mA bias current and a 15mA peak-to-peak driving current are adopted, which are the optimum values for IM/DD SSMF systems with transmission distances of interest of this Chapter [8]. In the receiver, a PIN photo-detector is employed having a quantum efficiency of 0.8 and a sensitivity of -19 dBm [corresponding to a 10 Gb/s NRZ data for a BER_T of1.0×10^{-9}].

5.3 Cross-Channel Complementary Modulation Format Mapping

To demonstrate the effectiveness of the WDM channel-bit-loading algorithm described in section 5.2, and to gain an in-depth understanding of the results presented in the following sections, discussions are first made of distributions of signal modulation formats across different subcarriers for five WDM channels with the same signal polarization states at the input of the transmission system. The simulated results are illustrated in Figure 5.2 which obtain that the transmission distance and the optical launch power per channel are fixed at 40km and 0dBm, respectively.

As a direct result of the triangle-shaped signal spectral distortion across the entire WDM window, cross-channel complementary modulation format mapping occurs, as seen in Figure 5.2, i.e., relatively high signal- modulation formats are taken on high-frequency subcarriers for wavelength channel 1 and wavelength channel 2, while relatively low-signal-modulation formats are taken on high-frequency subcarriers for wavelength channel 4 and wavelength channel 5. Such a cross-channel complementary nature is possible only when AMOOFDM is applied, indicating that AMOOFDM can mitigate, to some extent, the FWM effect and subsequently leads to improvements in both the overall signal capacity of the entire WDM transmission system and each individual WDM channel capacity, in comparison with the conventional OOFDM technique.

It can also be seen in Figure 5.2 that, for each individual WDM channel, relatively low-signal modulation formats appear on both sides of the signal spectrum. The low-modulation formats on the low-frequency subcarriers are due to the *subcarrier* × *subcarrier* intermixing effect, which takes place upon direct photon detection in the receiver [14], [16], and the low-signal modulation formats on the high-frequency subcarriers are mainly because of the effects of the DML-induced frequency chirp and system frequency response roll-off [6], [14], [15].

As the FWM effect causes the central channel to have the worst transmission performance among all the WDM channels, only the transmission performance of the central channel is, therefore, presented in all the following sections.

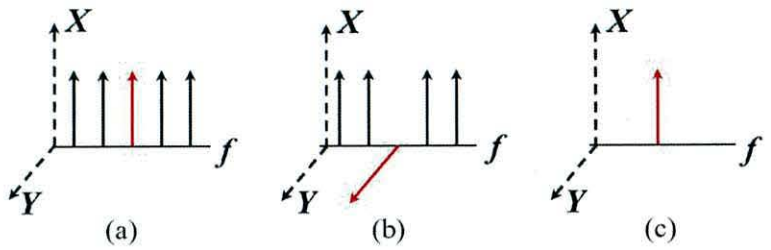

Figure 5.3: Polarization states of five WDM channels at the input facet of a transmission system. (a) All x-polarized WDM channels, (b) 4 x-polarized and 1 y-polarized WDM channels, and (c) a single x-polarized channel.

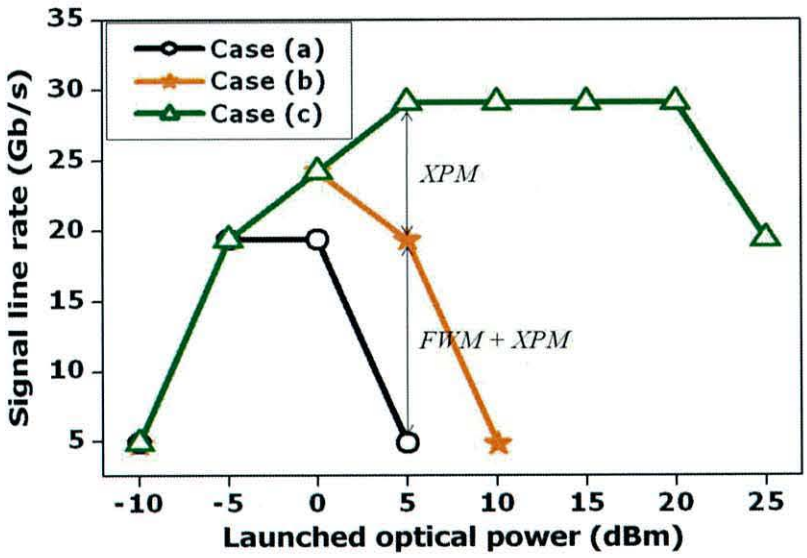

Figure 5.4: Transmission capacity versus optical launch power over DML-based 40km SSMF systems. The conventional OOFDM technique, using identical modulation formats across all the subcarriers, is used for Case (a), Case (b), and Case (c) defined in Figure 5.3.

5.4 Adaptive-Modulation-Induced Reduction in WDM Impairments

To investigate in detail the impacts of the effects of XPM and FWM on the transmission performance of the worst-case central WDM channel, numerical simulations are undertaken for three different polarization conditions at the input facet of a transmission system, as shown in Figure 5.3: Case (a) consists of five x-polarized WDM channels, the central channel experiences the XPM, and FWM effects; in Case (b), the central channel is set at y-polarization, and the other four WDM channels remain at x-polarization. Such a signal polarization arrangement leads to the central channel suffering from the XPM effect only, which is one third weaker than that in Case (a) [17]. Finally, Case (c) just includes a single x-polarized channel, where the XPM and FWM impairments do not exist. It should be pointed out that the similar SPM effect is always present in each WDM channel for all three different cases.

The signal line rate of the central WDM channel versus optical launch power per channel is plotted in Figure 5.4 for a DML-based 40km IM/DD transmission system subject to three polarization conditions defined in Figure 5.3. To highlight the XPM and FWM effects only, in simulating Figure 5.4, the conventional OOFDM technique is considered for all the WDM channels. The developing trends of signal transmission capacity shown in Figure 5.4 are very similar to those observed in Ref. [9]. By comparing the three different curves shown in Figure 5.4, it is clear that XPM plays a dominant role in determining the maximum achievable transmission performance of the central channel for optical launch powers larger than 0dBm. Compared with the XPM effect, the FWM effect is relatively weaker, which, however, increases

exponentially with decreasing channel spacing. On the other hand, for optical launch powers less than 0dBm, the XPM- and FWM-induced nonlinear WDM impairments are negligible, implying that the use of VOAs in evaluating the WDM network performance is sufficiently accurate. However, for optical launch powers beyond such a value, the linear network evaluation approach is not valid. In Case (c), the reduction in signal transmission capacity for optical launch powers of > 20dBm is contributed by the SPM effect.

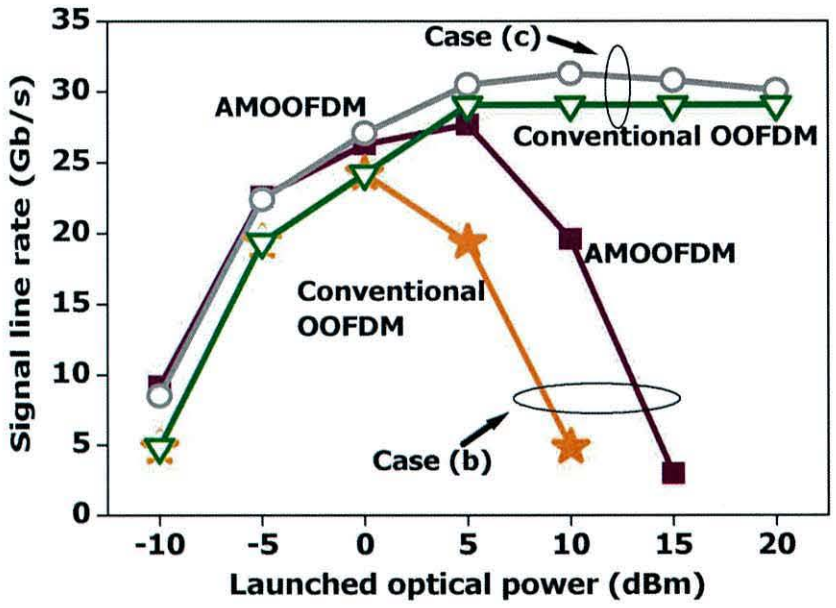

Figure 5.5: Signals capacity versus optical launch power over DML-based 40km IM/DD SMF systems subject to different polarization launch conditions. Case (b) and Case (c) defined in Figure 5.3.

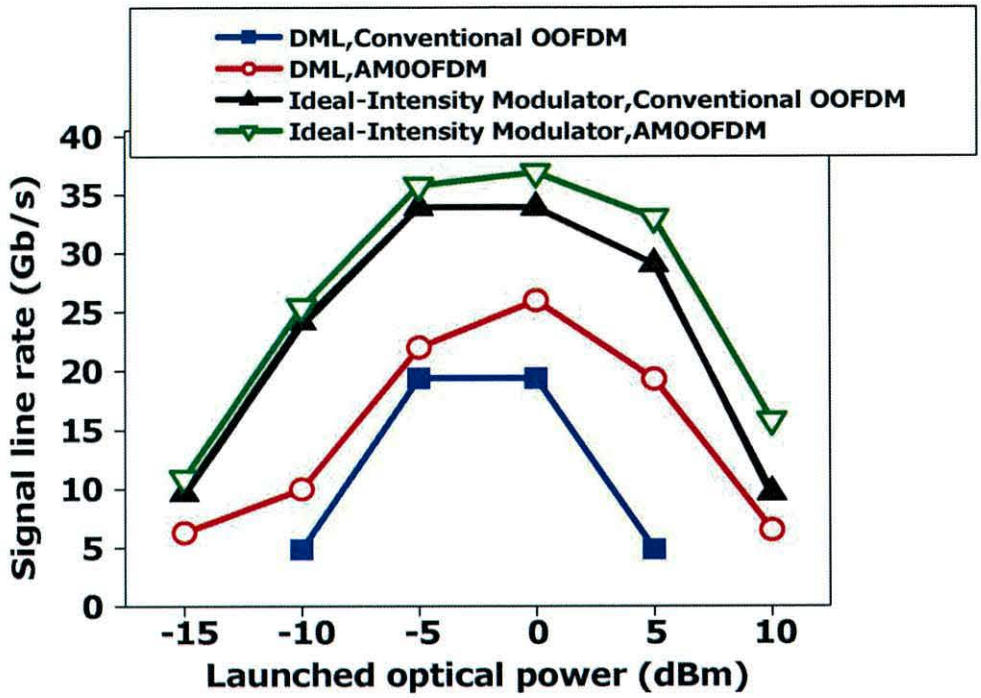

Figure 5.6: Transmission capacity versus optical launch power for AMOOFDM and conventional OOFDM over 40km IM/DD systems including and excluding DMLs. Case (a) is considered.

It is very interesting to note that the use of AMOOFDM can considerably reduce the nonlinear WDM impairments induced by XPM and FWM, as seen in Figures 5.5 and 5.6. In Figure 5.5, performance comparisons are made between AMOOFDM and conventional OOFDM for Case (b) and Case (c), and in Figure 5.6, similar comparisons are made for Case (a). These Figures show that, as a direct result of cross-channel complementary modulation format mapping presented in section 5.3, the adaptive modulation-enabled performance enhancement is more pronounced for the WDM case than that for the single-channel case. In addition, compared with conventional OOFDM, in the WDM nonlinearity-limited performance region, AMOOFDM not only improves the maximum achievable signal bit rate by a factor of > 1.3 but also extends the optimum optical launch power by about 5dB.

Apart from the reduction in the FWM-induced crosstalk effect via cross-channel complementary modulation format mapping, the significantly improved transmission performance observed in Figures 5.5 and 5.6 is also due to the fact that the AMOOFDM can also produce a signal PAPR lower than that corresponding to conventional OOFDM. This is because AMOOFDM decreases the probability of independently modulated subcarriers being added up coherently by the IFFT. This statement is confirmed in Figure 5.7, where the signal peak occurrence probability density versus PAPR is plotted for AMOOFDM and conventional OOFDM. The signal peak occurrence probability density ρ is defined as

$$\rho = \frac{n_{PAPR}}{n_T} \tag{5.4}$$

where n_{PAPR} is the total number of signal peaks occurring within a power variation range of 1dB with respect to a specific PAPR value, and n_T is the total number of signal peaks occurring within the entire PAPR range. It should be noted that, in calculating Figure 5.7, use is made of the optical signals emerging at the output facet of a 40km transmission system at an input optical power of 5dBm.

It can be seen in Figure 5.7 that, in comparison with conventional OOFDM, AMOOFDM produces more signal peaks in a low-PAPR region of < 4dB and fewer signal peaks in a high-PAPR region of > 4dB. As the XPM-related optical phase is proportional to the intensity of the other signal channel travelling simultaneously over the same fibre, a small PAPR gives rise to the reduced XPM effect, as seen in Figures 5.5 – 5.6. In addition, it is also easy to understand that a low PAPR also results in a reduction in the FWM effect [17].

According to the above analyses, it is very easy to understand that the effectiveness of utilizing adaptive modulation to compensate for the nonlinear WDM impairments can be enhanced considerably with increasing transmission distance. As an example, in comparison with conventional OOFDM, for a transmission distance of 80km, numerical simulations show that AMOOFDM can improve the maximum achievable signal bit rate of the central channel by a factor of 3.6, which is approximately three times higher than that corresponding to the 40km transmission distance case.

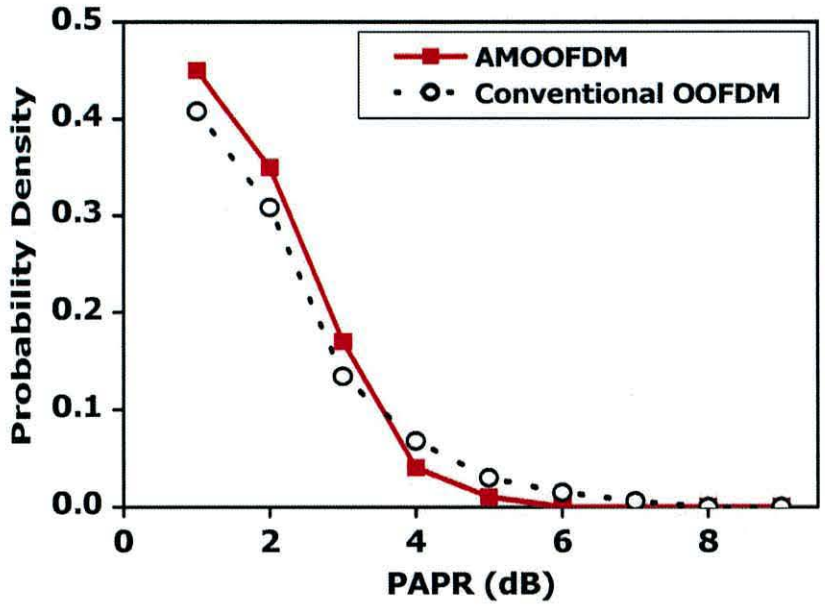

Figure 5.7: Signal peak occurrence probability density versus PAPR for AMOOFDM and conventional OOFDM. The optical launch power is fixed at 5 dBm, and the transmission link is 40km.

5.5 DML Frequency Chirp Compensation

Apart from the aforementioned significant reduction in the XPM and FWM effects, use can also be made of AMOOFDM to effectively compensate for the DML-induced frequency chirp effect, as shown in Figure 5.6, where comparisons of the

transmission performances for Case (a) are made between a DML and an ideal-intensity modulator to distinguish clearly the impacts of the DML-induced frequency chirp effect. The output optical signal from the ideal-intensity modulator $S_O(t)$ can be written as

$$S_o(t) = \sqrt{S_e(t)} \tag{5.5}$$

where $S_e(t)$ is the total electrical current applied to the DML. It is shown in Figure 5.6 that the DML-induced frequency chirp effect degrades dramatically the transmission performance. This is in very good agreement with results presented in Refs. [8], [15]. More importantly, compared with conventional OOFDM, AMOOFDM is capable of improving considerably the transmission performance across the entire optical launch power range, especially for optical launch powers of > 0dBm. Such behaviours can be explained by considering the fact that the DML frequency chirp distorts considerably the optical signal spectrum via lifting up the high-frequency spectral region by approximately 10dB after transmitting through 40km SSMFs [8]. AMOOFDM can fully utilize all parts of the spectrum by taking low-signal-modulation formats on the most distorted spectral regions, as illustrated in Figure 5.2. This causes the transmission performance enhancement over the entire optical launch power region of interest of the present work. Moreover, AMOOFDM can also reduce the signal PAPR, resulting in a small electrical signal current variation and, thus, a low DML frequency chirp [12]. Such an effect is more significant for high optical launch powers. It is also worth pointing out that the DML-induced frequency chirp increases the walk-off effect between different wavelength channels, whose contribution to the FWM effect is, however, negligible, as the AMOOFDM signals

have noise-like time-domain waveforms with approximated Gaussian probability density functions [8], [11], [13].

5.6 Conclusion

The transmission performance of multi-channel AMOOFDM signals has been explored numerically, for the first time, in DML-based IM/DD SSMF systems without involving in-line optical amplification and CD compensation for ER-DWDM-PONs. It has been shown that AMOOFDM cannot only significantly reduce the nonlinear WDM impairments induced by the XPM and FWM effects but can also effectively compensate for the frequency chirp effect associated with the DMLs. Investigations have also revealed that, in comparison with conventional OOFDM, AMOOFDM improves the maximum achievable signal transmission capacity of a central WDM channel by a factor of 1.3 and 3.6 for 40km and 80km SSMFs, respectively, with the corresponding dynamic input optical power range being extended by approximately 5dB. In addition, the adaptive modulation-enabled performance enhancement is more pronounced for optical launch powers of > 0dBm. Furthermore, AMOOFDM also enables the occurrence of cross-channel complementary modulation format mapping, leading to considerably improved transmission capacities for each individual WDM channel and the entire WDM transmission system.

The present work suggests that AMOOFDM is promising for practical implementation in ER-DWDM-PONs. From the practical implementation point of view, the maximum achievable signal-transmission capacity of the system of interest

of this Chapter is mainly limited by the following three factors including properties of DACs/ADCs adopted, DML-induced relatively small-signal extinction ratio, and subcarrier intermixing upon direct photon detection in the receivers. It is also worth mentioning that following the successful experimental demonstration of 11.25 Gb/s real-time end-to-end OOFDM transceivers [20], experimental verifications of the theoretical predictions are currently being undertaken, and results will be reported elsewhere in due course.

References

[1] T. Koonen, "Fiber to the home/fiber to the premises: What, where, and when",[Proc. IEEE, vol. 94, no. 5, pp. 911–934, May 2006.

[2] P. W. Shumate, "Fibre-to-the-home: 1977-2007", IEEE J. Lightw. Technol., vol. 26, no. 9, pp. 1093–1103, May 2008.

[3] C.-W. Chow, C.-H. Yeh, C.-H. Wang, F.-Y. Shih, C.-L. Pan, and S. Chi, "WDM extended reach passive optical networks using OFDM-QAM", Opt. Express, vol. 16, no. 16, pp. 12096–12101, Aug. 2008.

[4] D. Qian, N. Cvijetic, J. Hu, and T. Wang, "Optical OFDM transmission in metro/access networks", presented at the Optical Fiber Communication/Nat. Fiber Optic Engineers Conf. (OFC/NFOEC), San Diego, CA, 2009, Paper OMV1.

[5] N. E. Jolley, H. Kee, R. Rickard, J. Tang, and K. Cordina, "Generation and propagation of a 1550 nm 10 Gb/s optical orthogonal frequency division multiplexed signal over 1000 m of multimode fibre using a directly modulated DFB", presented at

the Optical Fiber Communication/Nat. Fiber Optic Engineers Conf. (OFC/NFOEC), Anaheim, CA, 2005, Paper OFP3.

[6] X. Q. Jin, R. P. Giddings, E. Hugues-Salas, and J. M. Tang, "Real-time demonstration of 128-QAM-encoded optical OFDM transmission with a 5.25 bit/s/Hz spectral efficiency in simple IMDD systems utilizing directly modulated DFB Lasers", Opt. Express, vol. 17, no. 22, pp. 20484–20493, Oct. 2009.

[7] R. P. Giddings, X. Q. Jin, and J. M. Tang, "First experimental demonstration of 6 Gb/s real-time optical OFDM transceivers incorporating channel estimation and variable power loading", Opt. Express, vol. 17, no. 22, pp. 19727–19738, Oct. 2009.

[8] J. M. Tang and K. A. Shore, '30-Gb/s signal transmission over 40-km directly modulated DFB-laser-based singlemode- fibre links without optical amplification and dispersion compensation", J. Lightw. Technol., vol. 24, no. 6, pp. 2318–2327, Jun. 2006.

[9] A. J. Lowery, L. B. Du, and J. Armstrong, "Performance of optical OFDM in ultra-long-haul WDM lightwave systems", IEEE J. Lightw. Technol., vol. 25, no. 1, pp. 131–138, Jan. 2007.

[10] D. Qian, J. Yu, J. Hu, L. Zhou, L. Xu, and T. Tang, B10 Gb/s WDM-SSB-OFDM transmission over 1000 km SSMF using conventional DFB lasers and direct-detection", Electron. Lett., vol. 44, no. 3, pp. 223–225, Jan. 2008.

[11] J. M. Tang, P. M. Lane, and K. A. Shore, "High-speed transmission of adaptively modulated optical OFDM signals over multimode fibres using directly modulated DFBs", IEEE J. Lightw. Technol., vol. 24, no. 1, pp. 429–441, Jan. 2006.

[12] J. A. P. Morgado and A. V. T. Cartaxo, "Directly modulated laser parameter optimisation for metropolitan area networks utilizing negative dispersion fibres,", IEEE J. Sel. Topics Quantum Electron., vol. 9, no. 5, pp. 1315–1324, Sep./Oct. 2003.

[13] J. L. Wei, X. L. Yang, J. M. Tang, and R. P. Giddings, "Colourless adaptively modulated optical OFDM transmitters using SOAs as intensity modulators", Opt. Express, vol. 17, no. 11, pp. 9012–9027, May 2009.

[14] J. L. Wei, X. Q. Jin, and J. M. Tang, "The influence of directly modulated DFB lasers on the transmission performance of carrier suppressed single sideband optical OFDM signals over IMDD SMF systems", IEEE J. Lightw. Technol., vol. 27, no. 13, pp. 2412–2419, Jul. 2009.

[15] E. Giacoumidis, J. L. Wei, X. Q. Jin, and J. M. Tang, "Improved transmission performance of adaptively modulated optical OFDM signals over directly modulated DFB laser-based IMDD links using adaptive cyclic prefix", Opt. Express, vol. 16, no. 13, pp. 9480–9494, Jun. 2008.

[16] X. Zheng, J. L. Wei, and J. M. Tang, "Transmission performance of adaptively modulated optical OFDM modems using subcarrier modulation over SMF IMDD links for access and metropolitan area networks", Opt. Express, vol. 16, no. 25, pp. 20 427–20 440, Dec. 2008.

[17] T. Schneider, Nonlinear Optics in Telecommunications. New York: Springer-Verlag, 2004.

[18] S. C. J. Lee, F. Breyer, S. Randel, D. Cardenas, H. P. A. Boom, and A. M. J. Koonen, "Discrete multi-tone modulation for high-speed data transmission over multimode fibres using 850-nm VCSEL", presented at the Optical Fiber

Communication/Nat. Fiber Optic Engineers Conf. (OFC/NFOEC), San Diego, CA, 2009, Paper OWM2.

[19] J. M. Tang and K. A. Shore, "Maximizing the transmission performance of adaptively modulated optical OFDM signals in multimode-fiber links by optimizing analog-to-digital converters", IEEE J. Lightw. Technol., vol. 25, no. 3, pp. 787–798, Mar. 2007.

[20] R. P. Giddings, X. Q. Jin, E. Hugues-Salas, E. Giacoumidis, and J. M. Tang, "Experimental demonstration of a record high 11.25 Gb/s real-time optical OFDM transceivers supporting 25 km SMF end-to-end transmission in simple IMDD systems", Opt. Express, vol. 18, no. 6, pp. 5541–5555, Mar. 2010.

CHAPTER 6

Filter Concatenation Impairments Reduction using AMOOFDM

Contents

6.1 Introduction.....183

6.2 Transmission System Model.....184

6.3 Conventional OOFDM using Identical Modulation.....188

6.4 OOFDM with Adaptive Modulation 192

6.5 Conclusions.....199

References.....200

6.1 Introduction

Due to the cost-sensitive nature, transparent optical Metropolitan/Regional networks not employing optoelectronic regeneration are preferred. To enable such networks to handle dynamical traffic in a cost-effective manner and to address the challenges of high traffic churn and exponential traffic growth, ROADMs have been extensively utilized as an effective bandwidth management solution [1], [2], [3].

In cost-sensitive transparent optical metropolitan/regional networks, IM/DD OOFDM is a promising transmission technique with great potential for practical deployment [4], [5].

In Metropolitan/Regional networks using ROADMs, one significant source of penalty is signal degradation due to transmission through cascaded ROADMs, referred to as the filter concatenation effect [3]. This effect gives rise to a power penalty because of signal spectral clipping arising from the overall filter passband narrowing effect [3]. In addition, filter concatenation effect also causes the strong CD effect due to variations in filter phase profiles [6], LR and GDRs appearing at the slot boundaries [7], [8]. A GDR normally occurs because of the design and manufacturing compromises for the filters. The GDR effect has been identified as one paramount factor causing transmission penalties associated with the use of filters [9], [10]. Furthermore, for a specific transmission system, the filter concatenation effect is more severe when an offset exists between the optical signal frequency and the centre position of the overall filter passband profile [6].

The effect of filter concatenation has been investigated in long-haul CO-OFDM systems using conventional OOFDM which employs an identical signal modulation

format across all subcarriers [3]. Given the fact that, compared with the employment of an identical signal modulation, the use of adaptive modulation in OOFDM (AMOOFDM) can further improve the signal transmission capacity, network flexibility and performance robustness [4], [5], it is, therefore, envisaged that adaptive modulation can enhance the ROADM-based transparent network tolerance to the filter concatenation impairments, because low signal modulation formats are adopted on subcarriers located on the filter side lobes, which experience low SNRs. Similarly, it is also expected that adaptive modulation can enhance the network tolerance to passband LR, GDR and frequency dip because of the use of low signal modulation formats on subcarriers located in such regions.

In this Chapter, the use of IM/DD OOFDM with adaptive modulation (AMOOFDM) to improve the network tolerance to the filter concatenation effect is theoretically investigated, for the first time, in transparent Metropolitan/Regional networks employing ROADMs based on different filters including fiber FBG, Chebyshev, thin film and cascaded WB/WSS devices. It is shown that, compared to the conventional identical modulation OOFDM technique, adaptive modulation can not only improve the maximum achievable transmission capacity by up to 60%, but also enhances the network tolerance to the filter impairments including filter passband LRs, GDRs and frequency dips.

6.2 Transmission System Model

In numerical simulations, the filter concatenation effect is extensively explored in a 200km Metropolitan/Regional system, which consists of ten transmission spans. Each span is composed of a 20km SSMF, one Erbium-Doped Fibre Amplifier (EDFA) with

a 5dB noise figure and a ROADM node. The purpose of using an EDFA in each span is to compensate for the signal attenuation [8]. The ROADM is based on either FBG, thin film, Chebyshev or a specific type of WB/WSS device. Throughout this Chapter, a single wavelength channel is considered to distinguish the filter concatenation effect from other nonlinear WDM impairments such as XPM and inter-channel FWM. The IM/DD OOFDM link diagram is shown in Figure 6.1, where an ideal-intensity modulator is utilized and simulated following procedures similar to those reported in [4], [5]. In the receiver, the transmitted signal is detected using a PIN-detector, and this is followed by an inverse procedure for the transmitter in the electrical domain.

In this Chapter, filters of the following four types are considered:

- FBG filters, which are uniform-strength-grating zero-chirp reflection filters. These filters have passband characteristics with strong side lobes. The intrinsic dispersion of the grating is also included and the GDR value is taken to be 12ps peak-to-peak;
- Thin film filters, which are known to have Butterworth frequency responses and are modelled using 3rd order Butterworth filters [11];
- Chebyshev filters, which are designed to have passband frequency LRs ranging from 0.1 to 2dB.
- WBs/WSSs, whose frequency ripples are approximated by inverse first-order Gaussian functions and sigmoid functions are used to describe each GDR [10]. The corresponding normalized expressions for the optical field amplitude and group delay terms are given in Ref. [12]. The parameters of the WB/WSS devices are based on those reported in Ref. [9] including, a 0.2dB amplitude

dip and a 20 GHz frequency width. The GDR value is taken to be 12ps peak-to-peak.

The numerical simulation results presented in this Chapter pertain specifically to the aforementioned four filters. These filters are representative of a significant subset of WDM filters and the results are, therefore, sufficiently generic to be of interest for use in practical Metropolitan/Regional networks.

To achieve adaptive modulation, each individual subcarrier signal modulation format varies from DBPSK, DQPSK, and from 8QAM to 256QAM. Depending upon the system frequency response, through negotiations between the transmitter and the receiver, as shown in Figure 6.1, an appropriate signal modulation format is selected for each individual subcarrier to ensure that subcarrier *BERs* detected in the receiver are uniformly distributed among all the subcarriers, and that the corresponding total channel *BER* is $< 1.0\times10^{-3}$. When the individual subcarrier *BER* is too high ($>>1.0\times10^{-3}$) even when DBPSK is used, the subcarrier is dropped completely.

Parameter	Value
Data-carrying subcarriers	31
Signal modulation formats used	DBPSK, DQPSK, 8 QAM–256 QAM
DAC & ADC sampling rate	12.5 GS/s
CP	25%
Quantization bits	7
Clipping ratio	13 dB
PIN-detector sensitivity	−19 dBm
EDFA noise figure	5 dB
SSMF dispersion parameter at 1550 nm	17 ps/(nm km)
SSMF attenuation at 1550 nm	0.2 dB/km

Table 6.1: OOFDM transceiver parameters.

In numerical simulations, for a specific transmission system, the highest possible signal modulation format of 256QAM is first taken on each individual subcarrier. The

OOFDM signal is then transmitted through the system. After transmission, the total channel *BER* and the individual subcarrier *BER* are calculated in the receiver. If the total channel *BER* is less than 1.0×10^{-3}, then the corresponding signal line rate is considered to be the final result. On the other hand, if the total channel *BER* is larger than 1.0×10^{-3}, the signal modulation format taken on each subcarrier with a subcarrier *BER* of larger than 1.0×10^{-3} is reduced to its adjacent low level. After that, a new OOFDM signal is generated and the above-mentioned procedures are repeated until the total channel *BER* of 1.0×10^{-3} is achieved. It should be noted that identical powers are used for all non-dropped subcarriers. Details of the description of the adaptive modulation algorithm are given in Refs. [4], [5].

An ideal-intensity modulator at 1550nm is considered in order to distinguish the filter concatenation effect from other laser impairments such as the frequency chirp effect. In simulating the OOFDM transceivers, 31 data-carrying subcarriers are used, a DAC/ADC converter operates at an optimum 7-bit resolution and at 12.5 GS/s sampling rate. The signal clipping level is fixed at 13dB and the CP parameter is fixed at 25% [4], [5]. In the OOFDM receiver a PIN-detector is employed, which has a quantum efficiency of 0.8 and a -19 dBm sensitivity (corresponding to a 10 Gb/s NRZ at a *BER* of 1.0×10^{-9}). Using a VOA, the optical launch power is fixed at 5dBm.

The widely adopted split-step Fourier method is employed to model the propagation of the optical signal down a SSMF [4], [5]. It is well known that for a sufficiently small fibre split-step length, the theoretical treatment yields an accurate approximation to the real effects [4], [5]. In the SSMF model, the effects of loss, CD, PMD and optical power dependence of the refractive index are included. The effect of fibre nonlinearity-induced phase noise on intensity noise conversion is also

considered upon photon detection in the receiver. The SSMF model has been successfully used in Refs. [4], [5]. The key OOFDM transceiver parameters are summarized in Table 6.1.

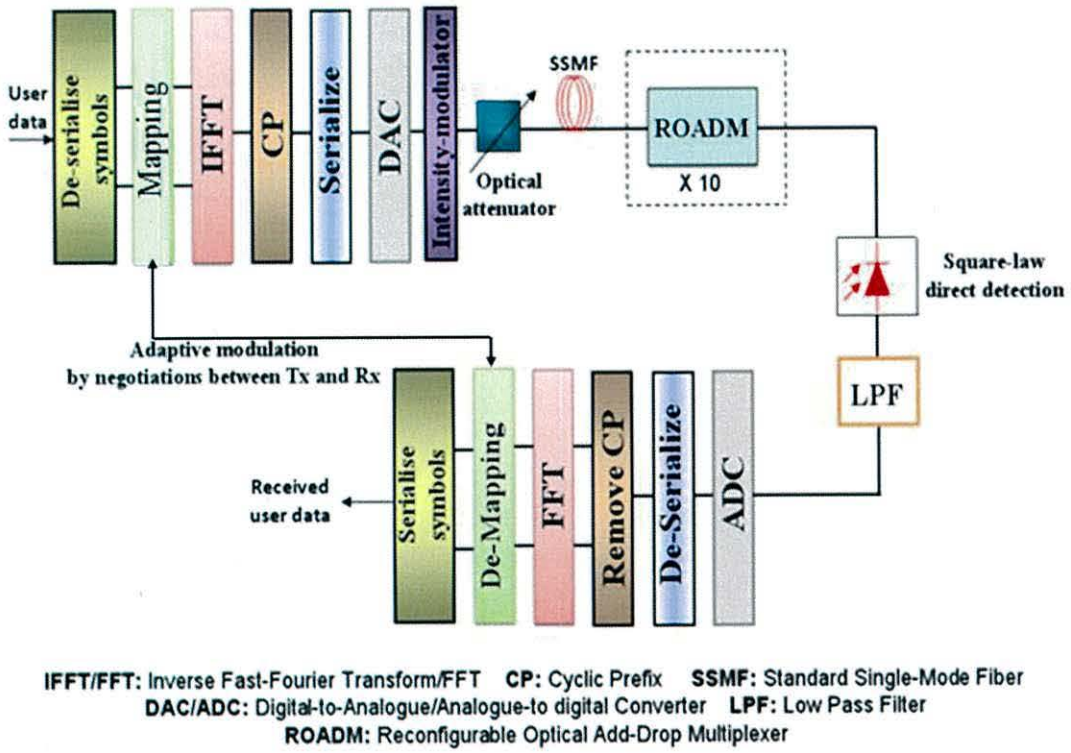

Figure 6.1: Simulation schematic diagram of IM/DD OOFDM system using both adaptive and identical modulation techniques.

6.3 Conventional OOFDM using Identical Modulation

To highlight the effectiveness of adaptive modulation, in this section, the transmission performances of OOFDM signals using identical signal modulation are explored,

which are then treated as baseline cases for comparing results obtained when adaptive modulation is adopted. For a realistic system a frequency misalignment between the optical signal frequency and the centre of the filter passband profile often exists. The impact of a misaligned FBG filter on the overall cascadability is depicted in Figure 6.2 parametrically for different maximum allowable detuning offsets. In particular, in Figures 6.2(b) and 6.2(c), the *BER* as a function of the filter misalignment is illustrated when five FBG filters and ten FBG filters are cascaded, respectively, for different signal modulation formats. When five and ten FBG filters are cascaded, this corresponds to 5×40km and 10×20km spans, respectively. Moreover, in Figure 6.2(a) the *BER* for the cases of excluding filtering is illustrated for comparison purposes. It should be noted that for all simulations, the filter misalignment effect is modelled as being uniformly distributed within the spectral range specified. A 5 GHz filter misalignment is used as a default parameter in this Chapter. This misalignment value has been used in a previous study of filter concatenation in CO-OFDM systems [3].

Figure 6.2 shows that a high signal modulation format results in a large *BER*. This occurs, firstly, due to time-domain signal distortions arising from clipping of the signal spectrum, and, secondly due to the excess optical power loss caused by the effects of filter concatenation and narrowing [6]. These effects are enhanced with increasing levels of signal modulation formats. In addition to the vendor-specified insertion loss which is usually specified at the centre of a filter passband, an excess loss is a result of the increased attenuation at a frequency on either side of the filter centre [6]. In particular, in Figure 6.2(a), all signal modulation formats correspond to *BER*s of $<1.0\times10^{-4}$ and in Figure 6.2(b) *BER*s of $<1.0\times10^{-3}$ are still observed for all the signal modulation formats considered. In comparison with Figure 6.2(a), the

increase in *BER* for all signal modulation formats is a direct result of the use of the five FBG filters. In Figure 6.2(c), due to a further increase in the number of the concatenated FBG filters, the targeted total *BER*s of 1.0×10^{-3} are achieved only for DBPSK, DQPSK, 8QAM and 16QAM.

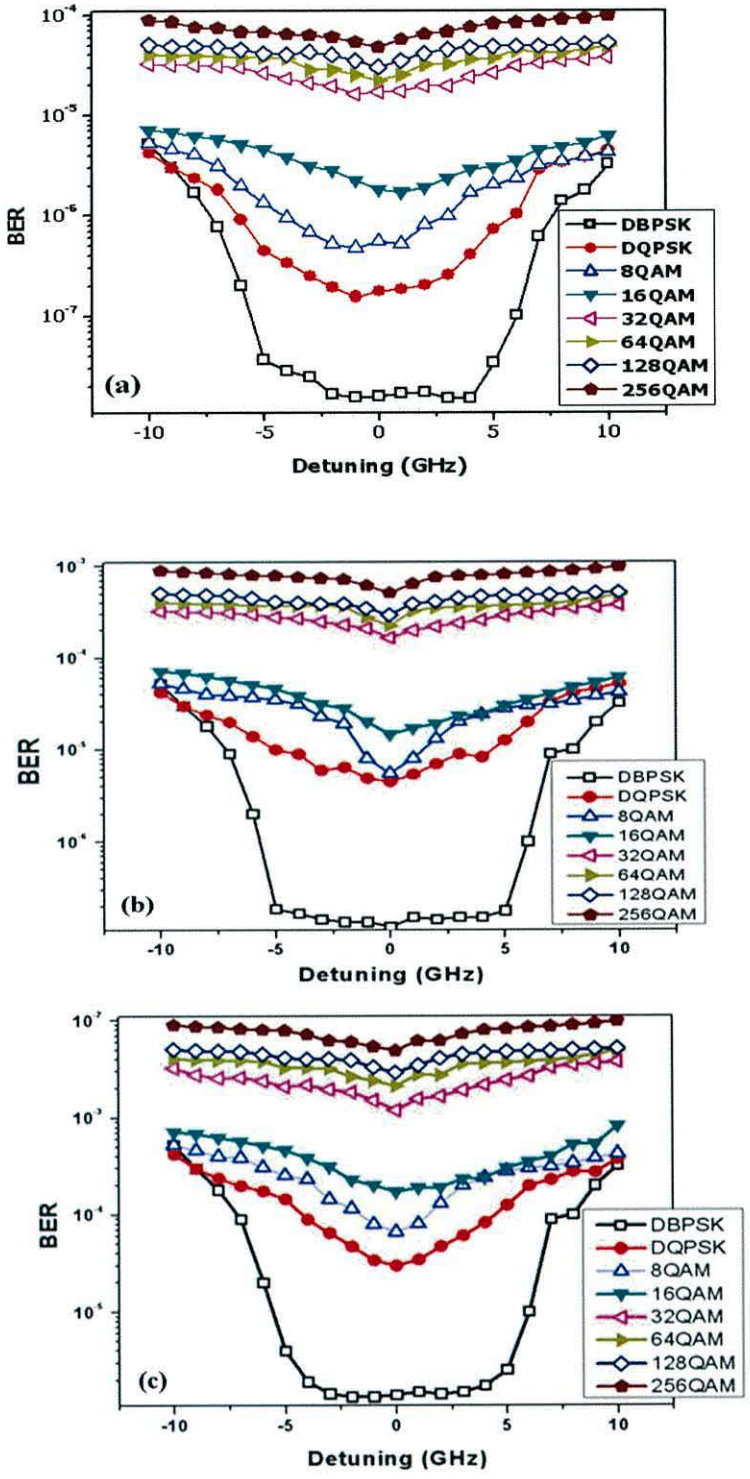

Figure 6.2: *BER* versus laser detuning for different signal modulation formats for (a) no filtering, (b) five FBGs, and (b) ten FBGs.

Making use of the conventional identical modulation technique, in Figure 6.3, the *BER* as a function of laser detuning is examined for ten Chebyshev filters having different values of frequency passband LR (ranging from 0.5dB to 2dB). For this example the highest signal modulation format of 256QAM is used on all the subcarriers. It is shown that the *BER* degradation strongly depends on the passband LR.

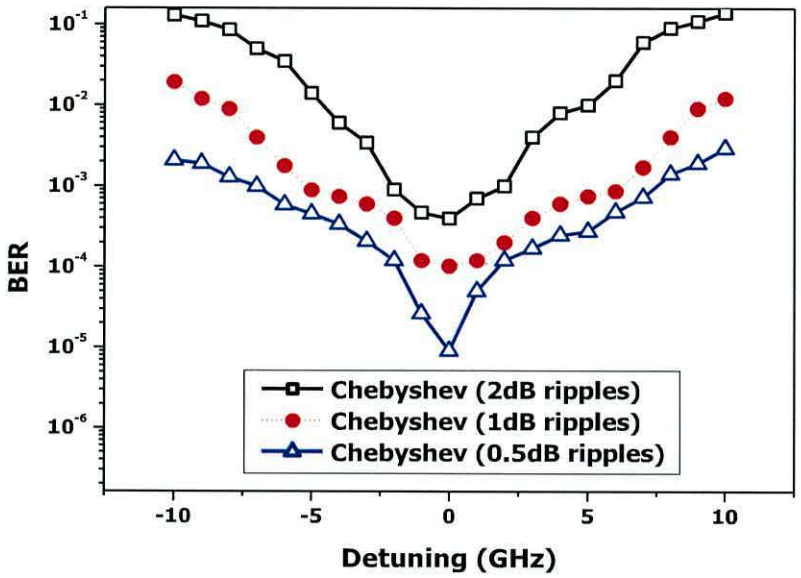

Figure 6.3: *BER* versus laser detuning for ten Chebyshev filters with different ripple factors. 256QAM is used on all subcarriers.

6.4 OOFDM with Adaptive Modulation

In this section, detailed performance comparisons are made between the conventional identical signal modulation technique and the adaptive modulation technique for filters of various types. For this purpose, initially optical filters of two types including FBG and WB/WSS are employed. In Figure 6.4, the transmission performance of the

OOFDM system using adaptive modulation is explored and compared with the conventional identical modulation technique when ten FBG filters and WB/WSS devices are employed. It is shown that, for both FBGs and WB/WSSs, the signal capacity achieved using adaptive modulation can be improved by up to 60% within the entire detuning range when compared to conventional identical modulation. Such a signal capacity improvement can be explained by considering Figures 6.5 – 6.6:

In Figure 6.5 the FBG amplitude response and GDR are plotted together with the signal modulation format allocation on each subcarrier. For this example only, 22 subcarriers are shown. High transmission loss regions are observed where the GDRs are increased to 6 ps (12 ps peak-to-peak) and the passband LRs are also high at the FBG frequency response side lobes. This results in low signal modulation formats occurring at the side lobes. However, high signal modulation formats occur in the centre of the frequency range, where the passband LRs and GDRs are very low (GDR values are about 2 ps peak-to-peak). This gives rise to a total signal capacity of 26 Gb/s corresponding to a total *BER* of 1.0×10^{-3}. However, using conventional identical modulation on these subcarriers, the maximum signal capacity reaches just 14.53 Gb/s (corresponding to 8QAM).

In Figure 6.6, the WB/WSS amplitude responses and corresponding GDRs are plotted together with the signal modulation format allocation on the subcarriers. This example presents 29 of the 31 subcarriers, since two subcarriers are dropped due to occurrence of an extremely high *BER* ($>>1.0\times10^{-3}$). It is observed that, at the centre frequency (a frequency dip at -57dBm is shown) and the side lobes of the spectrum, the passband LR and GDR are high, resulting in low signal modulation formats, whilst the highest signal modulation formats are taken on the low roll-off regions where the

passband LRs and GDRs are also very low (GDR values are about 1 ps peak-to-peak). This leads to a total signal capacity of 26.094 Gb/s at a total *BER* of 1.0×10^{-3}. However, using conventional identical modulation, the maximum signal capacity reaches just 19.375 Gb/s (corresponding to 16QAM).

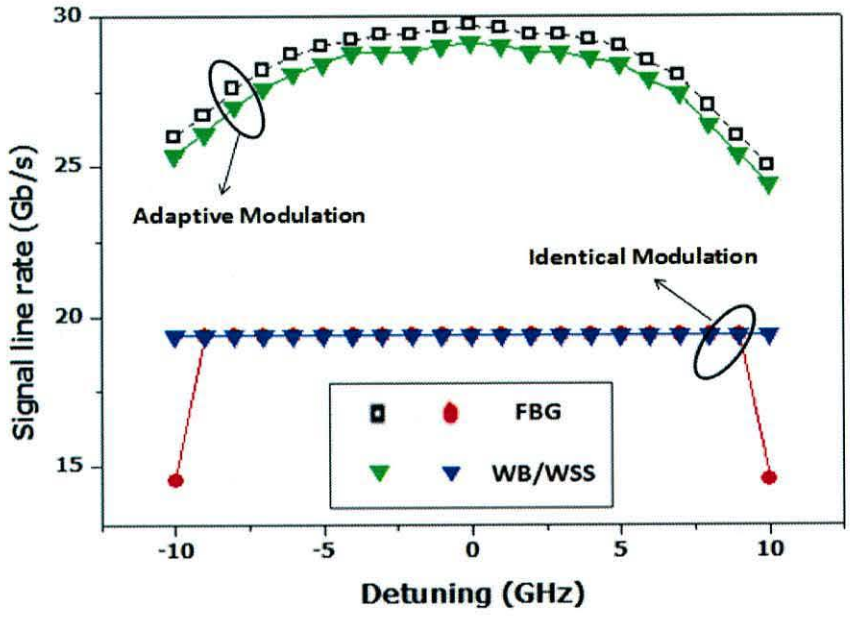

Figure 6.4: Signal capacity versus laser detuning for ten FBGs and WB/WSS devices using adaptive and identical modulation.

Having investigated the influence of adaptive modulation on the filter concatenation effect for optical filters of two types, the next step is to explore the impact of adaptive modulation for filters of other types. In addition, the node number-dependent transmission performance is also studied. In Figures 6.7 and 6.8, the transmission performance is explored for FBGs, thin films and Chebyshev filters. For Chebyshev filters, the impact of adaptive modulation on 2dB of frequency passband LR is also examined.

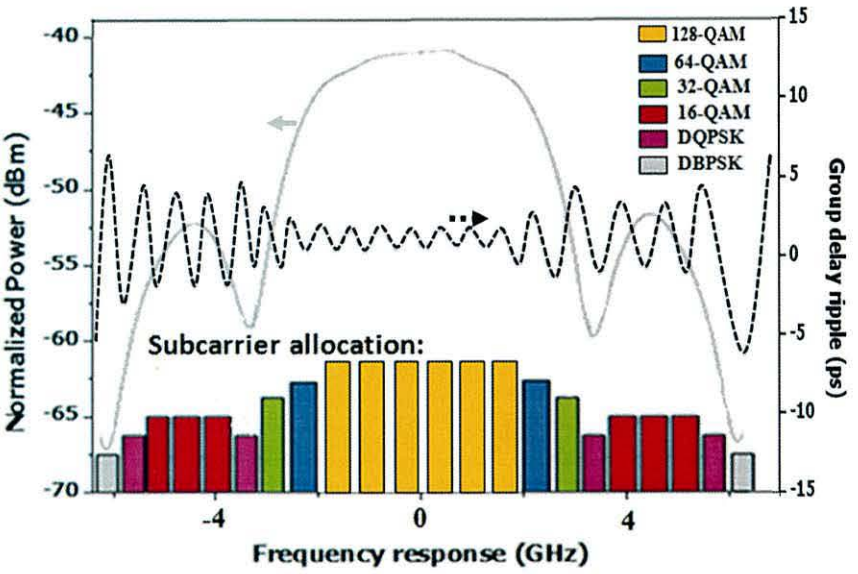

Figure 6.5: Example of adaptive modulation allocation on subcarriers, for FBG amplitude response and group delay ripple. This simple example shows 22 subcarriers.

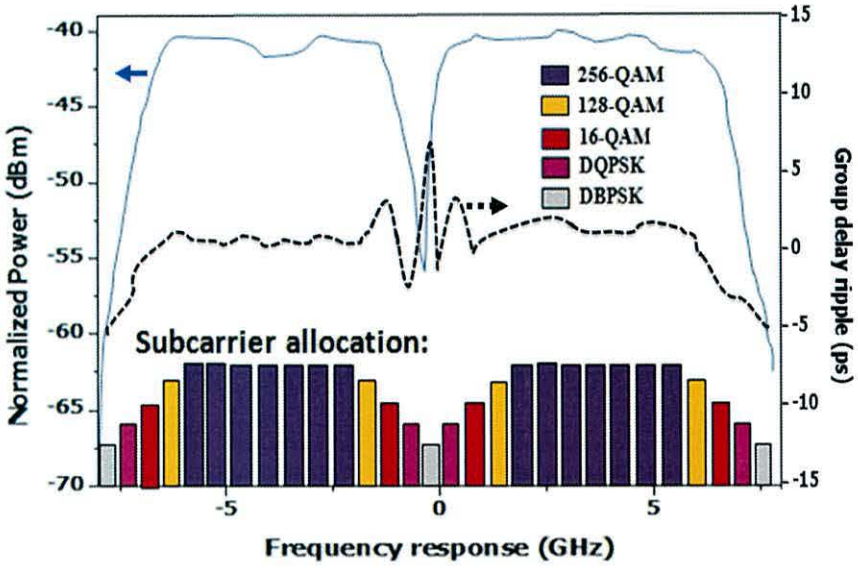

Figure 6.6: Example of adaptive modulation allocation on subcarriers, for WB/WSS amplitude response and group delay ripple. This example shows 29 of the 32 generated subcarriers, since 2 are dropped due to very high *BERs* even when DBPSK is used, and, 1 carries no information (zero power).

For the conventional identical modulation technique, the observed performances are very similar for the three aforementioned filters, except for the cases where the Chebyshev filters are used for large laser detuning and large number of nodes. The difference is due to the 2dB ripple factor. On the other hand, using adaptive modulation, the thin film filters have better performance compared to the FBGs and Chebyshev-with-LR filters, because the improved steepness of the responses of these FBG/Chebyshev filters results in an increase in both the filter dispersion effect and the transmission loss. The validity of the statement has been confirmed in Ref. [13].

From Figures 6.7 and 6.8, it is verified that adaptive modulation can be considered as an effective signal modulation scheme for filters of different types and can increase the transmission performance significantly (up to 60%), compared to the conventional identical modulation technique. Furthermore, adaptive modulation is not only effective over a wide range of laser frequency detuning but also for any number of nodes. Increasing the number of nodes, the subcarrier SNR is degraded due to the accumulation of the filter characteristic which results as a noise for these subcarriers. This kind of distortion can be tolerated by using low signal modulation formats on these subcarriers. Moreover, adaptive modulation can improve the tolerance to the filter passband LR impairments, as shown in the related graphs for ten Chebyshev filters having a 2 dB ripple factor. This occurs due to the effective signal modulation format allocation over the LR region.

In Figures 6.8(a) – 6.8(b) the signal capacity versus node number for the cases including/excluding filter misalignment is plotted in order to investigate the filter misalignment impact on cascaded filters. It is revealed that the adaptive modulation improvement in signal capacity against the conventional identical modulation is more

pronounced when the filter misalignment is considered for a number of the cascaded filters of <7.

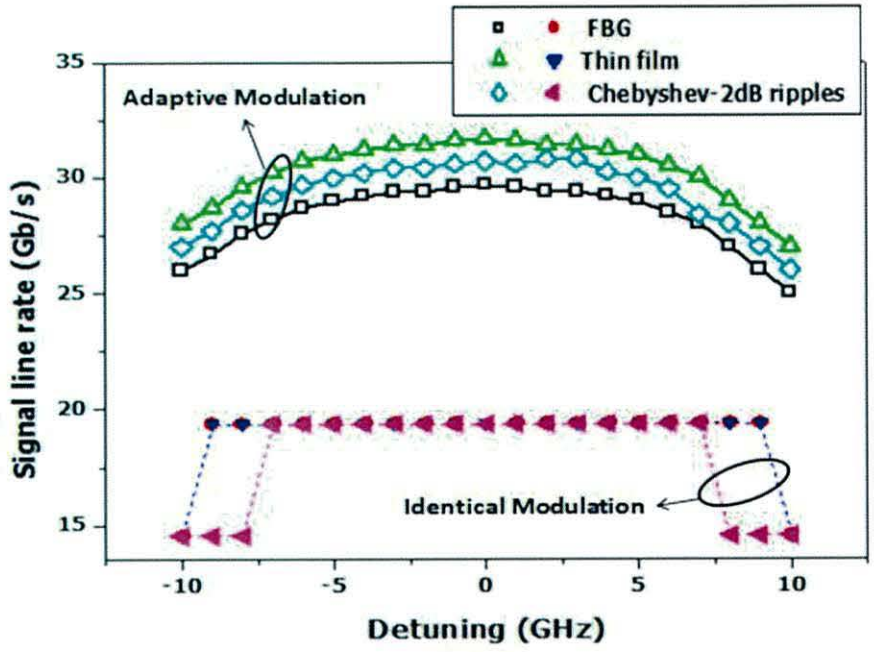

Figure 6.7: Signal capacity versus laser detuning for ten FBGs, thin films and Chebyshevs with 2dB ripple factor, using both adaptive and identical modulation.

On the other hand, when the number of the cascaded filters is larger than 7, the signal capacity improvement offered by adaptive modulation is almost the same for the two cases considered here. The aforementioned statement and the graph trends can be explained by considering Figure 6.9, where the Q penalty as a function of node number is depicted for the cases including/excluding filter misalignment. In obtaining Figure 6.9, use is made of conventional identical modulation of 64QAM on all subcarriers and FBG filters. The Q penalty is defined in Ref. [14]. It can be seen that when the FBG filters and signal laser are perfectly aligned, a penalty occurs only for >7 cascaded filters. The reason behind this is that, even though the majority of the IM/DD OOFDM signal spectrum will be confined within the filter passband, some

parts of the signal spectrum are eventually confined outside that range. Figures 6.8 and 6.9 reveal that the utilization of adaptive modulation is essential in ROADM-based transparent optical Metropolitan/Regional networks.

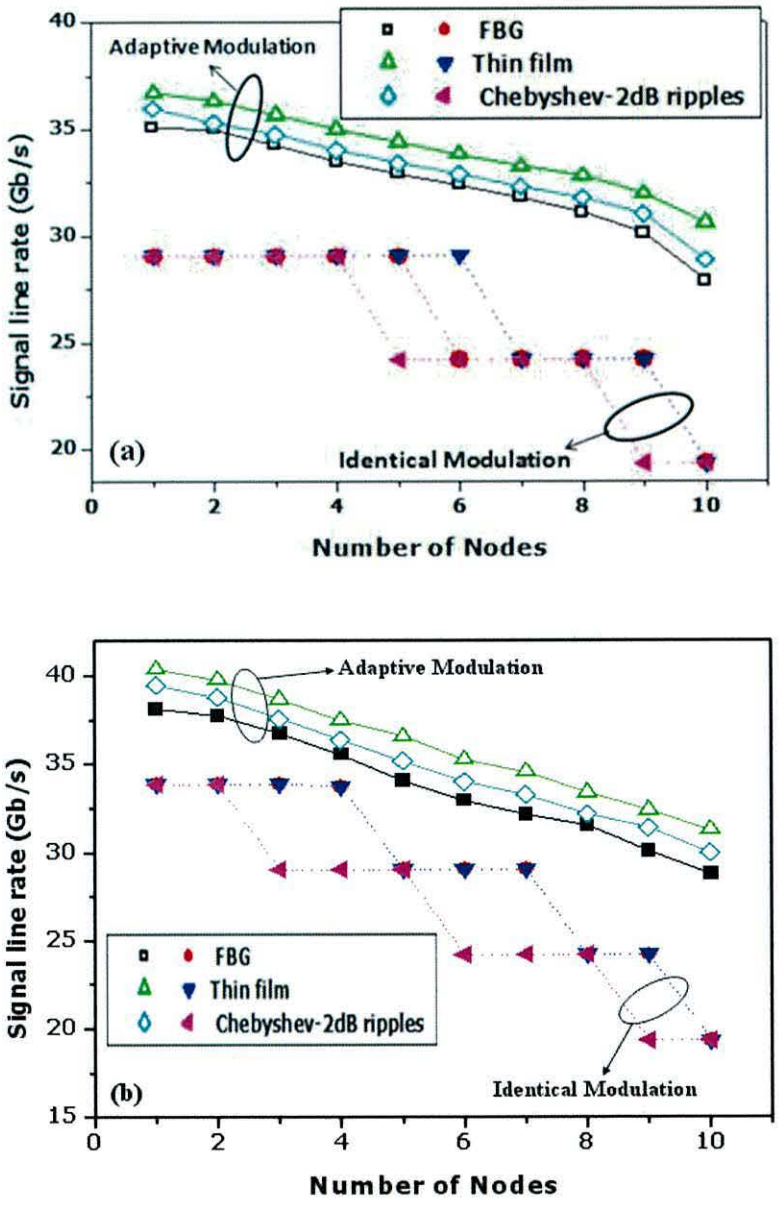

Figure 6.8: Signal capacity versus node number with (a) filter misalignment and (b) without filter misalignment for FBGs, thin films and Chebyshevs filters with 2dB ripple factor, using both adaptive and identical modulation.

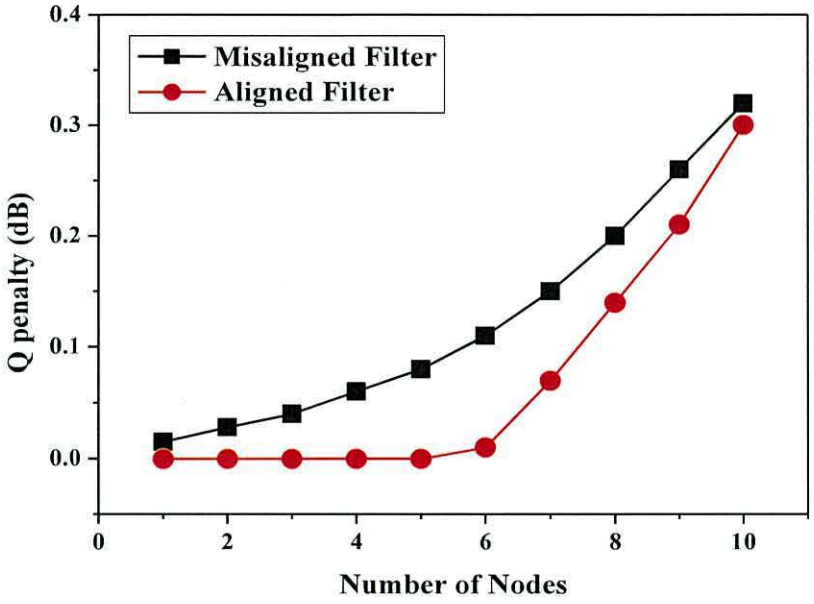

Figure 6.9: Q penalty versus node number for cases of including/excluding filter misalignment. FBG filters are considered and 64 QAM is taken on all the subcarriers.

6.5 Conclusions

We have performed numerical simulations of the impact of adaptive modulation on the filter concatenation effect in transparent Metropolitan/Regional optical networks. For conventional identical OOFDM signal modulation and adaptive OOFDM signal modulation, we have evaluated the system performance for optical filters of four types including FBG, WB/WSS, thin film and Chebyshev. It has been shown that, in comparison with conventional identical modulation, adaptive modulation can increase the transmission performance by up to 60%. Moreover, adaptive modulation is also capable of improving the network tolerance to passband LR, GDR and frequency dip due to the use of low signal modulation formats on subcarriers with degraded SNRs.

Numerical simulation results also indicate that adaptive modulation is effective when the number of nodes is less than 7. More importantly, it has been shown that the utilization of adaptive modulation is essential due to its vital tolerance to filter misalignment.

It is worth pointing out the following two points: a) The use of adaptive modulation increases the DSP complexity of the OOFDM transceivers, which may, however, not increase the actual cost of the transceivers for mass production. On the other hand, the OOFDM transceivers can significantly lower the system installation cost as adaptive modulation can relax the requirements on optical component parameters, thus allowing the use of low-cost optical components in practical system designs. b) The conclusions obtained in this Chapter may also be applicable for long-haul transmission systems.

References

[1] I. Papagiannakis, D. Klonidis, J. Kikidis, A. N. Birbas, and, I. Tomkos, "Electronic mitigation of the filter concatenation effect of low-cost 2.5 Gb/s rated DMLs sources operated at 10 Gb/s", Optical Fiber Communication Conf./National Fiber Optic Engineers Conf. (OFC/NFOEC), (Anaheim, CA, 2009), Paper OWE3.

[2] I. Tomkos, R. Hesse, N. Antoniades, and A. Boskovic "Impact of filter concatenation on the performance of metropolitan area optical networks utilizing directly modulated lasers", Optical Fiber Communication Conf./National Fiber Optic Engineers Conf. (OFC/NFOEC), (Anaheim, CA, 2000), Paper WBB4.

[3] Y. Tang and W. Shieh, "Filter concatenation impact on 107-Gb/s coherent optical OFDM system", OptoElectronics and Communications Conference (OECC), pp. 1–2, 2009.

[4] E. Giacoumidis, J. L. Wei, X. L. Yang, A. Tsokanos, and, J. M. Tang, "Adaptive-Modulation-Enabled WDM Impairment Reduction in Multichannel Optical OFDM Transmission Systems for Next-Generation PONs", IEEE Journal of Photonics, vol. .2, pp. 130–140, 2010.

[5] J. M. Tang and K. A. Shore, "30-Gb/s signal transmission over 40-km directly modulated DFB-laser-based singlemode-fibre links without optical amplification and dispersion compensation", IEEE J. Lightw. Technol., vol. 24, pp. 2318–2327, 2006.

[6] J. D. Downie, I. Tomkos, N. Antoniades, and A. Boskovic, "Effects of Filter Concatenation for Directly Modulated Transmission Lasers at 2.5 and 10 Gb/s", IEEE J. Lightwave Technol., vol. 20, pp. 218–228, 2002.

[7] X. Liu, X. Wei, A. H. Gnauck, C. R. Doerr, and S. Chandrasekhar, "Analysis of Loss Ripple and Its Application to the Mitigation of Optical Filtering Penalty", IEEE Photon. Technol. Lett., vol. 17, pp. 82–84, 2005.

[8] N. N. Khrais, A. F. Elrefaie, R. E. Wagner, and S. Ahmed, "Performance of Cascaded Misaligned Optical (De)multiplexers in Multiwavelength Optical Networks", IEEE Photon. Technol. Lett., vol.8, pp. 1073–1075, 1996.

[9] J. K. Rhee, "Variable passband optical add-drop multiplexer using wavelength selective switch," in Proc. 27th Eur. Conf. Optical Commun., vol. 4, pp. 550–551, 2001.

[10] S. Sygletos, A. Tzanakaki, and I. Tomkos, "Numerical Study of Cascadability Performance of Continuous Spectrum Wavelength Blocker/Selective Switch at 10/40/160 Gb/s", IEEE Photon. Technol. Lett., vol. 18, pp. 2608–2610, 2006.

[11] H. Fadhil, S. Aljunid, and B. Ahmed, "Performance of OCDMA Systems Using Random Diagonal Code for Different Decoders Architecture Schemes", The International Arab Journal of Information Technology, vol. 7, no. 1, pp. 1–5, 2010.

[12] R. Ramaswami and K. N. Sivarajan, *Optical Networks: A Practical Perspective*, 2nd ed. Morgan Kauffman, San Mateo, CA, 2001.

[13] G. Lenz, B. Eggleton, C. Madsen, C. Giles, and G. Nykolak, "Optimal Dispersion of Optical Filters for WDM Systems," IEEE Photon. Technol. Lett., vol. 10, pp. 567–569, 1998.

[14] J. D. Downie, "Relationship of Q Penalty to Eye-Closure Penalty for NRZ and RZ Signals With Signal-Dependent Noise" J. Lightw. Technol., vol. 23, no. 6, pp. 2031–2038, 2005.

CHAPTER 7

Conclusions and Future Work

7.1 Conclusions

To accommodate the ever increase in bandwidth requirement from both individual and business users, cost-sensitive MMF-based LANs, SMF-based PONs face tremendous challenges for upgrading into high-speed solutions in a cost-effective manner. OOFDM as a promising technique for future high-capacity optical networks has found its place in optical networks of various architectures [1].

In this thesis, extensive investigations have been theoretically undertaken of the feasibility of the OOFDM technique in simple cost-effective IM/DD transmission systems for different application scenarios. As high-speed and cost-effectiveness are the main targets in designing any optical systems, from the operators' point of view, the use of low-cost electro-optic converters is also critical to substantially reduce the operation cost, and hence reduce the CAPEX/OPEX of the transmission systems. Whilst external modulation schemes such as EAM and MZM are the dominant technologies for long-haul applications, their usage in LANs and PONs is, however, limited since they are expensive and bulky. This problem can be solved successfully by the utilization of DMLs because of their potentially low cost, compact size, low

power consumption and high optical output power characteristics when compared with other transmitter source using external modulation schemes [2].

The PON industry and standardization body are currently making great effort to implement high-capacity FTTH systems in a cost-effective manner. To achieve the aforementioned objectives, full use of DSP-based OOFDM adaptability is very promising to deliver high-speed and low-cost transceivers with improved robustness to the MMF/SMF impairments. In Chapter 3, the impact of ACP has been investigated on the transmission performance of AMOOFDM over DML-based, IM/DD systems using both MMFs and SMFs. Three ACP mechanisms have been identified, each of which can, depending upon the system properties, affect significantly the AMOOFDM transmission performance. In comparison with AMOOFDM having a fixed cyclic prefix duration of 25%, AMOOFDM with ACP can not only improve the transmission capacity by a factor of >2 (>1.3) for >1000m MMFs (<80km SMFs) with 1dB link loss margin enhancement, but also relax considerably the requirement on the DFB modulation bandwidth.

In Chapter 4, to further maximize the OOFDM transmission performance and simultaneously improve the system flexibility and performance robustness, full use has been made of orthogonality among different subcarriers within an OOFDM symbol by applying various adaptive loading algorithms on each individual subcarrier, according to the SNR experienced by the subcarrier [3]. The widely adopted adaptive loading algorithms include BL, PL, and BPL, all of which can be implemented using the well-known "water-filling" approach. Hence, it is of great importance to compare the performance of the three adaptive loading algorithms over OOFDM MMF and SMF systems. Therefore, detailed investigations of the

performance of the widely adopted adaptive loading algorithms including BL, PL and BPL have been compared for different transceiver parameters in both SMF and MMF systems. It has been shown that the BPL (PL) algorithm always offers the best (worst) transmission performance. The absolute transmission capacity differences between these algorithms are independent of signal bit rate and increase with both transmission distance and DAC/ADC sampling rate. More importantly, numerical results have also indicated that, for PON systems and worst-case MMF links of less than 300 m, in comparison with the most sophisticated BPL algorithm, the simplest PL algorithm is sufficiently effective in escalating the OOFDM system performance to its maximum potential. The effectiveness of the PL algorithm can be further improved when a large number of subcarriers are utilized. On the other hand, for relatively transmission systems with their 3-dB bandwidths being much less than the transmitted OOFDM signal spectrum, the BPL algorithm has to be adopted. The aforementioned results have great potential for practical cost-effective OOFDM transceiver architecture design.

In all previously published works related to AMOOFDM [1], [2], [4], discussions of the transmission performance of the AMOOFDM technique have been made only for single-channel transmission. Hence, in Chapter 5, the AMOOFDM technique has been investigated over IM/DD DML-based multi-channel PON. It has been shown that AMOOFDM can significantly reduce the nonlinear WDM impairments induced by the XPM and FWM effects. Investigations have also revealed that, in comparison with conventional OOFDM, AMOOFDM improves the maximum achievable signal transmission capacity of a central WDM channel by a factor of 1.3 and 3.6 for 40km and 80km SSMFs, respectively, with the corresponding dynamic input optical power

range being extended by approximately 5dB. In addition, the adaptive modulation-enabled performance enhancement is more pronounced for optical launch powers of > 0dBm. Furthermore, AMOOFDM also enables the occurrence of cross-channel complementary modulation format mapping, leading to considerably improved transmission capacities for each individual WDM channel and the entire WDM transmission system.

Having explored OOFDM in cost-sensitive LANs and PONs, further investigations of the OOFDM technique have been undertaken in transparent optical Metro/Regional networks without employing optoelectronic regeneration. To enable such networks to handle dynamical traffic in a cost-effective manner and to address the challenges in high traffic churn and exponential traffic growth, ROADMs have been extensively utilized as an effective bandwidth management solution [5], [6], [7]. In the cost-sensitive transparent optical Metro/Regional networks using ROADMs, one significant source of penalty is signal degradation due to transmission through cascaded ROADMs, referred to as the filter concatenation effect [5], [7]. This effect gives rise to a power penalty because of signal spectral clipping arising from the overall filter passband narrowing effect [7]. In addition, the filter concatenation effect also causes the strong CD effect due to nonlinear filter phase profiles [8], and wider passband, LR and GDR appearing at the slot boundaries [9], [10]. In Chapter 6, the use of AMOOFDM to improve the network tolerance to the filter concatenation effect has been theoretically investigated in transparent Metro/Regional networks employing ROADMs based on different filters including FBG, Chebyshev, thin film and a WB/WSS device. It has been shown that, compared to the conventional identical modulation OOFDM, adaptive modulation can not only improve the maximum

achievable transmission capacity by up to 60%, but also enhances the network tolerance to the filter impairments including filter passband LR, GDR and frequency dip. Numerical simulation results also indicated that adaptive modulation is effective for any amount of nodes and laser frequency detuning. More importantly, it has also been shown that the utilization of adaptive modulation is essential due to its vital tolerance to the filter misalignment penalty.

The aforementioned investigations are the brief summaries of the research work carried out in this thesis. Future works on the OOFDM technique are presented in next section.

7.2 Future Work

Although extensive research works have been undertaken in this Thesis, a number of issues related to OOFDM-based LANs PONs and even MANs are important for future investigations. The short-term works are listed as follows:

1) Experimental demonstration of AMOOFDM transmission in WDM-PONs using real-time OOFDM transceivers.

Real-time experimental demonstrations of AMOOFDM transmission is critical for not only evaluating the true potential of the AMOOFDM transmission WDM-PONs, but also identifying the limitations set by hardware that theoretical simulations may not be able to cover.

2) Rayleigh backscattering mitigation in OOFDM WDM-PONs.

One of the key objectives in OOFDM WDM-PONs is to achieve a full bidirectional transmission system. If downstream and upstream spectra

overlap, the Rayleigh backscattering may become a substantial interference to the received signal, for fibre lengths > 10km [11]. In order to solve this, a couple of approaches are proposed: dual laser configuration (one used as a reference for detection, and the other for upstream transmission), and inclusion of a wavelength shifter at the ONU, using a wavelength shifting device [12].

3) Utilization of novel signal modulation techniques such as Fast-OFDM (FOFDM) for LANs, MANs and NG-PONs.

Based on the author's very recent investigations on FOFDM [13], in which the frequency spacing between subcarriers is reduced by half in contrast to conventional OFDM, bandwidth-efficient transceivers can be designed. FOFDM has been effectively implemented in both MMF [13] and SMF [14] transmission systems. Investigations on Fast-OFDM can trigger a new generation of bandwidth-efficient optical networks including a new breed of NG-PONs.

The long-term work is to investigate high-speed OOFDM signals for ≥40Gb/s transmission over SMF-based IM/DD WDM-PONs with extended reach and high power split ratio. Such an advanced PON system can provide individual and business users with "future proof" solutions to satisfy the requirements in bandwidth and allowable power budget.

References

[1] N. E. Jolley, H. Kee, R. Rickard, J. Tang, and K. Cordina, "Generation and propagation of a 1550 nm 10 Gb/s optical orthogonal frequency division multiplexed signal over 1000 m of multimode fibre using a directly modulated DFB", presented at the Optical Fiber Communication Conf./National Fiber Optic Engineers Conf. (OFC/NFOEC), (OSA, 2005), Paper OFP3.

[2] J. M. Tang, P. M. Lane, and K. A. Shore, "High-speed transmission of adaptively modulated optical OFDM signals over multimode fibres using directly modulated DFBs", IEEE J. Lightwave. Technol., vol. 24, no. 1, pp. 429–441, 2006.

[3] Y. Li and W. E. Ryan, "Mutual-Information-Based Adaptive Bit-Loading Algorithms for LDPC-Coded OFDM", Wireless Commun., vol. 6, no. 5, May 2007.

[4] J. M. Tang and K. A. Shore, "30 Gb/s signal transmission over 40-km directly modulated DFB-laser-based single-mode-fibre links without optical amplification and dispersion compensation", IEEE J. Lightwave. Technol. vol. 24, no. 6, pp. 2318-2327, 2006.

[5] I. Papagiannakis, D. Klonidis, J. Kikidis, A. N. Birbas, and, I. Tomkos, "Electronic mitigation of the filter concatenation effect of low-cost 2.5 Gb/s rated DMLs sources operated at 10 Gb/s", Optical Fiber Communication Conf./National Fiber Optic Engineers Conf. (OFC/NFOEC), (Anaheim, CA, 2009), Paper OWE3.

[6] I. Tomkos, R. Hesse, N. Antoniades, and A. Boskovic "Impact of filter concatenation on the performance of metropolitan area optical networks utilizing directly modulated lasers", Optical Fiber Communication Conf./National Fiber Optic Engineers Conf. (OFC/NFOEC), (Anaheim, CA, 2000), Paper WBB4.

[7] Y. Tang and W. Shieh, "Filter concatenation impact on 107-Gb/s coherent optical OFDM system", OptoElectronics and Communications Conference (OECC), pp. 1–2, 2009.

[8] J. D. Downie, I. Tomkos, N. Antoniades, and A. Boskovic, "Effects of Filter Concatenation for Directly Modulated Transmission Lasers at 2.5 and 10 Gb/s", IEEE J. Lightwave Technol., vol. 20, pp. 218–228, 2002.

[9] X. Liu, X. Wei, A. H. Gnauck, C. R. Doerr, and S. Chandrasekhar, "Analysis of Loss Ripple and Its Application to the Mitigation of Optical Filtering Penalty", IEEE Photon. Technol. Lett., vol. 17, pp. 82–84, 2005.

[10] N. N. Khrais, A. F. Elrefaie, R. E. Wagner, and S. Ahmed, "Performance of Cascaded Misaligned Optical (De)multiplexers in Multiwavelength Optical Networks", IEEE Photon. Technol. Lett., vol.8, pp. 1073–1075, 1996.

[11] M. O. van Deventer, Fundamentals of Bidirectional Transmission over a Single Optical Fibre, Kluwer academic press, 1996.

[12] M. Omella, J. Lazaro, and J. Prat, "Driving Requirements for Wavelength Shifting in Colorless ONU with Dual-Arm Modulator", IEEE Journal of Lightwave Technology, vol. 27, no. 17, 2009.

[13] E. Giacoumidis, I. Tomkos, and J. Tang, "Performance of Optical Fast-OFDM in MMF-Based Links", in Optical Fiber Communication Conference, OSA Technical Digest (CD) (Optical Society of America, 2011), paper OWU3.

[14] S. K. Ibrahim et al., "Demonstration of world-first experimental fast OFDM system at 7.174Gbit/s and 14.348Gbit/s", ECOC'2010, PD3.4.

Appendix

A.1 Journal Publications

[1] E. Giacoumidis, I. Tomkos, and J. M. Tang, "Adaptive Modulation-Induced Reduction in Filter Concatenation Impairment for Optical OFDM Metro/Regional4Systems", IEEE/OSA J. Opt. Commun. Netw. (JOCN), vol. 3, pp. 587 – 593, 2011.

[2] E. Giacoumidis, X. Q. Jin, A. Tsokanos, and J. M. Tang, "Statistical Performance Comparisons of Optical OFDM Adaptive Loading Algorithms in Multimode Fiber-Based Transmission Systems", IEEE Journal of Photonics, vol. 2, pp. 1051 – 1059, 2010.

[3] A. Tsokanos, C. Mouchos, E. Giacoumidis, and J. M. Tang, "A Scalable Model for the Performance Evaluation of ROADMs with Generic Switching Capabilities", Journal of Networks (JNW), vol. 5, no. 10, pp. 1215 – 1220, 2010.

[4] E. Giacoumidis, J. L. Wei, X. L. Yang, A. Tsokanos, and J. M. Tang, "Adaptive Modulation-Enabled WDM Impairment Reduction in Multi-Channel Optical OFDM Transmission Systems for Next Generation PONs", IEEE Journal of Photonics, vol. 2, pp. 130 – 140, 2010.

[5] R. P. Giddings, X. Q. Jin, E. Hugues-Salas, E. Giacoumidis, J. L. Wei, and J. M. Tang, "Experimental demonstration of record high 11.25Gb/s real-time end-to-end optical OFDM transceivers for PONs", Optics Express, vol. 18, pp. 5541 – 5555, 2010.

[6] E. Giacoumidis, J. L. Wei, X. Q. Jin, and J. M. Tang, "Improved transmission performance of adaptively modulated optical OFDM signals over directly modulated DFB laser-based IMDD links using adaptive cyclic prefix", Optics Express, vol. 16, pp. 9480 – 9494, 2008.

A.2 Conference Publications

[7] E. Giacoumidis, J. L. Wei, E. Hugues Salas, J. M. Tang, and I. Tomkos, "Adaptive Loading Algorithms Evaluations for IMDD SMF System-Based Optical OFDM Transceivers", Progress In Electromagnetics Research Symposium (PIERS), Suzhou, China, Sept. 2011.

[8] E. Giacoumidis, I. Tomkos, and J. M. Tang, "Group Delay Ripple Reduction in Cascaded ROADMs by Adaptively Modulated Optical OFDM signals for Metro/Regional Networks", IEEE 16th European Conference on Networks and Optical Communications (NOC) and 6th Conference on Optical Cabling and Infrastructure (OC&I), Northumbria University, Newcastle upon Tyne, UK, July 2011.

[9] E. Giacoumidis, J. L. Wei, A. Tsokanos, A. Kavatzikidis, E. Hugues-Salas, J. M. Tang, and I. Tomkos, "Performance Optimization of Adaptive Loading Algorithms for SMF-Based Optical OFDM Transceivers", IEEE 16th European Conference on Networks and Optical Communications (NOC) and 6th Conference on Optical Cabling and Infrastructure (OC&I), Northumbria University, Newcastle upon Tyne, UK, July 2011.

[10] E. Giacoumidis, A. Kavatzikidis, I. Cano, M. C. Santos, J. M. Tang, J. Prat, and I. Tomkos, "Mitigation techniques for peak-to-average power ratio and optical beat interference in OFDMA-PONs", IEEE International Conference on Transparent Optical Networks (ICTON), Stockholm, Sweden, June 2011, (Invited).

[11] E. Giacoumidis, I. Tomkos, and J. M. Tang, "Filter Concatenation Impairments Reduction by Adaptively Modulated Optical OFDM Signals for Metro/Regional Networks", IEEE Future Network & MobileSummit, Warsaw, Poland, June 2011.

[12] J. M. Tang, R. P. Giddings, X. Q. Jin, J. L. Wei, X. Zheng, E. Giacoumidis, et al., "Real-Time Optical OFDM Transceivers for PON Applications", Optical Fiber Communication Conference and Exposition (OFC) and the National Fiber Optic Engineers Conference (NFOEC), Los Angeles, California, USA, March 2011, (Invited) Paper OTuK3.

[13] E. Giacoumidis and J. M. Tang, "Statistical Investigations of Optical OFDM Adaptive Loading Algorithm over 1000 Worst-Case MMFs", Optical Fiber Communication Conference and Exposition (OFC) and the National Fiber Optic Engineers Conference (NFOEC), Los Angeles, California, USA, March 2011, Paper JWA089.

[14] E. Giacoumidis, J. L. Wei, and J. M. Tang, "Adaptive Modulation Induced WDM Impairment Reduction in Optical OFDM PONs", IEEE Future Network & MobileSummit, Florence, Italy, June 2010.

[15] R. P. Giddings, X. Q. Jin, E. Hugues-Salas, E. Giacoumidis, and J. M. Tang, "Experimental demonstration of record high 11.25Gb/s real-time end-to-end optical OFDM transceivers for PONs", IEEE Future Network & MobileSummit, Florence, Italy, June 2010.

[16] E. Giacoumidis and J. M. Tang, "Improved transmission performance of Adaptively Modulated Optical OFDM signals over MMFs using adaptive cyclic prefix", IEEE OptoElectronics and Communications Conference and the Australian Conference on Optical Fiber Technology (OECC/ACOFT), Sydney Convention & Exhibition Centre, Australia, July 2008.

[17] E. Giacoumidis, J. L. Wei, and J. M. Tang, "Influence of Adaptive Cyclic Prefix on the Transmission Performance of Adaptively Modulated Optical OFDM Signals over Directly Modulated Laser-Based IMDD Links", Semiconductor & Integrated Optoelectronics (IEE/SIOE), Cardiff, Wales, April 2008.

[18] M. A. Jarajreh, E. Giacoumidis, and J. M. Tang, "Quantization and Clipping Effects on the Transmission Performance of Coherent Optical OFDM Signals over AWGN Channels", Semiconductor & Integrated Optoelectronics (IEE/SIOE), Cardiff, Wales, April 2007.

[19] E. Giacoumidis, M. A. Jarajreh, and J. M. Tang, "Effect of Analogue-to-Digital Conversion on the Performance of Optical OFDM Modems in Coherent and IMDD Transmission Links", Semiconductor & Integrated Optoelectronics (IEE/SIOE), Cardiff, Wales, April 2007.